INFORMATION TO USERS

This manuscript has been reproduced from the microfilm master. UMI films the text directly from the original or copy submitted. Thus, some thesis and dissertation copies are in typewriter face, while others may be from any type of computer printer.

The quality of this reproduction is dependent upon the quality of the copy submitted. Broken or indistinct print, colored or poor quality illustrations and photographs, print bleedthrough, substandard margins, and improper alignment can adversely affect reproduction.

In the unlikely event that the author did not send UMI a complete manuscript and there are missing pages, these will be noted. Also, if unauthorized copyright material had to be removed, a note will indicate the deletion.

Oversize materials (e.g., maps, drawings, charts) are reproduced by sectioning the original, beginning at the upper left-hand corner and continuing from left to right in equal sections with small overlaps.

Photographs included in the original manuscript have been reproduced xerographically in this copy. Higher quality 6" x 9" black and white photographic prints are available for any photographs or illustrations appearing in this copy for an additional charge. Contact UMI directly to order.

Bell & Howell Information and Learning
300 North Zeeb Road, Ann Arbor, MI 48106-1346 USA
800-521-0600

Université d'Ottawa · University of Ottawa

VIBRATION AND STABILITY ANALYSIS OF TOROIDAL SHELLS

by

Bo Xu

A thesis submitted to
the Faculty of Graduate Studies and Research
in partial fulfilment of the requirements
for the degree of

M. A. Sc. in Mechanical Engineering

UNIVERSITY OF OTTAWA

Abstract

The present study is concerned with the vibration and stability analysis of toroidal shells. The study was conducted in two parts. The first part dealt with the vibration of toroidal panels, and the second with the stability of complete toroidal shells under distributed and concentrated loading.

The natural frequency and mode shape analysis of toroidal panels formed the first part of the study. The problem has potential application to reactor vessels. Panels were considered cut from different positions of a toroidal surface. Solutions were set up using the Fourier series approach, finite element method, and the differential quadrature method. Comparisons between results were made, and parametric studies considering the effect of position, thickness, and boundary conditions were carried out.

The linear elastic stability analysis of a partially submerged toroidal shell subject to concentrated loads forms the second part of the study. The problem has potential application to an offshore platform. The loading applied to the shell is idealized as a set of pads of normal surface stresses. A theoretical solution for the smallest buckling load based on the Donnell stability equations is developed. Sample results for the critical load and buckling mode are determined using the finite element method. Finally a hybrid solution based on shell theory and the differential quadrature method is presented.

Acknowledgements

I would like to express my sincere gratitude to all members of the department of mechanical engineering who made contributions towards my studies and research.

I am grateful to my supervisor, Dr. D. Redekop, for his continuous encouragement, invaluable suggestions, and patient guidance throughout the whole research process.

Special thanks go to my parents and sister and brother for their moral support and encouragement during my study.

The financial support provided by the Natural Sciences and Engineering Research Council of Canada is gratefully acknowledged.

Contents

1 Introduction

2 Literature Survey

3 Vibration of Toroidal Panels

4 Stability of Toroidal Shells

5 Conclusions

List of Tables

List of Figures

Nomenclature

a,b,c,d	constant coefficients
A_1, A_2	Lame parameters
D	bending rigidity, defined as $Eh^3/[12(1-v^2)]$
E	Young's modulus
$\mathbf{e_r}, \mathbf{e_\phi}, \mathbf{e_\theta}$	toroidal base unit vectors at point P
h	shell thickness
$\mathbf{i}, \mathbf{j}, \mathbf{k}$	cartesian unit vectors
K	extensional rigidity, defined as $Eh/[(1-v^2)]$
M,N	truncation integers
$M_\theta, M_\eta, M_{\theta\eta}$	moment resultants
$N_\theta, N_\eta, N_{\theta\eta}$	in-plane resultants
p	magnitude of normal pressure
Q_θ, Q_η	transverse shear resultants
r	cross-sectional radius of shell
$\mathbf{r}$	radius vector
R	toroidal bend radius
R_1, R_2	radii of curvature
t	time
u,v,w	displacement components
x,y,z	Cartesian coordinates
$\alpha, \hat{\beta}$	extent and center of load pad in meridional direction
β	frequency parameter
γ	radius ratio, defined as r/R
$\epsilon_\theta, \epsilon_\eta, \epsilon_{\theta\eta}$	in-plane strain components
ζ	$= 1 + \gamma \cos\theta$

η	toroidal circumferential coordinate, defined as ϕ/γ
θ	toroidal meridional coordinate
$\kappa_\theta, \kappa_\eta, \kappa_{\theta\eta}$	change of curvature components
λ	buckling load parameter
ν	Poisson's ratio
ϕ	toroidal circumferential coordinate
ψ	circumferential angle
ω	natural circular frequency in rad/s

Chapter 1

Introduction

1.1 Toroidal shells

Thin-shell structures have been studied extensively over the last century (Noor (1990), Yang (1990)). Applications of shells include aircraft, cooling towers, nuclear reactors, steel silos and tanks for bulk solid and liquid storage, pressure vessels, pipelines, and space station structures. The most important types of shells are cylindrical, spherical, and conical. Of considerable importance also is the toroidal shell, which forms the subject of this study.

The toroidal shell is doubly-curved and although less used than the other main types, does have such applications as aircraft and automobile tires, nuclear reactor vessels, and offshore platforms. Segments of such shells also form impellers of pumps and fluid couplings. In particular, the toroidal geometrical shape forms a basic structural element in the Tokamak-type fusion reactor, rotating space station, and in space vehicle liquid storage containers.

A toroidal coordinate system is given in Fig. 1.1, which depicts one quadrant of a toroidal shell. A complete toroidal shell spans through 360^o arcs in the meridional

and circumferential directions. It has a bend radius of R, a cross-sectional radius of r, and a thickness of h. A general point P on the shell mid-surface is defined by meridional and circumferential angular coordinates θ and ϕ. The radius vector $\mathbf{r}$ to P is given by

$$\mathbf{r} = (R + r\cos\theta)\sin\phi\mathbf{i} + (R + r\cos\theta)\cos\phi\mathbf{j} + r\sin\theta\mathbf{k} \qquad (1.1)$$

where i, j, and k are unit vectors forming a base in the cartesian x, y, z coordinate system. Both ϕ and $\eta = \phi/\gamma$ are used in the following as the circumferential coordinate, with $\gamma = r/R$. The Lamé parameters A_1 and A_2, and the principal radii of curvatures R_1 and R_2 are given by

$$A_1 = r;\ A_2 = r\zeta;\ R_1 = r;\ R_2 = r\zeta/(\gamma\cos\theta) \qquad (1.2)$$
$$\zeta = 1 + \gamma\cos\theta$$

The loading on the shell is considered to be restricted to normal pressure. Such a loading leads to displacements u, v, and w in the meridional, circumferential, and normal directions respectively. Stresses induced are represented by in-plane stress resultants N_θ, N_η, $N_{\theta\eta}$, moment resultants M_θ, M_η, $M_{\theta\eta}$, and transverse shear force resultants Q_θ, Q_η. The convention for displacement components and stress resultants is given in Fig 1.2.

Toroidal shells of complete and incomplete geometric form have found engineering application. In the present study two of these geometries are considered. The first consists of toroidal panels, which are defined as being incomplete toroidal shells bounded by two circumferential and two meridional arcs. This geometry has application to complete toroidal shells constructed of panels, such as the TOKAMAK

breeder reactor vessel (Fig. 1.3). The problem considered for this geometry is that of vibration. The second geometry deals with a complete toroidal shell. The intended application is to a marine bouyancy unit consisting of a complete toroidal shell (Fig. 1.4), which supports through a series of columns an overhead platform. A stability problem is considered with respect to this geometry.

Various methods are available for shell vibration and stability analysis. The theoretical method using Fourier series expansions has long been popular due to its efficiency. The finite element method (FEM) has become popular in recent decades due to its generality. A new method, the differential quadrature method (DQM), is rapidly gaining popularity due to its ability to combine efficiency with generality. In this thesis the theoretical method is used as the main tool of study, while the FEM and DQM are used as means of validation. The fundamental principles of each of these three methods will now be presented.

1.2 Theoretical method

The basic concepts of thin-shell theory have been presented in a number of standard references such as those by Novozhilov (1959), Soedel (1992), and Yamaki (1984). The various shell theories that are in use at present all stem from the equations of Love developed towards the end of the 19th century. This theory was developed for linear elastic behaviour of isotropic shells such as those considered in the present study.

Among the many shell theories in current use is that of Mushtari, Donnell and

Vlasov (MVD). This theory has found perhaps the widest application in vibration and buckling analysis. The theory considers both bending and membrane effects, applies to shells that are loaded normally to their surface, and concentrates on transverse deflection behavior.

A number of assumptions are made in the MVD theory which modify it relative to the original Love theory. The first basic assumption is that the contributions of in-plane deflections can be neglected in the bending strain expressions but not in the membrane ones. The next assumption is that the influence of inertia in the in-plane direction is negligible. The theory is then restricted to normal loading. Finally, the shear terms in the Love equations are neglected in the two tangential force equilibrium equations. The remaining moment equilibrium equations remain unchanged.

In some problems of thin shells, the bending and twisting moments, as well as the transverse shearing forces, are so small that they may be neglected. Consequently, the stresses in the shell are mainly due to the membrane forces and the shell is said to be in a membrane state. In such a theory of thin shells, i. e. in the membrane theory, the following assumptions are made about the stress and moment resultants $M_\theta = M_\eta = M_{\theta\eta} = Q_\theta = Q_\eta = 0$. In the present study the MVD theory is used as the main tool in the theoretical method and it is used to develop the solution for the problems of the vibration of a toroidal panel and the instability of the platform shell. The shell membrane theory is used solely to set up the static solution for the prebuckling effects in the platform shell problem.

1.3 Finite element method

The finite element method (FEM) is a numerical procedure which has been used extensively for shell analysis (Mackerle (1993), Yang (1990)). Standard references on this method include those of Bathe (1996) and Zienkiewicz and Taylor (1989). The method combines several mathematical concepts to produce a system of linear or nonlinear equations and has two characteristics that distinguish it from other numerical procedures:

1. The method utilizes an integral formulation to generate a system of algebraic equations.
2. The method uses continuous piecewise smooth functions for approximating the unknown quantity or quantities.

In this method a mathematical model is generated by subdividing the actual structure into a finite number of small regions called elements. Within an element displacements and stresses are approximated using polynomial shape functions. An element is connected to adjacent elements at a finite number of points called nodes. Interaction among elements is solely through the forces they exert at the nodes. Element material properties and geometry are used to generate the stiffness of the entire structure, discretized at the nodes. Known loads acting on the structure are represented as forces, also at the nodes. The solution requires using these known loads and stiffnesses to solve for unknown displacements. The displacements are then used to find element results such as force per unit length, stress, strain, etc.

A major advantage of the FEM is its versatility and universality of application. Unlike the theoretical method, the FEM method can readily be applied to problems

of irregular geometry, arbitrary boundary conditions, and materials of arbitrary properties. A disadvantage of the method is its relatively high cost. Hence there is still room in shell analysis for specialized solutions which can be economically used to carry out parametric studies.

A number of commercial computer codes based on the theory of finite elements are currently on the market. One of these, NE/Nastran (1996) was adopted to carry out the FEM analysis of the present study. This code features a four-node flat plate element that can be used in static, vibration and linear buckling analysis of toroidal shells. Results obtained from this code are presented in chapters 3 and 4, and serve to validate results from the theoretical method, as well as to provide supplementary data.

1.4 Differential quadrature method

The differential quadrature method (DQM) was introduced to problems of shell analysis by Bert and Malik (1995). The method has already been applied to several shell vibration and buckling problems. The fundamental principles of the method have been presented in a review paper by Bert and Malik (1996).

The basis of the DQM is the representation of the derivatives of a function f(x) by a weighted sum of the function values at sampling points in the domain. The weighting coefficients can be determined for some appropriately chosen set of test or trial functions. Once the test functions are selected the derivative can be considered known. The number of trial functions N is arbitrarily chosen but must be equal to

at least one plus the order of the highest order derivative. N will also correspond to the number of sampling points in the domain.

The weighting coefficients are functions of the sampling points only. Explicit formulas can be used to find these coefficients. For example, formulas for polynomial test functions are given by Shu and Richards (1992). The weighting coefficients for higher order derivatives may be obtained through recurrence relationships.

Each sampling point is used to either represent the DQM analogue of a governing equation for the domain, or to satisfy a boundary condition. For shells there are four boundary conditions at each end, while there are only three governing equations. It is therefore necessary to enforce one of the boundary equations at an interior point. This point, a 'δ point', is taken a short distance ($\delta \cong 10^{-5}$ on a unit domain) from the boundary.

The DQM in this study is used as a second means of validating results and providing supplementary data. For the first case involving the vibration of toroidal panels the 1D or semi- analytical DQM is used. For the second case involving the buckling of a toroidal platform shell the 2D or fully numerical DQM is used. In both cases there is a full development of relevant theory. For the vibration case results are also obtained to compare with the results from the theoretical solution and FEM.

1.5 Scope of the current study

In Chapter 1 the toroidal shell is introduced and the three methods of analysis used in the study are outlined. Chapter 2 contains a literature survey that gives a

description of previous work on vibration and buckling of shells with emphasis on toroidal shells. Chapters 3 gives new detailed solutions for the vibration of toroidal panels including results from the theoretical, FEM and DQM analyses. Chapter 4 gives the development of new theory for the stability of complete toroidal platform shells using the theoretical and DQM approaches, as well as results from the FEM. Finally Chapter 5 contains conclusions about the technical significance of the calculated results and solution methods, as well as suggestions for further research.

Chapter 2

Literature Survey

2.1 Introduction

Shell structures have been studied extensively for over a hundred years since Love formulated his now famous equations (Noor (1990)). The Love equations are eighth-order partial differential equations, that were difficult to solve prior to the computer era, but may now be handled with comparative ease. There are a large number of potential shell geometries, but the study of shell structures is devoted largely to cylindrical, spherical, conical, and toroidal shapes. While the early work on shells dealt mainly with the static, i.e. the equilibrium problem, later work has concentrated on the main concerns related to the thin nature of shells, namely vibration and buckling.

The standard references on shell vibration analysis include those of Leissa (1973) and Soedel (1992). In his research monograph Leissa (1973) compares results from most of the popular shell theories including those of Love and Timoshenko, Byrne and Flügge, Vlasov, Reissner, Berry and Naghdi, Sanders, Donnell, and Flügge. The book gives an overall view of the development and difference of these thin shell theories.

As well detailed results are presented of applications principally for cylindrical and spherical shells.

In his popular text Soedel (1992) begins the development of the governing shell equations from Love theory, since it can be shown that all the other linear thin shell theories represent relatively minor extensions to it. The Love equations are applied to different shell structures and are extended to include the influence of large initial stress fields, transverse shear strain, shear deflection, shear deformation, etc. Hamilton's principle is used for derivations throughout the book. Approximate solution techniques such as the Galerkin technique, and the Rayleigh-Ritz method are discussed. As well extensive results are given.

Among the standard references on shell buckling are the works of Yamaki (1984) and Samuelson and Eggwertz (1992). In the research text by Yamaki (1984) the coverage is exclusively of cylindrical shells. The form and predictions of several of the principal shell theories are treated in considerable detail. Extensive results are given not only for simple uniform loading cases, but also for more difficult and practical loadings.

The engineering handbook by Samuelson and Eggwertz (1992) covers shell forms of practical interest in industrial applications. Numerous buckling formulas derived over the years are summarized, and examples of applications are given.

2.2 Vibration of cylindrical panels

There is an ample literature on the vibration of shell panels, mainly of the

cylindrical form (Redekop and Azar (1991)). In 1968 Tsui studied the natural vibration of moderately thick cylindrical panels using equations derived from the three-dimensional theory of elasticity. Petyt (1971) compared the results from four different methods on the vibration of rectangular thin cylindrical panels. Leissa and Kadi (1971) studied the effect of curvature on shallow shell vibrations. Kanazawa and Hangai (1975) presented results on linear and non-linear vibrations of panels of constant curvature. The effects of boundary conditions were studied by a number of researchers. Sewall (1967) did some early theoretical and experimental work on clamped and simply supported conditions. Leissa, Lee and Wang (1981) considered the vibration of cantilever cylindrical panels.

Among more recent work is that of Shen and Wan (1987) who used B-spline functions to analyze panels of single and double curvature. Mizusawa (1988) used the spline strip method to analyze the vibration of simply supported cylindrical panels. Lim and Liew (1994) developed a solution for rectangular panels using a pb-2 Ritz formulation. Finally Selmane and Lakis (1997) have studied anisotropic cylindrical panels using the FEM.

Few studies have dealt with the vibration of toroidal panels. In 1994 Redekop investigated the dynamic response of a toroidal shell panel to blast loading. The governing equations were in terms of the transverse displacement of the shell and a stress function. A series solution was obtained corresponding to a loading which was uniformly distributed and contained the Friedlander time decay function. Time integration of the equation was performed directly, using the Newmark method.

2.3 Vibration of toroidal shells

The books by Leissa (1973) and Soedel (1992) make only limited references to toroidal shells. Significant studies of the vibration of toroidal shells have been conducted only recently.

In 1973 Balderes and Armenakas investigated the free vibrations of ring-stiffened toroidal shells, using the Love-Reissner shell theory. A set of linear homogeneous algebraic equations were solved by a fast converging iteration technique. The results obtained indicate that the frequencies increase with increasing t/r, and decreasing r/R. When stiffening rings are added to the toroidal shells, the authors observed that the frequencies either remain the same or increase substantially.

The Ritz method was used to calculate the lowest natural vibration frequencies of a thin toroidal shell by Bulygin (1975). He asserted that there is an instability in the computational process when using the finite-difference scheme, and that poor convergence is obtained when using the trigonometric series approach. Thus the asymptotic method based on the assumption of small shell thickness is adopted in the paper.

In 1975 Gavelya and Kononenko conducted a study on the characteristic oscillations and waves of a toroidal shell. An algorithm based on the use of special matrices belonging to the type of the Green matrices is realized in their work.

In 1985-6, Kosawada et al analysed the free vibrations of thin and thick toroidal shells of circular cross section. The equations of motion and the boundary conditions

are derived from the stationary conditions of the Lagrangian of the toroidal shell. These equations are solved exactly by a power series expansion. The results are confirmed by comparing with those by other approximate methods. The authors observe that prior to their work 'no analytical solutions have been published' for the problem of toroidal shell vibrations.

In 1994 and 1995 Leung and Kwok studied the free vibration of toroidal shells. They used the MVD thin shell theory. Fourier series and Galerkin's method were used. The behavior of the vibration of cylindrical shell, as a special case of toroidal shell, is discussed. Also, a 90 degree curved pipe bend is studied numerically. Results obtained by their method are compared to results obtained by finite element and other methods.

In 1994 Redekop studied the natural frequencies for a short curved pipe with shear diaphragm supports. The shell theory used was developed in toroidal coordinates, based on the Mushtari-Vlasov-Donnell assumptions. To validate the theory the end exponential decay coefficients were calculated and compared with those from another theory. The theory for the determination of the natural frequencies of vibration in symmetric and anti-symmetric modes was presented. For a slightly curved pipe the results agreed well with results for straight pipes.

In 1997 Huang, Redekop and Xu used the linear elastic Sanders shell theory to solve the problem of the free vibration of a curved pipe with rigid diaphragm end supports. A numerical solution based on the finite element method was also given. The FEM results agreed well with those of the Sanders theory.

2.4 Buckling of shells

Recent reviews by Teng (1996), and Grigorenko and Gulyaev (1991) indicate that the shell buckling problem remains a major concern in structural engineering. Numerous other specialized review articles on thin shell buckling have also been written. Among these are ones focusing on the effect of various boundary conditions, elastic postbuckling and imperfection sensitivity, dynamic buckling, and plastic buckling. Because of the thinness of shell structures, buckling is often the controlling failure mode in industrial applications. It is therefore essential that buckling behavior be properly understood so that suitable design methods can be established.

Despite extensive research over many decades, our knowledge of many shell buckling problems is still very limited. Consequently, shell stability design criteria contained in design codes for various structures such as tanks, pressure vessels and offshore platforms generally cover only the basic geometries of cylinders, cones, and spheres, and simple loading conditions such as uniform axial compression, uniform normal pressure, uniform torsion and bending, or a combination of them. This limitation also applies to the general code for steel shell buckling.

This lack of knowledge has been due to two main difficulties encountered in shell buckling research in the previous decades. First, the buckling phenomenon in shells is a highly complex one, described by nonlinear partial differential equations too difficult to solve except for a few simple cases before the computer era. Second, buckling of shells is generally sensitive to small geometric imperfections induced in the fabrication process. Theoretical buckling loads obtained assuming a perfect geometry

often greatly overestimate the actual strength of a shell. Indeed, it was pointed out that there was a great need for more experimental data in the area of shell buckling.

The availability of powerful computers and development of sophisticated finite element and other numerical techniques in recent years have changed the situation drastically. It is no longer impossible to solve numerically a specific complicated nonlinear buckling problem. Great strides can now be made in understanding the buckling behavior of shells for a much wider range of problems.

A study on cylindrical shell buckling of particular significance to the present work is that due to Tooth and Fernandez (1979). These researchers studied the buckling behaviour of horizontally supported thin walled cylindrical liquid storage tanks. The Donnell's linear stability equations were adopted contaning as unknowns the membrane stress function and the radial deflection. Expressing the deflected buckled form as a double series in two unknowns, and applying the Galerkin method, a prediction for the buckling load was developed.

2.5 Stability of toroidal shells

The literature contains many studies dealing with stability studies of toroidal shells. Early works include those of Stein and McElman (1965), Hutchinson (1967), Bushnell (1967).

Sobel and Flügge (1967) investigated the elastic stability of general axisymmetric shells subjected to arbitrary loads, and applied the governing equations to the particular case of a toroidal shell loaded by uniform external pressure. The critical

buckling mode is asymmetric with respect to the generator axis, and either symmetric or nonsymmetric with respect to the midplane of the toroid. Their test results compared well with the theoretical predictions. However, the toroids tested by them had geometries defined by the ratios R/r=8 and r/t=70 to 80. The authors note that the predictions may not be as satisfactory for smaller values of R/r such as 3, which is in the range of the present study.

In 1971 Nordell and Crawford studied experimentally seven epoxy toroidal shell models which were subjected to hydrostatic pressure. The results were compared with those from analytical solutions. The toroidal shells had a mean radius about the axis of revolution of 6 in., a mean tube radius of 2 in., and a mean shell thickness of 0.086 in. The static elastic strain response of the epoxy models was in satisfactory agreement with that computed using a finite element analysis. Critical buckling pressures for the models were within 5 percent of the analytical prediction.

In 1971 Kosheleva and Myachenkov investigated the stability of toroidal shells with localized loadings using the finite difference method. The governing equation adopted were from the Mushtari thin shell theory. The authors studied toroidal shells loaded by an annular force distributed uniformly over the major circumference of the torus. They found that if subcritical distortion is not taken into account, a large value is obtained for the critical load, and with the increase of the R/r this difference increases rapidly. For a semitorus, loaded along the major diameter by a uniformly distributed edge torque, the same trend was obtained.

In 1981 Bushnell studied straight and curved pipe models subjected to external

or internal pressure, simulated by thermal loading. The model included geometric and material nonlinearity in the prebuckling analysis and bifurcation buckling from the nonlinear prebuckled state. The author compared the theoretical results with previous work and test results, and observed that the degree of ovalization of the straight pipe cross section under bending is very much affected by the external pressure. In the case of bending of curved pipes, the straight legs act to prevent ovalization near the ends of the curved portion.

In 1985 Panagiotopoulos presented a finite element formulation for the stress and stability analysis of toroidal pressure vessels under hydrostatic pressure. The follower force effect of the external pressure and the contributions of prebuckling bending moments were considered in the stability equations. The linear bifurcation buckling loads and corresponding mode shapes obtained agreed well with experimental results.

In 1991 Anwen and Wei derived stability equations for toroidal shells under hydrostatic pressure from Sanders' non-linear equations of equilibrium and kinematic relations of the middle surface for general shells. The asymptotic method was used to solve the stability equations. The authors obtained good agreement between the theoretically predicted buckling pressures and existing experimental results. The influence of prebuckling deflection on the critical load was investigated in their study.

In 1992 Bielski discussed the influence of geometrical imperfections in the meridional shape and thickness of elastic toroidal shells on buckling pressure and post-buckling behavior. It was concluded that the imperfections in wall thickness distribution exert only a minor influence on the critical (bifurcation) pressure value. However,

they may cause a change in the post-critical behavior from stable to unstable. Much greater sensitivity of a shell to an ovalization imperfection was observed.

In 1995 Galletly and Blachut investigated the stability of complete circular and non-circular toroidal shells. The various numerical buckling pressures in the literature are compared with recent results obtained by the authors using the BOSOR 5 program. The accuracy of the latter was checked by comparing the numerical values with those of two other programs. Experimental results obtained on complete plastic toroidal shells in the United States and metallic ones in Russia are given. These are compared with numerical predictions of the buckling pressures.

In 1996 Galletly and Galletly compared results of various theoretical methods for predicting the elastic buckling pressures of externally pressurized complete circular toroidal shells. The accuracy of the latter was checked using two independent programs. The experimental results on toroidal shells are summarized and their buckling pressures calculated using the BOSOR5 computer program which is based on the finite difference method. A simple equation for predicting the buckling pressures of these shells is also briefly reviewed. The buckling of externally pressurized complete elliptical toroidal shells is then discussed. Depending on the major/manor axis ratio, the buckling pressures of the elliptical toroids can be larger or smaller than those of the corresponding circular toroids. Buckling due to internal pressure is considered in the third part of the paper. It is predicted to occur for several complete toroids of elliptical cross-section. It is believed that this is a new result. It still has to be verified experimentally.

In 1997 Redekop considered the elastic instability of a thin curved pipe under three-point bending. The loading was idealized as a set of pads of uniform pressure applied radially on discrete regions of the pipe surface. The governing equation was developed from the Donnell-type linearized stability equation.

2.6 Summary

In summary there is a rather limited literature on vibration and buckling of toroidal shells. It is observed that only a few researchers have used the methods adopted in the current study. Some numerical results are available for vibration and buckling which can serve to validate results from the current study.

Chapter 3

Vibration of Toroidal Panels

3.1 Introduction

In the present chapter the free vibration of panels of toroidal shells is investigated. Such panels have application for example to breeder reactor vessels such as the TOKAMAK (Fig. 1.3). A new theoretical solution is developed as well as one based on the DQM. Results for the natural frequencies of vibration are found using these solutions. The results are validated by comparisons with results from a previously published paper and FEM results. Mode shapes corresponding to the frequencies are also given. These were obtained solely using the FEM. Aside from the papers by Redekop and Xu (1997 and 1998) the problem outlined here has apparently not been considered previously in the literature.

3.1.1 Shell geometry

Toroidal panels are assumed taken from a toroidal shell surface (Fig. 1.1). A half-ring spanning through 180^o in the meridional direction is considered taken from the upper half of a toroidal shell. The panels are then obtained by dividing the half ring into two, four, or eight parts, with meridional arcs $2\theta_o$ of 90^o, 45^o and 22.5^o

respectively (Fig. 3.1). The circumferential arc of the ring ψ is selected to give a nearly-square geometric shape for the panel. The ψ is chosen so that the angular arcs of the panel are related by

$$\psi = 2\theta_o \frac{r}{R} \tag{3.1}$$

Thus a panel adjacent to the crown ($\theta = 90°$) is nearly square in shape.

Each of the toroidal panels is assumed to be separately supported. Vibration characteristics are to be determined for each of these. It is clear that the panels at the extrados have positive Gaussian curvatures, while the panels at the intrados have negative Gaussian curvatures, which will lead to differences in the natural frequencies.

A development for the theoretical solution is first presented. This is followed by outlines of the FEM and DQM solutions. Finally results are given from the three methods and conclusions are drawn.

3.2 Theoretical method

The theoretical solution is developed based on the Mushtari-Vlasov-Donnell (MVD) assumptions. For thin-walled isotropic shells with only normal loading the governing equations may be expressed in terms of the normal displacement component w, and the Airy stress function Ψ in the form

$$D \nabla^4 w - \hat{D}\Psi = p \tag{3.2}$$

$$(Eh)^{-1} \nabla^4 \Psi + \hat{D} w = 0$$

where $D = Eh^3/[12(1-\nu^2)]$, E is the Young's modulus, and ν is Poisson's ratio. Function $p = p(\theta, \eta)$ represents the equivalent normal load, which is used to account

for inertial effects in the normal direction through the D'Alembert principle. Inertial effects in the meridional and circumferential directions are taken as zero, as are rotary inertia effects. The operator ∇^4 and $\hat{D}$ are given by

$$\begin{aligned} \nabla^4 &= \nabla^2 \nabla^2 \\ \nabla^2 &= \frac{1}{r^2}\left(\frac{\partial^2}{\partial\theta^2} - \frac{\gamma}{\zeta}\sin\theta\frac{\partial}{\partial\theta} + \frac{1}{\zeta^2}\frac{\partial^2}{\partial\eta^2}\right) \\ \hat{D} &= \frac{1}{r^3\zeta}\left(\gamma\cos\theta\frac{\partial^2}{\partial\theta^2} - \gamma\sin\theta\frac{\partial}{\partial\theta} + \frac{1}{\zeta}\frac{\partial^2}{\partial\eta^2}\right) \end{aligned} \tag{3.3}$$

where $\zeta = 1 + \gamma\cos\theta$. A solution is set up in this study for a small value of the parameter γ. Thus the expansions for ζ^{-1} and ζ^{-2} are truncated to

$$\begin{aligned} \zeta^{-1} &= 1 + 0.5\gamma^2 - \gamma\cos\theta + 0.5\gamma^2\cos 2\theta \\ \zeta^{-2} &= 1 + 1.5\gamma^2 - 2\gamma\cos\theta + 1.5\gamma^2\cos 2\theta \end{aligned} \tag{3.4}$$

For $\gamma \leq 0.2$ the maximum error in these series is about 4.4%.

To determine the natural frequencies for the panel, series expansions are written for the normal displacement component, Airy stress function, and equivalent normal load as

$$\begin{aligned} w &= \Sigma\Sigma w_{mn}\sin\kappa_n\theta\sin\mu_m\eta\sin\omega t \\ \Psi &= \Sigma\Sigma\Psi_{mn}\sin\kappa_n\theta sin\mu_m\eta\sin\omega t \\ p &= \Sigma\Sigma(-\rho h\ddot{w}_{mn})\sin\kappa_n\theta\sin\mu_m\eta\sin\omega t \end{aligned} \tag{3.5}$$

where $\kappa_n = (2n-1)\pi/2\theta_o$, $\mu_m = (2m-1)\pi/\psi$, $m = 1, 2, \ldots, M$, $n = 1, 2, \ldots, N$, ω is the natural circular frequency (rad/sec), and t is the time. Solely modes which are symmetrical with respect to the panel center lines are represented in these ex-

pansions. Antisymmetrical modes are readily obtainable by modifying the selection of trigonometric terms and κ_n, μ_m parameters.

Diaphragm type supports which are rigid in their own planes are considered to be applied on the boundaries of the panel. Thus the following boundary conditions are satisfied

$$N_\eta = u = w = M_\eta = 0 \ (\phi = 0°, \psi) \tag{3.6}$$
$$N_\theta = v = w = M_\theta = 0 \ (\theta = \theta_L, \theta_H)$$

where θ_L and θ_H are the angles defining the meridional edges of the panel. The convention for displacement components and resultants is given in Fig. 1.2.

Next the expansions (3.5) are substituted into eqns (3.2) and the Galerkin method is used to enforce the governing equations in the domain. For a given m one obtains a homogeneous equation set which involves $2N$ linear equations in terms of the $2N$ unknown coefficients w_{mn}, Ψ_{mn}, and the frequency ω. The equations appear in pairs and have the form

$$\Sigma[(\frac{D}{r^4}\bar{S}_{mnl} + \beta T_{inl})w_{mn} - (\frac{1}{r^3}\hat{S}_{mnl})\Psi_{mn}] = 0 \tag{3.7}$$
$$\Sigma[(\frac{1}{r^3}\hat{S}_{mnl})w_{mn} + (\frac{1}{Ehr^4}\bar{S}_{mnl})\Psi_{mn}] = 0$$

where $\beta = 2\rho h\omega^2$, ℓ is the Galerkin index, and the summation in the equations is over n. In these equations the MVD conditions that $\kappa_n \gg 1$, and that $\mu_m \gg 1$ have been employed. The constants $\bar{S}_{mnl}$, $\hat{S}_{mnl}$, and T_{inl} are evaluated from

$$\begin{aligned} \bar{S}_{mnl} &= \Sigma F_{in} T_{inl};\ \hat{S}_{mnl} = \Sigma G_{in} T_{inl} \\ T_{inl} &= \frac{1}{\kappa_n - \kappa_l - 3 + i}[\sin(\kappa_n - \kappa_l - 3 + i)\theta_H \end{aligned} \tag{3.8}$$

$$
\begin{aligned}
&- \sin(\kappa_n - \kappa_l - 3 + i)\theta_L] \\
+ \quad &\frac{1}{\kappa_n - \kappa_l - 3 + i}[\sin(\kappa_n + \kappa_l - 3 + i)\theta_H \\
&- \sin(\kappa_n + \kappa_l - 3 + i)\theta_L]
\end{aligned}
$$

The summations in eqns (3.8) extend over $i = 1, 2, \ldots, 5$. The functions F_{in} and G_{in} are given by Redekop (1997).

For a non-trivial solution the determinant of the equation set 3.7 must be zero, i. e.

$$| B | = 0 \tag{3.9}$$

where B represents the matrix of the coefficients. Eqn. (3.9) is a non-linear algebraic equation in the frequency parameter β. The roots of this equation may be found using standard routines for eigenvalue problems.

The theory presented in the preceding was incorporated in the computer code Ommhqr.for. A listing of this program is given on p. 62. Results from this code are discussed in section 3.5.

3.3 Finite element method

The commercial program NE/Nastran (1996) was used to determine both the natural frequencies and mode shapes of the panels. A flat thin-shell four-noded element with six degrees of freedom per node is available for vibration analysis (Fig. 3.2). The program FEMAP was used for pre and post-processing of the data. All FEM work was done on a PC.

Using FEMAP models were developed for three types of divisions of the semi-meridional arc, namely division into two, four and eight parts. Results for each of the three division are given for two panels, one adjacent to the extrados, and the other adjacent to the intrados. For the divisions into four and eight parts results are also given for a panel at the crown of the shell.

The boundary conditions considered in the FEM solution correspond to diaphragm supports on the circumferential edges (ϕ = cnst). This requires the fixing of four degrees of freedom on the boundary nodes. On the meridional edges (θ = cnst.) boundary conditions were considered as clamped, diaphragm support, or free. In the first of these conditions all degrees of freedom on the boundary nodes are fixed, while in the last no degrees of freedom are fixed.

3.4 Differential quadrature method

To provide a second means of validating the theoretical solution a solution based on the DQM was developed. This new method of shell analysis is more flexible in dealing with boundary conditions than the theoretical method, and more computationally efficient than the FEM.

Shear diaphragm support conditions are assumed on the circumferential edges of the panels. Diaphragm, clamped and free support conditions are assumed on the meridional edges. Numerical results are computed using the DQM and these results are compared with results obtained using the theoretical and FEM approaches.

3.4.1 MVD shell theory

To facilitate satisfying the boundary conditions using this numerical method the MVD shell theory is developed in its displacement form (Redekop and Zhang (1992)). The governing equations for free vibrations may then be expressed in terms of the three displacement components u, v, and w (Fig. 1.2) as

$$
\begin{aligned}
&[\zeta^2\frac{\partial^2}{\partial\theta^2}+\nu_1\frac{\partial^2}{\partial\eta^2}-\gamma\zeta sin\theta\frac{\partial}{\partial\theta}-\nu\gamma\zeta cos\theta-\gamma^2sin^2\theta]u+\lambda u\zeta^2 \\
&+[\nu_2\zeta\frac{\partial^2}{\partial\theta\partial\eta}+\nu_3\gamma sin\theta\frac{\partial}{\partial\eta}]v+[(\zeta^2+\nu\gamma\zeta cos\theta)\frac{\partial}{\partial\theta}-\gamma\sin\theta]w=0 \\
&[\nu_2\zeta\frac{\partial^2}{\partial\theta\partial\eta}-\nu_3\gamma sin\theta\frac{\partial}{\partial\eta}]u \\
&+[\nu_1\zeta^2\frac{\partial^2}{\partial\theta^2}+\frac{\partial^2}{\partial\eta^2}-\nu_1\gamma\zeta sin\theta\frac{\partial}{\partial\theta}+\nu_1\gamma\zeta cos\theta-\nu_1\gamma^2sin^2\theta]v+\lambda v\zeta^2 \\
&+[(\gamma cos\theta+\nu\zeta)\frac{\partial}{\partial\eta}]w=0 \\
&-[(\zeta^4+\nu\gamma\zeta^3cos\theta)\frac{\partial}{\partial\theta}-\nu\gamma\zeta^3sin\theta-\gamma^2\zeta^2sin\theta cos\theta]u \\
&-[\gamma\zeta^2cos\theta+\nu\zeta^3)\frac{\partial}{\partial\eta}]v \\
&-[\zeta^4(\hat{k}\,\nabla^4+1)+2\nu\gamma\zeta^3cos\theta+\gamma^2\zeta^2cos^2\theta]w+\lambda w\zeta^4=0
\end{aligned}
\tag{3.10}
$$

where

$$
\begin{aligned}
&\lambda=(1-\nu^2)\rho r^2\omega^2/E;\ \hat{k}=(hr)^2/12; \\
&\nu_1=(1-\nu)/2;\ \nu_2=(1+\nu)/2;\ \nu_3=(3-\nu)/2 \\
&\nabla^4(\ldots)=\nabla^2\,\nabla^2\,(\ldots) \\
&\nabla^2(\ldots)=\frac{1}{r^2\zeta}[\zeta\frac{\partial^2}{\partial\theta^2}-\gamma\sin\theta\frac{\partial}{\partial\theta}+\frac{1}{\zeta}\frac{\partial^2}{\partial\eta^2}](\ldots)
\end{aligned}
\tag{3.11}
$$

As before E = Young's modulus, ν = Poisson ratio, ρ = unit mass, ω = natural circular frequency of vibration in rad/sec. Rotary inertia effects are again assumed

negligible. The objective is to determine the natural frequency parameter λ, and thus the natural frequencies, ω. It is noted that functions of the position variable θ are present, and thus the governing equations are ones with variable coefficients.

The strain-displacement and curvature-displacement relations in the MVD theory (Redekop and Zhang (1992)), expressed in toroidal coordinates, are

$$\begin{aligned}
\epsilon_\theta &= \frac{1}{r}(\frac{\partial u}{\partial \theta} + w) \\
\epsilon_\eta &= \frac{1}{r\zeta}(-\gamma sin\theta u + \frac{\partial v}{\partial \eta} + \gamma cos\theta w) \\
\epsilon_{\theta\eta} &= \frac{1}{2r\zeta}(\frac{\partial u}{\partial \eta} + \gamma sin\theta v) + \frac{1}{2r}\frac{\partial v}{\partial \theta} \\
\kappa_\theta &= \frac{1}{r^2}(\frac{\partial u}{\partial \theta} - \frac{\partial^2 w}{\partial \theta^2}) \\
\kappa_\eta &= -\frac{sin\theta}{rR\zeta}(u - \frac{\partial w}{\partial \theta}) + \frac{cos\theta}{rR\zeta^2}\frac{\partial v}{\partial \eta} - \frac{1}{(r\zeta)^2}\frac{\partial^2 w}{\partial \eta^2} \\
\kappa_{\theta\eta} &= \frac{1}{r^2\zeta}\frac{\partial u}{\partial \eta} + \frac{cos\theta}{rR\zeta}\frac{\partial v}{\partial \theta} + \frac{1}{R^2\zeta^2}cos\theta sin\theta v - \frac{1}{r^2\zeta}\frac{\partial^2 w}{\partial \theta \partial \eta} - \frac{\sin\theta}{rR\zeta^2}\frac{\partial w}{\partial \eta}
\end{aligned} \tag{3.12}$$

where $\epsilon_\theta, \kappa_\theta$ = mid-surface meridional strain, curvature; $\epsilon_\eta, \kappa_\eta$ = mid-surface circumferential strain, curvature; and $\epsilon_{\theta\eta}, \kappa_{\theta\eta}$ = mid-surface shear strain, curvature. The subscripts θ and η in eqns. (3.12) again indicate the panel meridional and circumferential directions respectively.

The membrane and bending stress resultants are expressed in terms of the mid-surface strain and curvature functions as

$$\begin{aligned}
N_\theta &= K(\epsilon_\theta + \nu\epsilon_\eta);\ M_\theta = D(\kappa_\theta + \nu\kappa_\eta) \\
N_\eta &= K(\epsilon_\eta + \nu\epsilon_\theta);\ M_\eta = D(\kappa_\eta + \nu\kappa_\theta) \\
N_{\theta\eta} &= K(1-\nu)\epsilon_{\theta\eta};\ M_{\theta\eta} = D(1-\nu)\kappa_{\theta\eta}
\end{aligned} \tag{3.13}$$

where $K = Eh/(1-\nu^2)$. The transverse shear stress resultants Q_θ, Q_η are available (Redekop and Zhang (1992)) from the displacement component w through

$$Q_\theta = -\frac{D}{r}\frac{\partial(\nabla^2 w)}{\partial\theta};\ Q_\eta = -\frac{D}{r\zeta}\frac{\partial(\nabla^2 w)}{\partial\eta} \tag{3.14}$$

The various displacement components and stress resultants are represented in their positive sense in Fig. 1.2.

Support at the boundaries of the panel on the circumferential edges is assumed to be by diaphragms which are rigid in their own planes. Thus the following boundary conditions are satisfied on the $\phi = 0^o, \psi$ edges

$$N_\eta = u = w = M_\eta = 0 \tag{3.15}$$

On the meridional edges of the panel three types of support conditions are considered, namely diaphragm, clamped, and free. Thus the conditions applied on the $\theta = \theta_L, \theta_H$ edges are

$$v = w = N_\theta = M_\theta = 0 \tag{3.16}$$

for the diaphragm supports,

$$u = v = w = (v \equiv -\frac{1}{r}\frac{\partial w}{\partial\theta} + \frac{u}{r}) = 0 \tag{3.17}$$

for the clamped supports, and

$$(T_{\theta\eta} \equiv N_{\theta\eta} + \frac{\gamma\cos\theta}{r\zeta}M_{\theta\eta}) = (V_\theta \equiv Q_\theta + \frac{1}{r\zeta}\frac{\partial M_{\theta\eta}}{\partial\eta}) = N_\theta = M_\theta = 0 \tag{3.18}$$

for the free supports. Here θ_L and θ_H are the angles defining the meridional edges of the panel, while v, $T_{\theta\eta}$, and V_θ are equivalent boundary values (Novozhilov (1959)).

To determine the natural frequencies for the panel, series expansions are written for the displacement components as

$$\begin{aligned} u &= \Sigma U_m(\theta) \sin \mu_m \eta e^{i\omega t} \\ v &= \Sigma V_m(\theta) \cos \mu_m \eta e^{i\omega t} \\ w &= \Sigma W_m(\theta) \sin \mu_m \eta e^{i\omega t} \end{aligned} \tag{3.19}$$

where $\mu_m = (2m-1)\pi\gamma/\psi^{rad}$, $m = 1, 2, \ldots, M$. U_m, V_m, W_m are unknown functions, dependent on θ only. The subscript m of these functions is omitted in the following. Solely modes which are symmetrical with respect to the panel center ($\eta = \eta_m$) are represented in these expansions. Antisymmetrical modes are readily obtained by modifying the selection of trigonometric terms. These expansions automatically satisfy the boundary conditions (3.15) on the circumferential edges.

3.4.2 One-dimensional DQM

The DQM approach is used to determine the unknown functions U_m, V_m, W_m. The semi-analytical or one-dimensional version is required for the current problem as the unknown functions are dependent on the θ variable only. A brief overview of the method is presented in the following for completeness.

The basis of the DQM is the representation of the derivatives of a function f(x) by a weighted sum of the function values in the domain, i. e.

$$\left.\frac{d^r f}{dx^r}\right|_{x=x_i} = \sum_{j=1}^{N} A_{ij}^{(r)} f(x_j) \tag{3.20}$$

Here the $A_{ij}^{(r)}$ are the unknown weighting coefficients of the r-th order derivative at the i-th sampling point in the domain. The weighting coefficients can be determined

for some appropriately chosen function (test function), which in the current case is taken as a polynomial. Once the test function is selected the r-th derivative can be considered known, given through (3.20). The integer N is arbitrarily chosen but must be equal to at least one plus the order of the highest order derivative. N corresponds to the number of sampling points in the domain.

Once the distribution of the sampling points is made the $A_{ij}^{(r)}$ can be found. For the case of polynomial test functions they may be found by solving the following N simultaneous linear equations

$$\sum_{j=1}^{N} x_j^{k-1} A_{ij}^{(r)} = \frac{d^r(x^{k-1})}{dx^r}\bigg|_{x=x_i};\ i,k = 1,2,\ldots,N \tag{3.21}$$

Alternatively, for greater accuracy, explicit formulas for the weighting coefficients given by Shu and Richards (1992) may be used. The explicit formulae for the weighting coefficients of the first order derivative are

$$A_{ij}^{(1)} = \frac{\pi(x_i)}{(x_i - x_j)\pi(x_j)};\ i,j = 1,2,\ldots,N;\ i \neq j \tag{3.22}$$

where

$$\pi(x_i) = \prod_{j=1}^{N}(x_i - x_j);\ i \neq j \tag{3.23}$$

The weighting coefficients for higher order derivatives may be obtained through the following recurrence relationship

$$A_{ij}^{(r)} = r[A_{ii}^{(r-1)} A_{ij}^{(1)} - \frac{A_{ij}^{(r-1)}}{x_i - x_j}]$$
$$i,j = 1,2,\ldots,N;\ i \neq j;\ 2 \leq r \leq (N-1) \tag{3.24}$$

and when i = j

$$A_{ij}^{(r)} = A_{ii}^{(r)} = -\sum_{k=1}^{N} A_{ik}^{(r)};\ i = 1,2,\ldots,N;\ i \neq k;\ 1 \leq r \leq (N-1) \tag{3.25}$$

From the equations (3.20-3.25) it is clear that the weighting coefficients are functions of the sampling points only.

In this study a choice is made for a set of unequally spaced sampling points that proved successful in previous shell problems. Each sampling point is used to either represent the DQM analogue of a governing equation for the domain, or to satisfy a boundary condition. For shells there are four boundary conditions at each end, while there are only three governing equations. It is necessary to enforce one of the boundary equations at an interior point. This point, a 'δ point', is taken a short distance ($\delta \cong 10^{-5}$ on a unit domain) from the boundary point.

As the variation of the displacements is assumed trigonometric in the η direction (eqn. 3.19), a semi-analytical approach is effectively being taken. Mathematically there is only one variable, that of θ. The sampling points are then taken only in the meridional direction. In light of the previous discussion the sampling points on a unit domain are taken as

$$\begin{aligned} &x(1) = 0;\ x(2) = 0.00001;\ x(N-1) = 0.99999;\ x(N) = 1 \\ &x(i) = \frac{1 - \cos\frac{\pi(i-2)}{N-3}}{2};\ 2 < i < (N-1) \end{aligned} \tag{3.26}$$

The meridional coordinates θ of the sampling points on the panel are then found from the relation $\theta(i) = \theta_L + [\theta_H - \theta_L]x(i)$.

Substitution of the expansions (3.19) into the governing equations (3.10), and use of the quadrature rules (3.20-3.25) for the θ derivatives, leads to the DQM domain

equations for the ith sampling point

$$[\sum A_{il}^{(2)} - \gamma\zeta^{-1}\sin\theta \sum A_{il}^{(1)}]U_l - \zeta^{-2}(\nu_1\mu_m^2 + \nu\gamma\zeta\cos\theta + \gamma^2\sin^2\theta)U_i$$
$$-\nu_2\zeta^{-1}\mu_m \sum A_{il}^{(1)}V_\mu - \zeta^{-2}\nu_3\gamma\sin\theta\mu_m V_j \qquad (3.27)$$
$$+(1 + \nu\gamma\zeta^{-1}\cos\theta)\sum A_{il}^{(1)}W_\upsilon - \zeta^{-2}\gamma(\zeta - \gamma\cos\theta)\sin\theta W_k = -\lambda U_i$$

$$\nu_2\zeta^{-1}\mu_m \sum A_{il}^{(1)}U_l - \zeta^{-2}\nu_3\gamma\mu_m\sin\theta U_i \qquad (3.28)$$
$$+[\nu_1 \sum A_{il}^{(2)} - \nu_1\gamma\zeta^{-1}\sin\theta\sum A_{il}^{(1)}]V_\mu - \zeta^{-2}(\mu_m^2 - \nu_1\gamma\zeta\cos\theta + \nu_1\gamma^2\sin^2\theta)V_j$$
$$+\mu_m\zeta^{-2}(\gamma\cos\theta + \nu\zeta)W_k = -\lambda V_j$$

$$-(1 + \nu\gamma\zeta^{-1}\cos\theta)\sum A_{il}^{(1)}U_l + \gamma\zeta^{-2}\sin\theta(\nu\zeta + \gamma\cos\theta)U_i$$
$$+\mu_m\zeta^{-2}(\gamma\cos\theta + \nu\zeta)V_j - (1 + 2\nu\gamma\zeta^{-1}\cos\theta + \gamma^2\zeta^{-2}\cos^2\theta)W_k$$
$$-\frac{1}{12}(\frac{t}{r})^2\zeta^{-4}\{\zeta^4\sum A_{il}^{(4)}W_\upsilon - 2\gamma\zeta^3\sin\theta\sum A_{il}^{(3)}W_\upsilon$$
$$-[\frac{\gamma^2\zeta^2}{2}(1 - \cos 2\theta) + 2\gamma\zeta^3\cos\theta + 2\mu_m^2\zeta^2]\sum A_{il}^{(2)}W_\upsilon \qquad (3.29)$$
$$-[\frac{\gamma^3\zeta}{2}(1 - \cos 2\theta) + 2\gamma^2\zeta^2\cos\theta - \gamma\zeta^3 + 2\gamma\mu_m^2\zeta]\sin\theta\sum A_{il}^{(1)}W_\upsilon$$
$$+[\mu_m^4 - \mu_m^2(2\gamma^2(1 - \cos 2\theta) + 2\gamma\zeta\cos\theta)]W_k\} = -\lambda W_k$$

where the indices i, j, k, and corresponding dummy indices l, μ, and υ are used for the displacement components U, V, and W (Bert and Malik (1995)). The function ζ is understood to be evaluated at $\theta(i)$. The range of indices is given by

$$i, l = 1, 2, \ldots, N;\ j = i + N;\ k = j + N$$
$$\mu = l + N;\ \upsilon = \mu + N \qquad (3.30)$$

Using the quadrature rules the displacement support conditions $u = 0$, $v = 0$, $w = 0$, $v = 0$ on the θ = cnst. edges can respectively be cast into

$$U_i = 0;\ V_j = 0;\ W_k = 0;\ -\sum A_{il}^{(1)}W_\upsilon + U_i = 0 \qquad (3.31)$$

where the functions are taken at the appropriate edge. The force support conditions $N_\theta = 0$, $M_\theta = 0$, $T_\theta = 0$, $V_\theta = 0$ can respectively be cast into

$$\begin{aligned}
&\sum A_{il}^{(1)} U_l - \nu\gamma\zeta^{-1}\sin\theta U_i - \nu\mu_m\zeta^{-1}V_j + (1+\nu\gamma\cos\theta)W_k = 0 \\
&\sum A_{il}^{(1)} U_l - \nu\gamma\zeta^{-1}\sin\theta U_i - \nu\mu_m\gamma\zeta^{-2}\cos\theta V_j - \sum A_{il}^{(2)} W_v \\
&+\nu\gamma\zeta^{-1}\sin\theta\sum A_{il}^{(1)} W_v + \nu\mu_m^2\zeta^{-2}W_k = 0 \\
&\mu_m(Gtr^2\zeta^{-1} + D'\gamma\zeta^{-2}\cos\theta)U_i + (Gtr^2 + D'\gamma^2\zeta^{-2}\cos^2\theta)\sum A_{il}^{(1)} V_\mu \\
&+Gt\gamma r^2\zeta^{-1}\sin\theta V_j - \mu_m D'\gamma\zeta^{-2}\cos\theta\sum A_{il}^{(1)} W_v - \mu_m D'\gamma\zeta^{-3}\sin\theta\cos\theta W_k = 0 \\
&-\mu_m^2 D'\zeta^{-2}U_i - \mu_m D'\gamma\zeta^{-2}\cos\theta\sum A_{il}^{(1)} V_\mu - D\sum A_{il}^{(3)} W_v \\
&+D\gamma\zeta^{-1}\sin\theta\sum A_{il}^{(2)} W_v + \mu_m^2\zeta^{-2}(D+D')\sum A_{il}^{(1)} W_v \\
&+\mu_m^2\zeta^{-3}(2\gamma D + D')\sin\theta W_k = 0
\end{aligned} \tag{3.32}$$

where $D' = Eh^3/[12(1+\nu)]$.

The assembly of the domain and boundary equations yields a set of simultaneous linear equations of the form

$$\begin{bmatrix} S_{bb} & S_{bd} \\ S_{db} & S_{dd} \end{bmatrix} \begin{Bmatrix} (\Delta_b) \\ (\Delta_d) \end{Bmatrix} = \begin{Bmatrix} (0) \\ \lambda(\Delta_d) \end{Bmatrix} \tag{3.33}$$

The sub-matrices S_{bb} and S_{bd} stem from the boundary conditions, and are of size 8×8, and $8 \times (3N-8)$ respectively. Sub-matrices S_{db} and S_{dd} stem from the governing equations, and are of size $(3N-8)\times 8$, and $(3N-8)\times(3N-8)$ respectively. The vector (Δ_b) contains the displacements corresponding to the boundary points and is eliminated to produce a standard eigenvalue problem. Using the static condensation technique the matrix equation (3.33) is reduced into the form

$$[-S_{db}S_{bb}^{-1}S_{bd} + S_{dd}]\{\Delta_d\} = \lambda\{\Delta_d\} \tag{3.34}$$

from which the eigenvalue parameters λ and the corresponding mode shapes $\{\Delta_d\}$ can be determined.

The preceding theory was coded in a Matlab computer program labelled *Tordqm.m*. A listing of this program is given on p. 79. Results based on this code are presented in the following section.

3.5 Numerical results

Numerical results are presented for the following values of the problem parameters

$$\rho = 7770kg/m^3;\ \nu = 0.3;\ E = 207,000MPa$$
$$R = 3.2m;\ r = 0.56m;\ h = 0.0056m \tag{3.35}$$

Solutions are given for three types of division of the semi-meridional arc, namely division into two, four and eight parts. Results for the three types of division are generally given for three panels, one adjacent to the extrados, one adjacent to the crown (extrados side), and the other adjacent to the intrados. A total of eight panel cases, as described in Table 3.1, are studied in detail.

Numerical results from the three methods for the eight cases are given in Tables 3.2-3.7. The values represented in each case are the circular frequencies, ω in rad/sec. The frequencies f in cycles/sec may be obtained from these values through the relation $f = \omega/(2\pi)$.

The convergence of the theoretical (FS) and the DQM solutions is indicated in

Table 3.2. Symbol 'm' represents the number of terms in the 'θ' function of the theoretical solution, while 'N' represents the number of sampling points in the meridional direction of the DQM solution. Rapid convergence is indicated for both methods indicating high efficiencies. For further work on the theoretical and DQM solutions values of $m = 21$ and $N = 20$ were taken. The final column of the table gives previously published results by Leissa and Kadi (1971) which were found using an approximate theory assuming constant radii of curvatures. There is good agreement of the current results with the published ones.

The influence on the frequencies of the δ value used in enforcing the boundary conditions 3.16-3.18 is indicated in Table 3.3. Fundamental frequencies are given for the diaphragm and free boundary conditions, for δ values of 10^{-3}, 10^{-5}, 10^{-6}, 10^{-7}, and 10^{-9}. It is seen that the results for the diaphragm conditions are very stable with regard to changes in δ. The results for the clamped conditions closely resembled those of the diaphragm ones and are thus not shown. The results for the free boundary conditions are seen to be sensitive to changes in δ for values smaller than 10^{-5}. Based on the results of this table the value of δ was taken as 10^{-5} for all subsequent work of this study.

A study of convergence of the FEM results for panels corresponding to cases 1 and 2 is given in Table 3.4. Sample meshes are given in Figs. 3.3-3.4. A mesh of 40 $\times$ 40 was considered to represent a converged solution, and was used in subsequent work.

In Table 3.5 are given the results for the fundamental frequencies for the eight

cases indicated in Table 3.1. These values stem from the theoretical, FEM and DQM approaches and are given generally for three types of boundary supports on the meridional edges. The theoretical solution values are available only for the diaphragm supports, as a lengthy new theoretical development is required for each set of boundary conditions with this method. Diaphragm supports are invariably assumed on the circumferential ($\eta = cnst$) edges. Values marked by * indicate the lowest frequencies corresponding to symmetrical η modes as predicted by the FS method. Best agreement for the three methods is obtained for the diaphragm support condition. For clamped supports there is good agreement throughout between the FEM and DQM results. For free supports there are some important differences, due partly to the fact that free supports are defined somewhat differently in the two methods, and partly due to the variability of the DQM results with the δ value. The use of the DQM approach with free boundary conditions requires further study.

For diaphragm supports on the meridional edges in the case of two and four-part meridional divisions the fundamental frequencies decrease going from an extrados location to an intrados location. This is as expected since there is a change from positive to negative Gaussian curvature. As expected the frequencies are highest for the clamped supports, and lowest for the free supports. There is an increase in the fundamental frequencies in going from a two-part division to an eight-part division.

Results indicating the effect of panel thickness are given in Table 3.6. The calculations are for the case of diaphragm supports on the meridional edges. As expected the fundamental frequencies increase as the panel thickness increases. There

is good agreement in the results from the three methods over the entire range of thicknesses studied.

In Figs. 3.5-3.12 are presented the first four mode shapes for the eight panel cases of Table 3.1. Corresponding frequencies are available in Table 3.7. These results were all found using the FEM and apply to diaphragm support conditions. Passing from a division into two parts (Figs. 3.5-3.6) into a division into eight parts (Figs. 3.10-3.12) there is an increasing tendency toward plate-like behavior, i. e. the first mode can be approximated by a half sine wave in each direction and higher modes by higher order sine waves. Comparison of modes with cylindrical panel modes given by Lim and Liew (1994) indicates a similarity in shape for the panels at the crown.

In Figs 3.13-3.20 are shown the effects on the fundamental modes of changing the boundary conditions on the meridional edges. The panels with clamped supports have more complex mode shapes compared with those with free supports. The panels with diaphragm supports have modes in between those of the other two supports.

3.6 Conclusions

A theoretical solution for the natural frequencies of toroidal panels based on the MVD shell theory has been developed, as well as a solution based on the one-dimensional DQM approach. Numerical results are obtained using the theoretical and DQM solutions and are compared with published results as well as with FEM results. Close agreement is observed in the various sets of results.

Chapter 4

Stability of Toroidal Shells

4.1 Introduction

In this chapter a shell instability problem is considered which has application to a proposed offshore platform. The design, building and installation of offshore structures is currently one of the active concerns of structural engineering (Vugts, 1997). The basic structure consists of a partially submerged toroidal shell which is subjected to a set of concentrated loads acting downward at the crown of the shell. The problem is solved for simplified geometry, loading, and boundary conditions. A new theoretical solution based on the linearized Donnell-type stability equations is developed. Numerical results for the problem are determined using the finite element method. A solution procedure using the differential quadrature method is also presented. Aside from the paper by Xu and Redekop (1998) the problem outlined here has apparently not been considered previously in the literature.

4.1.1 Shell geometry

The toroidal shell (Figs. 1.1, 4.1) has a bend radius R, a cross-sectional radius r, and a thickness h as discussed in section 1.1. The loading on the shell comprises of

four pads of intense uniform pressure stemming from columns situated on the crown at the circumferential positions $\phi = 45^o, 135^o$, 225^o, and 315^o. The reaction is an axisymmetric pressure acting normally inward on the shell. As an approximation this reactive pressure is assumed to act uniformly on the bottom half of the shell.

For a shell with four equally spaced vertical concentrated loads along the crown consideration can be restricted to one x-y quadrant, say the first one. Selection of functions in the circumferential directions must be such as to satisfy the following symmetry conditions on the bordering planes $\phi = 0^\circ$ and $\phi = \psi = \pi/2$

$$N_{\eta\theta} = v = w_{,\eta} = M_{\eta\theta} = 0 \tag{4.1}$$

For the DQM method appropriate boundary conditions must be satisfied on these planes of symmetry. Relevant equations are given by Budiansky (1968) which include products of prebuckling resultants and buckling deformations. As in the present case the loading is self-equilibrated the values of the prebuckling resultants on the boundaries, i. e. planes of symmetry are expected to be small. Thus these terms are neglected and the conditions to be satisfied on the planes $\phi = 0^o$ and $\phi = \pi/2$ are taken as

$$\begin{aligned} & v = 0;\ (\gamma \cos\theta)v - \frac{\partial w}{\partial \eta} = 0 \\ & N_{\eta\theta} + (\frac{3}{2r} - \frac{\gamma \cos\theta}{2r\zeta}) M_{\eta\theta} = 0;\ \frac{\partial M_\eta}{\partial \eta} + 2\frac{\partial(\zeta M_{\eta\theta})}{\partial \theta} = 0 \end{aligned} \tag{4.2}$$

where $\zeta = 1 + \gamma \cos\theta$.

4.1.2 Shell membrane theory

The 'concentrated' load stemming from the columns and distributed load stem-

ming from the reactive water pressure can each be represented in the first quadrant by a quartet of uniform load pads situated symmetrically with respect to the coordinate lines $\phi = \psi/2, \theta = 0$. The center of the reference pad of the quartet has coordinates $\phi = \psi/2 - b, \theta = \hat{\beta}$, while the extent of the pad is $2c, 2\alpha$ in the ϕ and θ directions respectively. The Fourier representation of each of the two loading effects is given by the superposition of symmetrical and antisymmetrical components defined by

$$p = \sum_{\bar{m}=0,2,\ldots}^{\bar{m}_h} \Big(\sum_{\bar{n}=0,1,\ldots}^{\bar{n}_h} p_{\bar{m}\bar{n}s} \cos \bar{n}\theta + \sum_{\bar{n}=1,2,\ldots}^{\bar{n}_h+1} p_{\bar{m}\bar{n}a} \sin \bar{n}\theta \Big) \cos \mu_{\bar{m}}\phi$$

$$p_{\bar{m}\bar{n}s} = \frac{64 p_o}{\pi^2 \mu_{\bar{m}} \bar{n}} \cos \bar{n}\hat{\beta} \sin \bar{n}\alpha \cos \mu_{\bar{m}}(\psi/2 + b) \sin \mu_{\bar{m}} c \tag{4.3}$$

$$p_{\bar{m}\bar{n}a} = \frac{64 q_o}{\pi^2 \mu_{\bar{m}} \bar{n}} \sin \bar{n}\hat{\beta} \sin \bar{n}\alpha \cos \mu_{\bar{m}}(\psi/2 + b) \sin \mu_{\bar{m}} c$$

where $\mu_{\bar{m}} = 4m$, and special cases are given by

$$p_{oos} = \frac{16 c\alpha p_o}{\pi^2};\ p_{\bar{m}os} = \frac{32 \alpha p_o}{\mu_{\bar{m}} \pi^2} \cos \mu_{\bar{m}}(\psi/2 + b) \sin \mu_{\bar{m}} c \tag{4.4}$$

$$p_{o\bar{n}s} = \frac{32 c p_o}{\bar{n}\pi^2} \cos \bar{n}\hat{\beta} \sin \bar{n}\alpha;\ p_{o\bar{n}a} = \frac{32 c q_o}{\bar{n}\pi^2} \sin n\hat{\beta} \sin n\alpha$$

The absolute value of the symmetrical and nonsymmetrical load intensities p_o, and q_o is equal to half the actual load intensity $\bar{p}$ of the effect considered.

The 'concentrated' loads due to column action are assumed to extend through one sixth of a complete meridian and one thirty-sixth of a complete circumference. Considering the equilibrium of forces in the vertical direction the intensity of the pressure at the crown then must be twenty times that of the reactive pressure. The parameters in eqns (4.3-4.4) for the two loadings of this study thus are given by

$$\hat{\beta}_1 = \pi/2;\ \alpha_1 = \pi/6;\ b_1 = c_1 = \pi/80;\ \bar{p}_1 = 20.0 \tag{4.5}$$

$$\hat{\beta}_2 = \alpha_2 = \pi/2;\ b_2 = c_2 = \pi/8;\ \bar{p}_2 = 1.0$$

where the subscript 1 indicates the load at the crown and the subscript 2 the load due to the reactive pressure.

A Fourier series approach based on the membrane theory for shells of revolution (Budiansky (1968)) is used to determine the prebuckling effect. This series is used both in the theoretical and DQM solution. In toroidal coordinates the governing equations of the membrane theory are given by

$$\begin{aligned}
&\zeta\frac{\partial N_\theta}{\partial\theta} - \gamma\sin\phi(N_\theta - N_\eta) + \frac{\partial N_{\theta\eta}}{\partial\eta} = 0\\
&\zeta\frac{\partial N_{\theta\eta}}{\partial\theta} - 2\gamma\sin\phi N_{\theta\eta} + \frac{\partial N_\eta}{\partial\eta} = 0\\
&\frac{N_\theta}{r} + \frac{\gamma\cos\phi}{r\zeta}N_\eta = \bar{p}
\end{aligned} \tag{4.6}$$

where $\bar{p}$ represents the normal pressure.

The prebuckling stress resultants $N_{\eta o}$, $N_{\theta o}$, $N_{\theta\eta o}$ due to the loading (4.3-4.5), are expanded in a Fourier series as

$$\begin{aligned}
N_{\eta o} &= \sum_{\bar{m}=0,2,\ldots}^{\bar{m}_h}\Big[\sum_{\bar{n}=0,1,\ldots}^{\bar{n}_h} A_{\bar{m}\bar{n}s}\cos\bar{n}\theta + \sum_{\bar{n}=1,2,\ldots}^{\bar{n}_h+1} A_{\bar{m}\bar{n}a}\sin\bar{n}\theta\Big]\cos\mu_{\bar{m}}\eta\\
N_{\theta o} &= \sum_{\bar{m}=0,2,\ldots}^{\bar{m}_h}\Big[\sum_{\bar{n}=0,1,\ldots}^{\bar{n}_h} B_{\bar{m}\bar{n}s}\cos\bar{n}\theta + \sum_{\bar{n}=1,2,\ldots}^{\bar{n}_h+1} B_{\bar{m}\bar{n}a}\sin\bar{n}\theta\Big]\cos\mu_{\bar{m}}\eta\\
N_{\theta\eta o} &= \sum_{\bar{m}=0,2,\ldots}^{\bar{m}_h}\Big[\sum_{\bar{n}=0,1,\ldots}^{\bar{n}_h} C_{\bar{m}\bar{n}s}\sin\bar{n}\theta + \sum_{\bar{n}=1,2,\ldots}^{\bar{n}_h+1} C_{\bar{m}\bar{n}a}\cos\bar{n}\theta\Big]\cos\mu_{\bar{m}}\eta
\end{aligned} \tag{4.7}$$

where $\mu_m = 4m\gamma = \mu_{\bar{m}}\gamma$ and $A_{\bar{m}\bar{n}s}$, $B_{\bar{m}\bar{n}s}$, $C_{\bar{m}\bar{n}s}$, $A_{\bar{m}\bar{n}a}$, $B_{\bar{m}\bar{n}a}$, $C_{\bar{m}\bar{n}a}$ are constants of integration. The expansions (4.7) satisfy the symmetry conditions on the planes $\phi = 0^o$ and $\phi = \psi$ (eqns. 4.1).

The expansions for the loads and stress resultants are substituted into the governing equations (4.6). These equations are then solved for the integration constants,

after which the membrane stress resultants are completely determined. The three resultants may then be evaluated at each of the sampling points defined in the DQM discretization for the determination of the buckling effect.

4.2 Theoretical method

The theoretical solution is developed based on the Donnell-type linearized stability equations (Kosheleva and Myachenkov (1971), Tooth and Fernandez (1979)). These have the form

$$\begin{aligned} D\,\nabla^4 w_1 &- \hat{D}\Psi_1 - \lambda\{r^{-2}[N_{\theta o} w_{1,\theta\theta} + N_{\eta o}\bar{D}w_1] \\ &+ r^{-4}[w_{o,\theta\theta}\bar{D}\Psi_1 - \gamma\zeta^{-1}\sin\theta w_{o,\theta}\Psi_{1,\theta\theta}]\} = 0 \qquad (4.8) \\ (Eh)^{-1}\,\nabla^4\,\Psi_1 &+ \hat{D}w_1 + \lambda r^{-4}[w_{o,\theta\theta}\bar{D}w_1 - \gamma\zeta^{-1}\sin\theta w_{o,\theta} w_{1,\theta\theta}] = 0 \end{aligned}$$

where the operators are defined as

$$\begin{aligned} \nabla^4(\ldots) &= \nabla^2\,\nabla^2\,(\ldots) \\ \nabla^2(\ldots) &= r^{-2}[(\ldots)_{,\theta\theta} - \gamma\zeta^{-1}\sin\theta(\ldots)_{,\theta} + \zeta^{-2}(\ldots)_{,\eta\eta}] \qquad (4.9) \\ \bar{D}(\ldots) &= -\gamma\zeta^{-1}\sin\theta(\ldots)_{,\theta} + \zeta^{-2}(\ldots)_{,\eta\eta} \\ \hat{D}(\ldots) &= r^{-3}\zeta^{-1}[\gamma\cos\theta(\ldots)_{,\theta\theta} - \gamma\sin\theta(\ldots)_{,\theta} + \zeta^{-1}(\ldots)_{,\eta\eta}] \end{aligned}$$

and $D = Et^3/12(1-\nu^2)$, E is the Young's modulus, while ν is the Poisson ratio. w_1 and Ψ_1 are respectively the normal displacement and stress function in an assumed adjacent equilibrium state. w_o, $N_{\eta o}$, $N_{\theta o}$ are the displacement and stress resultants corresponding to a unit loading in the prebuckled state, and λ is a buckling load parameter. Following Mushtari and Galimov (1957) the membrane shear effect is neglected.

The initial bending stresses and displacement are not taken into consideration, and all approximations inherent in the Donnell shell theory are embedded in eqns (4.8-4.9). It has been reported by Yamaki (1984) that the Donnell stability solutions are practically accurate, at least for cylindrical shells, so long as the corresponding circumferential buckling wave number n exceeds 4.

A solution is set up for a small value of the bend curvature parameter γ. Thus the expansions for ζ^{-1} and ζ^{-2} are taken as

$$\zeta^{-1} = 1 + 0.5\gamma^2 - \gamma\cos\theta + 0.5\gamma^2\cos 2\theta \tag{4.10}$$

$$\zeta^{-2} = 1 + 1.5\gamma^2 - 2\gamma\cos\theta + 1.5\gamma^2\cos 2\theta$$

For $\gamma \leq 0.2$ the maximum error in these series is approximately 4.44%.

The stress resultants $N_{\eta o}$, $N_{\theta o}$, due to the loading (4.3-4.5), are taken from the shell membrane solution of section 4.1.2, while the prebuckling displacement w_o is taken as zero.

The solutions for w_1 and Ψ_1 are taken as

$$w_1 = \sum_{m=m_l,m_l+2,\ldots}^{m_h} \Big[\sum_{n=0,1,\ldots}^{n_h} w_{mns}\cos n\theta + \sum_{n=1,2,\ldots}^{n_h+1} w_{mna}\sin n\theta \Big] \cos\mu_m\eta \tag{4.11}$$

$$\Psi_1 = \sum_{m=m_l,m_l+2,\ldots}^{m_h} \Big[\sum_{n=0,1,\ldots}^{n_h} \Psi_{mns}\cos n\theta + \sum_{n=1,2,\ldots}^{n_h+1} \Psi_{mna}\sin n\theta \Big] \cos\mu_m\eta$$

where $\mu_m = 2m\pi\gamma/\psi$, and w_{mns}, Ψ_{mns} and w_{mna}, Ψ_{mna} are unknown constant coefficients. The expansions represent a preselected family of buckling modes. All modes represented have symmetry about the planes $\phi = 0^o, \psi$. the series parameters m_l, m_h, and n_h can be varied in the search for the mode corresponding to the lowest buckling

pressure. The first two of these parameters must necessarily be even. As a double series is involved selectivity must be exercised in the choice of the trial buckling modes to keep the numerical problem of a practical size.

Substitution of the expansions (4.7) and (4.11) into the governing equations (4.8), use of (4.9-4.10), and application of trigonometric identities leads to the requirements

$$
\begin{aligned}
\sum_{m=m_l,m_l+2,\ldots}^{m_h} \Big[\sum_{n=0,1,\ldots}^{n_h} \quad & \{[Dr^{-4}w_{mns}F_{mns}(\theta) - r^{-3}\Psi_{mns}G_{mns}(\theta)]\cos\mu_m\eta \\
& +\lambda[\frac{1}{4}r^{-2}w_{mns}\sum_{\bar{m}=0,2,\ldots}^{\bar{m}_h}(\sum_{\bar{n}=0,1,\ldots}^{\bar{n}_h}H_{mn\bar{m}\bar{n}s1}(\theta)+\sum_{n=1,2,\ldots}^{n_h+1}H_{mn\bar{m}\bar{n}s2}(\theta)) \\
& -\frac{1}{4}r^{-4}\Psi_{mns}\sum_{\bar{m}=0,2,\ldots}^{\bar{m}_h}(\sum_{\bar{n}=0,1,\ldots}^{\bar{n}_h}K_{mn\bar{m}\bar{n}s1}(\theta)+\sum_{n=1,2,\ldots}^{n_h+1}K_{mn\bar{m}\bar{n}s2}(\theta))]\times \\
& \times[\cos(\mu_m-\mu_{\bar{m}})\eta+\cos(\mu_m+\mu_{\bar{m}})\eta]\} \\
+\sum_{n=1,2,\ldots}^{n_h+1} \quad & \{[Dr^{-4}w_{mna}F_{mna}(\theta) - r^{-3}\Psi_{mna}G_{mna}(\theta)]\cos\mu_m\eta \\
& +\lambda[\frac{1}{4}r^{-2}w_{mna}\sum_{\bar{m}=0,2,\ldots}^{\bar{m}_h}(\sum_{\bar{n}=0,1,\ldots}^{\bar{n}_h}H_{mn\bar{m}\bar{n}a1}(\theta)+\sum_{n=1,2,\ldots}^{n_h+1}H_{mn\bar{m}\bar{n}a2}(\theta)) \\
& -\frac{1}{4}r^{-4}\Psi_{mna}\sum_{\bar{m}=0,2,\ldots}^{\bar{m}_h}(\sum_{\bar{n}=0,1,\ldots}^{\bar{n}_h}K_{mn\bar{m}\bar{n}a1}(\theta)+\sum_{n=1,2,\ldots}^{n_h+1}K_{mn\bar{m}\bar{n}a2}(\theta))]\times \\
& \times[\cos(\mu_m-\mu_{\bar{m}})\eta+\cos(\mu_m+\mu_{\bar{m}})\eta]\}] = 0 \qquad (4.12) \\
\sum_{m=m_l,m_l+2,\ldots}^{m_h} \Big[\sum_{n=0,1,\ldots}^{n_h} \quad & \{[r^{-3}w_{mns}G_{mns}(\theta) + (Ehr^4)^{-1}\Psi_{mns}F_{mns}(\theta)]\cos\mu_m\eta \\
& +\lambda[\frac{1}{4}r^{-4}w_{mns}\sum_{\bar{m}=0,2,\ldots}^{\bar{m}_h}(\sum_{\bar{n}=0,1,\ldots}^{\bar{n}_h}K_{mn\bar{m}\bar{n}s1}(\theta)+\sum_{n=1,2,\ldots}^{n_h+1}K_{mn\bar{m}\bar{n}s2}(\theta))]\times \\
& \times[\cos(\mu_m-\mu_{\bar{m}})\eta+\cos(\mu_m+\mu_{\bar{m}})\eta]\} \\
+\sum_{n=1,2,\ldots}^{n_h+1} \quad & \{[r^{-3}w_{mna}G_{mna}(\theta) + (Ehr^4)^{-1}\Psi_{mna}F_{mna}(\theta)]\cos\mu_m\eta \\
& +\lambda[\frac{1}{4}r^{-4}w_{mna}\sum_{\bar{m}=0,2,\ldots}^{\bar{m}_h}(\sum_{\bar{n}=0,1,\ldots}^{\bar{n}_h}K_{mn\bar{m}\bar{n}a1}(\theta)+\sum_{n=1,2,\ldots}^{n_h+1}K_{mn\bar{m}\bar{n}a2}(\theta))]\times
\end{aligned}
$$

$$\times[\cos(\mu_m - \mu_{\hat{m}})\eta + \cos(\mu_m + \mu_{\hat{m}})\eta]\}] = 0$$

The functions $F_{mns}(\theta)$, $G_{mns}(\theta)$, $H_{mn\hat{m}\hat{n}s1}(\theta)$, $K_{mn\hat{m}\hat{n}s1}(\theta)$, etc. are lengthy, but known. The equations (4.12) have the form

$$\begin{aligned}
\sum \; (\; & \sum[w_{mns}h_{1mn}(\theta,\eta) + \Psi_{mns}h_{2mn}(\theta,\eta)] \\
+ \; & \sum[w_{mna}h_{3mn}(\theta,\eta) + \Psi_{mna}h_{4mn}(\theta,\eta)]) = 0 \qquad (4.13) \\
\sum \; (\; & \sum[w_{mns}g_{1mn}(\theta,\eta) + \Psi_{mns}g_{2mn}(\theta,\eta)] \\
+ \; & \sum[w_{mna}g_{3mn}(\theta,\eta) + \Psi_{mna}g_{4mn}(\theta,\eta)]) = 0
\end{aligned}$$

Using the Galerkin approach these equations are multiplied by $\cos\hat{n}\theta\cos\mu_{\hat{m}}\eta$ and $\sin\hat{n}\theta\cos\mu_{\hat{m}}\eta$ and integrated over the shell surface, to obtain a set of linear equations in terms of the unknown constant coefficients. Here $\hat{n}$ and $\mu_{\hat{m}}$ cover the complete set of m, n combinations in the series for w_1, Ψ_1. The Galerkin approach leads to a linear matrix equation of the form

$$[A](\mathbf{a}) = \lambda[B](\mathbf{a}) \qquad (4.14)$$

where $\mathbf{a}$ represents the array of constant coefficients w_{mns}, Ψ_{mns}, w_{mna}, and Ψ_{mna}. This equation represents a general eigenvalue problem, which may be solved for the eigenvalues λ. A vector inverse iteration process outlined by Bathe (1996) can be used to determine the smallest eigenvalue, λ_{min}, which is the solution to the problem.

Based on the theory presented in the preceding a Matlab computer program labelled *formk.m* was developed. The listing of this program is available for future work.

4.3 Finite element method

The general structural FEM program NE/Nastran was used to determine the buckling loads and corresponding mode shapes for the toroidal shell. The flat four-noded eighteen degree-of-freedom shell element (Fig. 3.2) was employed for the linear buckling analysis.

One quarter of the shell was modelled, with symmetry assumed about the planes $\phi = 0^o, 90^o$. The program FEMAP was again used for pre and post-processing. A sample mesh with loading is given in Fig. 4.1. This model corresponds to a γ of 4. Additional models correspoding to γ values of 2 and 8 were also developed.

4.4 Differential quadrature method

In a recent study by Redekop, Xu and Zhang (1999) the DQM was applied to a stability problem involving a horizontal pipe elbow subjected to fluid loading. The theory developed for that study was adapted to cover the toroidal platform shell problem and is presented in the following.

The series solutions of section 4.1.2 based on shell membrane theory are used to give the prebuckling effect. Thus the difficulty that might arise from stringent mesh requirements for concentrated loadings in the DQM approach is circumvented. The buckling effects are found using the shell bending theory. As buckling modes are not necessarily axisymmetric the two-dimensional version of the DQM must be used.

4.4.1 Budiansky stability equations

To determine the buckling effects the Budiansky linearized first-order shell stability theory is employed (Budiansky (1968)). This theory is the stability counterpart to the Sanders linear shell bending theory (Sanders (1959)), which is considered one of the most accurate of the first order shell bending theories. The Budiansky theory is written here in the toroidal coordinate system. The governing equations, given in terms of the three displacement components u, v, and w, may be expressed as

$$
\begin{aligned}
&[\nu_1\frac{\partial^2}{\partial\theta^2}+\nu_2\frac{\partial^2}{\partial\eta^2}+\nu_3\frac{\partial}{\partial\theta}+\nu_4]u+[\nu_5\frac{\partial^2}{\partial\theta\partial\eta}+\nu_6\frac{\partial}{\partial\eta}]v\\
&+[\nu_7\frac{\partial^3}{\partial\theta^3}+\nu_8\frac{\partial^3}{\partial\theta\partial\eta^2}+\nu_9\frac{\partial^2}{\partial\theta^2}+\nu_{10}\frac{\partial^2}{\partial\eta^2}+\nu_{11}\frac{\partial}{\partial\theta}+\nu_{12}]w+\lambda E_1=0\\
&[\nu_{13}\frac{\partial^2}{\partial\theta\partial\eta}+\nu_{14}\frac{\partial}{\partial\eta}]u+[\nu_{15}\frac{\partial^2}{\partial\theta^2}+\nu_{16}\frac{\partial^2}{\partial\eta^2}+\nu_{17}\frac{\partial}{\partial\theta}+\nu_{18}]v\\
&+[\nu_{19}\frac{\partial^3}{\partial\eta^3}+\nu_{20}\frac{\partial^3}{\partial\theta^2\partial\eta}+\nu_{21}\frac{\partial^2}{\partial\theta\partial\eta}+\nu_{22}\frac{\partial}{\partial\eta}]w+\lambda E_2=0\\
&[\nu_{23}\frac{\partial^3}{\partial\theta^3}+\nu_{24}\frac{\partial^3}{\partial\theta\partial\eta^2}+\nu_{25}\frac{\partial^2}{\partial\eta^2}+\nu_{26}\frac{\partial^2}{\partial\theta^2}+\nu_{27}\frac{\partial}{\partial\theta}+\nu_{28}]u\\
&+[\nu_{29}\frac{\partial^3}{\partial\eta^3}+\nu_{30}\frac{\partial^3}{\partial\theta^2\partial\eta}+\nu_{31}\frac{\partial^2}{\partial\theta\partial\eta}+\nu_{32}\frac{\partial}{\partial\eta}]v\\
&+[\nu_{33}\frac{\partial^4}{\partial\theta^4}+\nu_{34}\frac{\partial^4}{\partial\eta^4}+\nu_{35}\frac{\partial^4}{\partial\theta^2\partial\eta^2}+\nu_{36}\frac{\partial^3}{\partial\theta^3}+\nu_{37}\frac{\partial^3}{\partial\theta\partial\eta^2}\\
&+\nu_{38}\frac{\partial^2}{\partial\eta^2}+\nu_{39}\frac{\partial^2}{\partial\theta^2}+\nu_{40}\frac{\partial}{\partial\theta}+\nu_{41}]w+\lambda E_3=0
\end{aligned}
\tag{4.15}
$$

where the ν_1 - ν_{41} are known functions of θ, given in full by Zhang and Redekop (1992). These functions depend also on the Poisson ratio ν, and the geometric parameters ζ, h, and γ. The buckling parameter λ and the quantities E_1, E_2, E_3 represent the Budiansky stability additions to the Sanders equations. The additional terms E_i are given in toroidal coordinates through

$$
\frac{12DE_1}{r^2h^2\zeta^3} = [\zeta n_{\theta o}\frac{\partial^2}{\partial\theta^2}+\zeta^{-1}n_{\eta o}\frac{\partial^2}{\partial\eta^2}-\gamma\sin\theta n_{\eta o}\frac{\partial}{\partial\theta}-(\gamma^2\zeta^{-1}\sin^2\theta n_{\eta o}+\zeta n_{\theta o})]u
$$

$$
\begin{aligned}
& +[2\gamma\zeta^{-1}\sin\theta n_{\eta o}\frac{\partial}{\partial\eta}]v+[2\zeta n_{\theta o}\frac{\partial}{\partial\theta}-\gamma\zeta^{-1}\sin\theta n_{\eta o}]w \\
\frac{DE_2}{r^2\zeta^3} &= [-2\gamma\zeta^{-1}\sin\theta n_{\eta o}\frac{\partial}{\partial\eta}]u+[\zeta n_{\theta o}\frac{\partial^2}{\partial\theta^2}+\zeta^{-1}n_{\eta o}\frac{\partial^2}{\partial\eta^2} \\
& -\gamma\sin\theta n_{\eta o}\frac{\partial}{\partial\theta}-\gamma^2\zeta^{-1}n_{\eta o}]v+[2\gamma\zeta^{-1}\cos\theta n_{\eta o}\frac{\partial}{\partial\eta}]w \qquad (4.16) \\
-\frac{DE_3}{r^2\zeta^3} &= [-2\zeta n_{\theta o}\frac{\partial}{\partial\theta}+\gamma\zeta^{-1}\sin\theta(1+2\gamma\cos\theta)n_{\eta o}]u+[-2\gamma\zeta^{-1}\cos\theta n_{\eta o}\frac{\partial}{\partial\eta}]v \\
& +[\zeta n_{\theta o}\frac{\partial^2}{\partial\theta^2}+\zeta^{-1}n_{\eta o}\frac{\partial^2}{\partial\eta^2}-\gamma\sin\theta n_{\eta o}\frac{\partial}{\partial\theta}-(\zeta n_{\theta o}+\gamma^2\zeta^{-1}\cos^2\theta n_{\eta o})]w
\end{aligned}
$$

where $n_{\theta o}$, $n_{\eta o}$ and $n_{\theta\eta o}$ are the membrane resultants of the pre-buckling state corresponding to a selected unit level of loading. The $n_{\theta\eta o}$ terms are often neglected in buckling analysis (Mushtari and Galimov (1957)) but they are included here in case the shearing action prior to buckling is significant.

4.4.2 Two-dimensional DQM

In the current study the two-dimensional DQM is required since the buckling mode need not be uniform in either the η or θ directions. The two-dimensional DQM has been used for a toroidal shell equilibrium problem by Zhang, Mirfakhraei, Xu and Redekop (1999), as well as for an ensuing stability study. A brief outline of the 2-D DQM is given in the following.

The basis of the DQM is still the representation in the domain of the derivatives of a function f(x) by a weighted sum of trial function values, i. e.

$$
\left.\frac{d^r f}{dx^r}\right|_{x=x_i}=\sum_{j=1}^{M}A_{ij}^{(r)}f(x_j) \qquad (4.17)
$$

Here the $A_{ij}^{(r)}$ are the unknown weighting coefficients of the r-th order derivative at the i-th sampling point in the x direction, and M is the number of sampling points

in this direction. For the current study sets of trial functions are required for both of the coordinate directions η and θ.

Polynomial trial functions are selected for the circumferential direction, and the variable x represents η. The functions are taken as

$$f(\eta) = 1, \eta, \eta^2, \ldots, \eta^{M-1} \tag{4.18}$$

For these functions explicit formulas for the weighting coefficients given by Shu and Richards (1992) may be used. For the first order derivative the formulas are

$$A_{ij}^{(1)} = \frac{\pi(\eta_i)}{(\eta_i - \eta_j)\pi(\eta_j)};\ i, j = 1, 2, \ldots, M;\ i \neq j \tag{4.19}$$
$$\pi(\eta_i) = \prod_{j=1}^{M} (\eta_i - \eta_j);\ i \neq j$$

while for the higher order derivatives the formulas are

$$A_{ij}^{(r)} = r[A_{ii}^{(r-1)} A_{ij}^{(1)} - \frac{A_{ij}^{(r-1)}}{\eta_i - \eta_j}];\ i, j = 1, 2, \ldots, M;\ i \neq j;\ 2 \leq r \leq (M-1)$$
$$A_{ij}^{(r)} = A_{ii}^{(r)} = -\sum_{k=1}^{M} A_{ik}^{(r)};\ i = 1, 2, \ldots, M;\ i \neq k;\ 1 \leq r \leq (M-1) \tag{4.20}$$

For the sampling points η_i in the circumferential direction the Chebyshev-Gauss-Lobatto spacing (Bert and Malik (1996)) is used. In this scheme the coordinates η_i are taken as $\eta_i \equiv x_i = \psi y_i$ where the y_i are given by

$$y_1 = 0;\ y_2 = 0.00001;\ y_{M-1} = 0.99999;\ y_M = 1 \tag{4.21}$$
$$y_i = \frac{1 - \cos\frac{\pi(i-2)}{M-3}}{2};\ 2 < i < (M-1)$$

At each sampling point either the DQM analogue of a governing equation for the domain is represented, or a boundary equation. For shells there are four conditions

at each boundary, while there are only three governing equations. It is necessary to enforce one of the boundary equations at an interior point. This point, a 'δ point', is taken a short distance ($\delta \cong 10^{-5}$ on a unit domain) from the boundary point. The boundaries of the current problem are located on circumferential edges of the shell, arising due to the use of symmetry conditions in the solution.

Harmonic trial functions (Malik and Bert (1994)) are used in the meridional direction in this problem having cyclic periodicity. Continuity conditions across $\theta = 360^0$ are then identically satisfied. The trial functions are thus taken as

$$f(\theta) = \cos[2(k-1)\pi\theta];\ k = 1, 2, 3, \ldots, N/2+1 \tag{4.22}$$
$$f(\theta) = \sin[2(k-N/2-1)\pi\theta];\ k = N/2+2, N/2+3, \ldots, N$$

where N is an even number. For equally spaced sampling points in the θ direction the weighting coefficients, labelled B_{ij} in the following, may be found explicitly from the inverse of the Vandermonde matrix (Malik and Bert (1994)).

Use of the quadrature rules (4.17-4.22) for the derivatives in the governing equation (4.15) leads to the transformed DQM domain equations

$$\begin{aligned}
&[\nu_1 \sum B_{ij}^{(2)} + \nu_3 \sum B_{ij}^{(1)}]U_{jh} + \nu_2 \sum A_{hl}^{(2)} U_{il} + \nu_4 U_{ih} + \nu_5 \sum\sum A_{hl}^{(1)} B_{ij}^{(1)} V_{jl} \\
&+\nu_6 \sum A_{hl}^{(1)} V_{il} + [\nu_7 \sum B_{ij}^{(3)} + \nu_9 \sum B_{ij}^{(2)} + \nu_{11} \sum B_{ij}^{(1)}]W_{jh} \\
&+\nu_8 \sum\sum A_{hl}^{(2)} B_{ij}^{(1)} W_{jl} + \nu_{10} \sum A_{hl}^{(2)} W_{il} + \nu_{12} W_{ih} + \lambda E_1 = 0 \\
&\nu_{13} \sum\sum A_{hl}^{(1)} B_{ij}^{(1)} U_{jl} + \nu_{14} \sum A_{hl}^{(1)} U_{il} + [\nu_{15} \sum B_{ij}^{(2)} + \nu_{17} \sum B_{ij}^{(1)}]V_{jh} \\
&+\nu_{16} \sum A_{hl}^{(2)} V_{il} + \nu_{18} V_{ih} + [\nu_{19} \sum A_{hl}^{(3)} + \nu_{22} \sum A_{hl}^{(1)}]W_{il} + [\nu_{20} \sum\sum A_{hl}^{(1)} B_{ij}^{(2)} \\
&+\nu_{21} \sum\sum A_{hl}^{(1)} B_{ij}^{(1)}]W_{jl} + \lambda E_2 = 0
\end{aligned} \tag{4.23}$$

$$[\nu_{23}\sum B_{ij}^{(3)} + \nu_{26}\sum B_{ij}^{(2)} + \nu_{27}\sum B_{ij}^{(1)}]U_{jh} + \nu_{24}\sum\sum A_{hl}^{(2)}B_{ij}^{(1)}U_{jl} + \nu_{25}\sum A_{hl}^{(2)}U_{il}$$
$$+\nu_{28}U_{ih} + [\nu_{29}\sum A_{hl}^{(3)} + \nu_{32}\sum A_{hl}^{(1)}]V_{il} + [\nu_{30}\sum\sum A_{hl}^{(1)}B_{ij}^{(2)}$$
$$+\nu_{31}\sum\sum A_{hl}^{(1)}B_{ij}^{(1)}]V_{jl} + [\nu_{33}\sum B_{ij}^{(4)} + \nu_{36}\sum B_{ij}^{(3)} + \nu_{40}\sum B_{ij}^{(1)}]W_{jh}$$
$$+[\nu_{34}\sum A_{hl}^{(4)} + \nu_{38}\sum A_{hl}^{(2)}]W_{il} + [\nu_{35}\sum\sum A_{hl}^{(2)}B_{ij}^{(2)} + \nu_{37}\sum\sum A_{hl}^{(2)}B_{ij}^{(1)}]W_{jl}$$
$$+\nu_{41}W_{ih} + \lambda E_3 = 0$$

The expressions involving the E_i of (4.16) and the symmetry conditions (4.2) may similarly be transformed.

The assembly of the domain and boundary equations yields a matrix equation of the form

$$\begin{bmatrix} S_{bb} & S_{bd} \\ S_{db} & S_{dd} \end{bmatrix} \begin{Bmatrix} (\Delta_b) \\ (\Delta_d) \end{Bmatrix} + \lambda \begin{bmatrix} 0 & 0 \\ S'_{db} & S'_{dd} \end{bmatrix} \begin{Bmatrix} (\Delta_b) \\ (\Delta_d) \end{Bmatrix} = \begin{Bmatrix} (0) \\ (0) \end{Bmatrix} \tag{4.24}$$

The sub-matrices S_{bb} and S_{bd} of the 'stiffness matrix' stem from the boundary conditions, and are of size $8N \times 8N$, and $8N \times (3MN - 8N)$ respectively. The sub-matrices S_{db} and S_{dd} of this matrix stem from the governing equations, and are of size $(3MN - 8N) \times 8N$, and $(3MN - 8N) \times (3MN - 8N)$ respectively. The sub-matrices S'_{db} and S'_{dd} of the 'stability matrix' stem from the E_i terms, and are of size $(3MN - 8N) \times 8N$, and $(3MN - 8N) \times (3MN - 8N)$ respectively. The vector Δ_b contains the displacements corresponding to the boundary points, and is eliminated using the static condensation technique. The matrix stability equation (4.24) is then reduced into the form

$$([-S_{db}S_{bb}^{-1}S_{bd} + S_{dd}] + \lambda[-S'_{db}S_{bb}^{-1}S_{bd} + S'_{dd}])\{\Delta_d\} = 0 \tag{4.25}$$

from which the eigenvalues λ and the mode shapes Δ_d are determined. The smallest

eigenvalue λ_{min} may be found directly using the inverse iteration method with shifting (Bathe (1996)).

A two-step procedure is used in the stability solution. In the first step, the pre-buckling analysis, series solutions for the membrane resultants $n_{\theta o}$, $n_{\eta o}$ and $n_{\theta \eta o}$ are found using the shell membrane theory. In the second step, the buckling analysis, the eigenvalue λ_{min} is found from the Budiansky equations (4.25) using the DQM. Based on this procedure a Matlab computer program labelled *plabuc.m* was developed. The listing of this program is available for future work.

4.5 Numerical Results

Sample numerical results are obtained for some shells discussed in the literature as well as for a toroidal platform shell with the following characteristics

$$E = 29 \times 10^6 psi\ (200MPa);\ \nu = 0.32 \qquad (4.26)$$

$$R = 400in\ (10.16m);\ r = 80in\ (2.032m)$$

All results given in this section were obtained using the FEM based on the NE/Nastran (1996) program.

Validation of the FEM results is made through comparison with the published results of Sobel and Flügge (1967) which are for a constant pressure loading. Table 4.1 lists results for the critical load λ obtained from the FEM and given by Sobel and Flügge. Two geometries corresponding to R/r values of four and two are represented. As there is close agreement in results the convergence characteristics and accuracy of the adopted FEM model are confirmed. Figure 4.2 gives the buckling modes for

the constant pressure loading cases. These modes compare well with those given by Sobel and Flügge.

Tables 4.2-4.4 give results for the critical load for the platform shell (Eqns. 4.5, 4.26). A total of eight platform shell cases are considered as described in Table 4.3. Table 4.2 shows the convergence of the FEM for this problem, while Table 4.3 gives the effect of the load area and of the shell thickness on the critical buckling load. It is seen that both factors have a major effect on the critical load. Finally Table 4.4 gives the first four buckling loads of the available platform shell cases.

In Figs. 4.3-4.10 are given the available mode shapes for the cases of Table 4.4. Generally there is a considerable variation of displacement in both the ϕ and θ directions corresponding to the local nature of the column loading. Buckling modes symmetrical about the plane $\phi = 45^o$ are mostly indicated, with substantial deformations taking place around the concentrated load areas.

4.6 Conclusions

A study on the instability of a partially submerged toroidal shell subject to concentrated loads at the crown has been conducted. A theoretical solution based on the linear Donnell stability equations is described. Numerical results obtained using the finite element method are presented, and these compare well with published results. Relevant theory for a solution based on the two-dimensional differential quadrature method is also presented.

Chapter 5

Conclusions

5.1 Panel Vibrations

Based on the current work on toroidal panel vibrations the following conclusions are drawn:

- results for frequencies from the three methods agree well with each other and with previously published results,
- relaxing of boundary conditions leads to lower frequencies,
- decrease of panel thickness leads to lower frequencies,
- corresponding to each natural frequency there is a unique mode shape,
- change of boundary conditions leads to large changes in mode shape,
- there is no clear trend in frequencies going from extrados to intrados.

5.2 Platform buckling

Based on the work on platform buckling the following conclusions are drawn:

- FEM results for buckling loads of complete toroidal shells under constant pressure agree well with previously published results,
- decrease of loaded area leads to lower buckling loads,
- decrease of shell thickness leads to sharply lower buckling loads,
- corresponding to each critical load there is a unique mode shape,
- analysis of one quadrant of the shell is justified as buckling, deformations are generally localized under the column load.

5.3 Methods of analyses

Three numerical methods are used in the study, a theoretical (Fourier series) method, the FEM, and the DQM. Generally the results obtained from the three methods agree well with each other, and with available results given in the literature.

Of the three methods, the theoretical method takes the least computer time, but requires the most time for theory and program development. Each new case of boundary conditions requires a new development of theory. The FEM takes the most computer time, but the least time for development. Formulating the FEM models using FEMAP is direct in the case of the simplified geometry and loading considered here. Conducting the vibration and stability analyses is straight-forward using the NE/Nastran program.

The DQM approach is the most recent of the three methods, and it must be considered still in the trial state. It has been demonstrated here that the DQM

approach provides an accurate, efficient means of solving vibration problems for shells, even in the case when the governing equations have variable coefficients. Work by others has demonstrated also the suitability of the DQM for shell buckling problems.

5.4 Suggestions for further research

Detailed results for vibration are given in the present study on panels taken from circular toroidal shells, and having meridional and circumferential dimensions approximately equal. Further work could be conducted on toroidal panels which are taken from shells that are not necessarily circular, and which don't necessarily have square planforms. An experimental study on toroidal panels could verify the theoretical models.

The present work has provided preliminary information about toroidal platform shell buckling, with numerical results found using the FEM. Further work could be done to obtain numerical results also from the theoretical and DQM solutions. Conducting of an experimental program on such shells would yield useful information about the accuracy of the various models.

References

Anwen, W. and Wei, Z., 1991, Asymptotic Solution for Buckling of Toroidal Shells, *Int. J. Pres. Ves. & Piping*, **45**, pp. 61-72.

Balderes, T. and Armenakas, 1973, Free Vibrations of Ring-Stiffened Toroidal Shells, *AIAA J.*, **11**, pp. 1637-1644.

Bathe, K. J., 1996, *Finite Element Procedures*, Prentice Hall, Englewood Cliffs, N. J.

Bert, C. W. and Malik, M., 1996, Differential Quadrature Method in Computational Mechanics; a Review, *ASME Appl. Mech. Rev.*, **49**, pp. 1-27.

Bert, C. W. and Malik, M., 1995, Free Vibration Analysis of Thin Cylindrical Shells by the Differential Quadrature Method, *ASME J. Press. Ves. Tech.*, **118**, pp. 1-12.

Bielski, J., 1992, Influence of Geometrical Imperfections on Buckling Pressure and Post-Buckling of Elastic Toroidal Shells, *Mech. Struct. & Mach.*, **20**, pp. 145-154.

Budiansky, B., 1968, Notes on Nonlinear Shell Theory, *ASME J. of Appl. Mech.*, **99**, pp. 393-401.

Bulygin, A. V., 1975, Calculation of Lowest Eigenfrequencies and Vibration Modes of Toroidal Shells, *Aeron. J.*, **18**, pp. 39-43.

Bushnell, D., 1981, Elastic-Plastic Bending and Buckling of Pipes and Elbows, *Comp. Struct.*, **13**, pp. 241-248.

Bushnell, D., 1967, Symmetric and Nonsymmetric Buckling of Finitely Deformed Eccentrically Stiffened Shells of Revolution, *AIAA J.*, **5**, pp. 1455-1462.

Galletly, G. D. and Galletly, D. A., 1996, Buckling of Complex Toroidal Shell Structures, *Thin-Walled Struct.*, **26**, pp. 195-212.

Galletly, G. D. and Blachut, J., 1995, Stability of Complete Circular and Non-Circular Toroidal Shells, *Proc. I. M. E., C*, **209**, pp. 245-255.

Gavelya, S. P. and Kononenko, N. I., 1975, Characteristic Oscillations and Waves on a

Toroidal Shell, *Sov. Appl. Mech.*, **11**, 31-35.

Grigorenko, Ya. M. and Gulyaev, V. I., 1991, Nonlinear Problems of Shell Theory and Their Solution Methods (Review), *Sov. Appl. Mech.*, **27**, pp. 929-946.

Huang, D. W., Redekop, D. and Xu, B., 1997, Natural Frequencies and Mode Shapes of Curved Pipes, *Comp. Struct.*, **63**, pp. 465-473.

Hutchinson, J. W., 1967, Initial Post-Buckling Behavior of Toroidal Shell Segments, *Int. J. Sol. Struct.*,, **3**, pp. 97-115.

Kanazawa K. and Hangai, Y., 1975, Nonlinear Flexural Vibrations of Thin Shallow Shells, *Theoretical and Applied Mechanics*, **25**, pp. 75-87.

Kosawada, T., Suzuki, D., and Takahashi, S., 1985, Free Vibrations of Toroidal Shells, *Bull. JSME*, **28**, pp. 2041-2047.

Kosawada, T., Suzuki, K., and Takahashi, S., 1986, Free Vibrations of Thick Toroidal Shells, *Bull. JSME*, **29**, pp. 3036-3042.

Kosheleva, T. I. and Myachenkov, V. I., 1971, Stability of Toroidal Shells with Localized Loadings, *Sov. App. Mech.*, **7,4**, pp. 370-373.

Leissa, A. W., 1973, *Vibration of Shells*, NASA, SP-288.

Leissa, A. W. and Kadi, A. S., 1971, Curvature Effects on Shallow Shell Vibrations, *J. Sound Vib.* **16**, pp. 173-187.

Leissa, A. W., Lee, J. K., and Wang, A. J., 1981, Vibrations of Cantilevered Shallow Cylindrical Shells of Rectangular Planform, *J. Sound Vib.*, **78**, pp. 311-328.

Leung, A. Y. T. and Kwok, N. T. C., 1995, Dynamic Stiffness Analysis of Toroidal Shells,, *Thin-Walled Struct.*, **21**, pp. 43-64.

Leung, A. Y. T. and Kwok, N. T. C., 1994, Free Vibration Analysis of a Toroidal Shell, *Thin-Walled Struct.*, **18**, pp. 317-332.

Lim, C. W. and Liew, K. M., 1994, A pb-2 Ritz Formulation for Flexural Vibration of Shallow Cylindrical Shells of Rectangular Planform, *J. Sound Vib.* **173(3)**, pp. 343-375.

Mackerle, J., 1993, Finite and Boundary Element Analyses of Shells- a Bibliography (1990-1992), *Fin. Elem. Analy. Des.*,**14**, pp. 73-84.

Malik, M. and Bert, C. W., 1994, Differential Quadrature Solutions for Steady-state Incompressible and Compresible Lubrication Problems, *ASME J. of Tribology*, **116**, pp. 296-302.

Mizusawa, T., 1988, Application of Spline Strip Method to Analyze Vibration of Open Cylindrical Shells, *Int. J. Num. Meth. Eng.*, **26**, pp 663-676.

Mushtari, D. M. and Galimov, K. Z., 1957, *Non-Linear Theory of Thin Elastic Shells*, Tatknigoizdat, Kazan, p. 103.

NE/Nastran, User's Manual, v. 2.3, Noran Engineering, Inc., Garden Grove, CA, 1996.

Noor, A. K., 1990, Bibliography on monographs and surveys on shells, *ASME Appl. Mech. Rev.*, **43**, pp. 223-234.

Nordell, W. J. and Crawford, J. E., 1971, Analysis of Behavior of Unstiffened Toroidal Shells, *IASS Pacific Symposium on Hydromechanically Loaded Shells*, Honolulu, pp. 304-314.

Novozhilov, V. V., 1959, *The Theory of Thin Shells*, P. Noordhoff, Groningen.

Panagiotopoulos, G. D., 1985, Stress and Stability Analysis of Toroidal Shells, *Int. J. Pres. Ves. & Piping*, **20**, pp. 87-100.

Petyt, M., 1971, Vibration of Curved Plates, *J. Sound Vib.*, **15**, pp. 381-395.

Redekop, D., Xu, B., and Zhang, Y. M., 1999, Stability of a Toroidal Fluid-Containing Shell, submitted for publication.

Redekop, D. and Xu, B., 1998, Natural Frequencies and Mode Shapes for Arbitrary Toroidal Panels, *Proc. CSME Forum 1998*, Ryerson, Toronto, **2**, pp. 109-113.

Redekop, D., 1997, Instability of a Curved Pipe under Three-Point Bending, *Int. J. Pres. Ves. & Piping*, **70**, pp. 91-96.

Redekop, D. and Xu, B., 1997, Natural Frequencies of a Toroidal Panel, *Proc. CANCAM 1997*, Laval, **1**, pp. 209-210.

Redekop, D., 1994, Dynamic Response of a Toroidal Shell Panel to Blast Loading, *Comp. Struct.*, **51** 235-239.

Redekop, D., 1994, Natural Frequencies of a Short Curved Pipe, *Trans. CSME*, **18** 35-45.

Redekop, D. and Zhang, F., 1992, Comparison of Elastic Solutions for Three-Point Bending of Curved Pipes, *Thin-Walled Structures*, **14**, pp. 223-239.

Redekop, D. and Azar, P., 1991, Dynamic Response of a Cylindrical Shell Panel to Explosive Loading, *ASME J. Vib. Acoust.*, **113**, pp. 273-278.

Samuelson, L. A. and Eggwertz, S., 1992, *Shell Stability Handbook*, Elsevier, London.

Sanders, J. L., 1959, An Improved First-Approximation Theory for Thin Shells, *NASA TR*, **R-24**, pp. 1-11.

Selmane, A. and Lakis, A. A., 1997, Dynamic Analysis of Anisotropic Open Cylindrical Shells, *Comput. Struct.*, **62**, pp 1-12.

Sewall, J. L., 1967, Vibration Analysis of Cylindrically Curved Panels with Simply Supported or Clamped Edges and Comparison with Some Experiments, *NASA TN*, **D-3791**, pp. 1-47.

Shen, P. C. and Wan, J. G., 1987, Vibration Analysis of Flat Shells by Using B Spline Functions, *Comput. Struct.*, **25**, pp 1-10.

Shu, C., & Richards, B. E., 1992, Application of Generalized Differential Quadrature to Solve Two-Dimensional Incompressible Navier-Stokes Equation, *Int. J. Numer. Meth. Fluids*, **15**, pp. 791-798.

Sobel, L. H. and Flügge, W., 1967, Stability of Toroidal Shells under Uniform External Pressure, *AIAA J*, **5**, pp. 425-431.

Soedel, W., 1992, *Vibration of Shells and Plates*, 2nd Ed., Marcell Dekker, New York.

Stein, M. and McElman, J. A., 1965, Buckling of Segments of Toroidal Shells, *AIAA J*, **3**, pp. 1704-1709.

Teng, J. G., 1996, Buckling of Thin Shells: Recent Advances and Trends, *ASME Appl.*

Mech. Rev., **49**, pp. 263-274.

Tooth, A. S. and Fernandez, J. A., 1979, A Study of the Buckling Behaviour of Horizontally Supported Thin-Walled Cylindrical Storage Vessels which Contain Fluid, in Richards, T. H. and Stanley, P. (Ed), *Proc. Stability Problems in Engineering Structures and Components*, Applied Science Publishers, London, pp. 315-340.

Tsui, E. Y. W., 1968, Natural Vibrations of Cylindrical Panels, *ASCE J. Eng. Mech.*, **94**, pp. 1425-1445.

Vugts, J. H. (ed.), 1997, BOSS '97 - The Behaviour of Offshore Structures, *Proc. 8th Int. Conf. of the Behaviour of Offshore Structures*, Elsevier, Delft.

Xu, B. and Redekop, D., 1998, Stability Analysis of a Partially Submerged Toroidal Shell with Concentated Loads, *Proceedings of Mechanics in Design Conference (MID '98)*, Nottingham, pp. 284-293.

Yamaki, N., 1984, *Elastic Stability of Circular Cylindrical Shells*, North-Holland, Amsterdam.

Yang, H. T. Y., 1990, Advances of Thin Shell Finite Elements and Some Applications, *Comput. Struct.*, **35**, pp 481-504.

Zhang, Y. M., Mirfakhraei, P., Xu, B., and Redekop, D., 1999, A Computer Program for the Elastostatics of a Toroidal Shell Using the Differential Quadrature Method, *Int. J. Press. Ves. & Piping*, in press.

Zhang, F. and Redekop, D., 1992, Surface Loading of a Thin-Walled Toroidal Shell, *Comput. Struct.*, **43**, pp. 1019-1028.

Zienkiewicz, O. C. and Taylor, R. L., 1989, *The Finite Element Method*, 4th Ed., McGraw Hill, New York.

Program Ommhqr.for

```
C********************  OMMHQR - FORTRAN ******************************
C     LAST MODIFICATION  -  DECEMBER 18, 1997
C     TO RUN ISSUE COMMAND - WATFOR77 OMMHQR
C     RESULTS IN  'OMMHQR.OUT'
C     NATURAL FREQUENCIES OF A TOROIDAL SHELL PANEL
C     MVD SHELL THEORY SOLUTION  - UP TO GAMA2 TERMS ONLY
C     READIN AND WRITEOUT ALL ANGLES IN DEGREES
      IMPLICIT DOUBLE PRECISION (A-H,O-Z)
      COMMON/FFF/TABA(10,21,4)
      COMMON/ZZZ/RS,RR,PSI,TOR,THIC,RO,POIS,EY,PL,PH,RL,RH,MHI,NHI,NDM
      OPEN(UNIT=8,FILE='OMMHQR.OUT')
      READ(5,5) NANALY
    5 FORMAT(I5)
C     LOOP OVER NUMBER OF ANALYSES TO BE CARRIED OUT
C     CAN VARY NDM, RARR, RATHIC, OR RS
      DO 100 KASE=1,NANALY
      WRITE(6,*) '  CALCULATIONS IN PROGRESS FOR KASE = ',KASE
      DO 10 M=1,MHI
      DO 11 N=1,NHI
      DO 12 J=1,4
   12 TABA(M,N,J)=.0
   11 CONTINUE
   10 CONTINUE
      KASEHI=1
      WRITE(8,6)
    6 FORMAT(' OMMHQR FORTRAN - NATURAL FREQUENCIES OF A TOROIDAL PANEL'
     1   / ' ==========================================================')
C     FIX PROBLEM PARAMETERS
      CALL INFIX
C     CALCULATE NAT FREQS FOR CYLINDRICAL PANEL
      CALL OMCYPA
C     CALCULATE NAT FREQS FOR TOROIDAL PANEL
      CALL OMEGAS
  100 CONTINUE
C     WRITE OUT TABLE FOR FUNDAMENTAL FREQUENCIES
      STOP
      END
C---------------------------------------------------------------------
      SUBROUTINE INFIX
C     INPUT DATA FIX GLOBAL CONSTANTS AND INITIALIZE
      IMPLICIT DOUBLE PRECISION (A-H,O-Z)
      COMMON/TTT/NMCASE,ATLO(16),ATHI(16)
      COMMON/ZZZ/RS,RR,PSI,TOR,THIC,RO,POIS,EY,PL,PH,RL,RH,MHI,NHI,NDM
      COMMON/DDD/TO,PI,WFACT,AKFAC,DEER4,ONER3,EHR4,R4D,RAT,AKL
      PI=3.141592653589793D0
      RAD=PI/180.D0
      READ(5,105) NDM,NMCASE,ENLR,RARR,RATHIC,RS
  105 FORMAT(2I5,4F10.3)
```

```
C     WRITEOUT THE INPUT DATA
      WRITE(8,106) MHI,NHI,NDM
  106 FORMAT(' SOLUTION PARAMETERS'/
     1       ' ------------------'/
     2 ' TERMS IN ETA DIRECTION (AXIAL DIRECT)       MHI = ',I5/
     3 ' TERMS IN THETA DIRECTION (NO OF ROOTS)      NHI = ',I5/
     4 ' NUMBER OF PANELS IN FULL MERIDIONAL DIRECT  NDM = ',I5/)
C     CALCULATE PARAMETERS
      TOLO=ATLO(NMCASE)
      TOHI=ATHI(NMCASE)
C     TO  =  SEMI    MERID  SPAN ANGLE OF PANEL
C     PSI = COMPLETE CIRCUM SPAN ANGLE OF PANEL
      TO=180./NDM
      PSI=360./(NDM*RARR*ENLR)
      TOR=TO*RAD
      PSIR=PSI*RAD
      RR=RARR*RS
      THIC=RATHIC*RS
      PH=2.DO*RS*DSIN(TOR)
      DH=RS*(1.DO-DCOS(TOR))
      RH=DH/PH
      PSIR2=PSIR/2.DO
      PL=(RS+RR)*2.DO*DSIN(PSIR2)
      DL=(RS+RR)*(1.DO-DCOS(PSIR2))
      RL=DL/PL
      XL=PSIR*(RR+RS)
C     OUT PUT PARAMETERS
      WRITE(8,116) PL,PH,RL,RH,RATHIC
  116 FORMAT(' TORUS PANEL DIMENSIONS (AT EXTRADOS)'/
     1       ' -----------------------------------'/
     2 ' PANEL LENGTH  (M)                        PL = ',F12.5/
     3 ' PANEL HEIGHT  (M)                        PH = ',F12.5/
     4 ' RISE RATIO LENGTH                        RL = ',F12.5/
     5 ' RISE RATIO HEIGHT                        RH = ',F12.5/
     6 ' SHELL THICKNESS RATIO H/R              THICR = ',F12.5/)
      WRITE(8,126) RS,RR,PSI,TO,THIC,TOLO,TOHI
  126 FORMAT(' TORUS DIMENSIONS AND ACTUAL PANEL EXTENT'/
     1       ' --------------------------------------'/
     2 ' SHELL RADIUS     (M)                     RS = ',F12.5/
     3 ' TOROIDAL RADIUS  (M)                     RR = ',F12.5/
     4 ' ANGULAR LENGTH (DEG)                    PSI = ',F12.5/
     5 ' ANGULAR WIDTH/2  (DEG)                   TO = ',F12.5/
     6 ' SHELL THICKNESS  (M)                   THIC = ',F12.5/
     7 ' ACTUAL PANEL START ANGLE (DEG)         TOLO = ',F12.5/
     8 ' ACTUAL PANEL END   ANGLE (DEG)         TOHI = ',F12.5/)
      WRITE(8,146)  POIS,EY,RO
  146 FORMAT(/' MATERIAL PARAMETERS'/
     1       ' ------------------'/
     2 ' POISSON RATIO                          POIS = ',F12.3/
     3 ' YOUNGS MODULUS (PA)                      EY = ',D12.3/
     4 ' MASS DENSITY (KG/M3)                     RO = ',F12.3/)
```

```
C     FIX VALUES FOR PROGRAM CONSTANTS
      DEE=EY*(THIC**3)/(12.*(1.-POIS*POIS) )
      V=POIS
      R4=RS*RS*RS*RS
      WFACT=RO*THIC
      AKFAC=.5*PI/TOR
      DEER4=DEE/R4
      ONER3=RS/R4
      EHR4=1./(EY*THIC*R4)
      R4D=R4/DEE
      RAT=RO*(1.-POIS*POIS)*RS*RS/EY
      AKL=THIC*THIC/(12.*RS*RS)
      RETURN
      END
C-----------------------------------------------------------------------
      SUBROUTINE OMCYPA
C     CYLD SHELL  BETA VS N  FOR M=1,2,3  SOEDEL P.97 FIG.5.5.2
      IMPLICIT DOUBLE PRECISION (A-H,O-Z)
      COMMON/ZZZ/RS,RR,PSI,TOR,THIC,RO,POIS,EY,PL,PH,RL,RH,MHI,NHI,NDM
      COMMON/FFF/TABA(10,21,4)
      PI=3.141592653589793D0
      RHO=RO
      HC=THIC
      RC=RS
      RC2=RC*RC
      POI=POIS
      AKH=12.*(1.-POI*POI)/(HC*HC)
      XL=PL
C     RISE RATIO
      RISE=RC*(1.D0-COS(TOR))
      RISER=RISE/PH
C     WRITEOUT THE INPUT DATA
      WRITE(8,106) RS,THIC,XL,RISER
  106 FORMAT(' CYLINDER PANEL DIMENSIONS'/
     1       ' ------------------------'/
     2 ' CYLD   RADIUS (M)                      RS = ',F12.5/
     3 ' CYLD   THICKNESS (M)                 THIC = ',F12.5/
     4 ' CYLD   LENGTH   (M)                    XL = ',F12.5/
     5 ' CYLD PANEL RISE RATIO               RISER = ',F12.5/)
      DEE=EY*HC**3/(12.*(1.-POI*POI))
      DROH=DEE/(RHO*HC)
C     LOOP OVER LONGITUDINAL WAVES
      DO 100 M=1,MHI
      EM=REAL(2*M-1)
      UM=EM*PI/XL
      UM2=UM*UM
      UM4=UM2*UM2
C     MVD THEORY - SYMMETRIC
      DO 110 N=1,NHI
      NN=2*N-1
      EN=REAL(NN)
```

```
      UN=EN*PI/(2.*TOR*RC)
      UN2=UN*UN
      SUM=UM2+UN2
      SUM2=SUM*SUM
      BRAC=SUM2+AKH*UM4/(SUM2*RC2)
      TABA(M,N,1)=DSQRT(DROH*BRAC)
  110 CONTINUE
  100 CONTINUE
      RETURN
      END
C-----------------------------------------------------------------------
      SUBROUTINE OMEGAS
C     CONTROL TO EVALUATE NATURAL FREQS FOR TOROIDAL PANEL
C     USING MAITER ROUTINE
      IMPLICIT DOUBLE PRECISION (A-H,O-Z)
      COMMON/DDD/TO,PI,WFACT,AKFAC,DEER4,ONER3,EHR4,R4D,RAT,AKL
      COMMON/ZZZ/RS,RR,PSI,TOR,THIC,RO,POIS,EY,PL,PH,RL,RH,MHI,NHI,NDM
      COMMON/HHH/X,X2,Y,Y2,Y4,EM,THETAL,THETAH
      COMMON/FFF/TABA(10,21,4)
      COMMON/TTT/NMCASE,ATLO(16),ATHI(16)
      DIMENSION XM(4),WRR(21)
      PSIR=PSI*PI/180.DO
      PIGAPS=PI*(RS/RR)/PSIR
      X=RS/RR
      X2=X*X
      THETLD=ATLO(NMCASE)
      THETAL=THETLD*PI/180.
      THETHD=ATHI(NMCASE)
      THETAH=THETHD*PI/180.
      TEEL=THETAL
      TEEH=THETAH
C     LOOP OVER LONGITUDINAL WAVES
      DO 100 LA=1,MHI
      Y=REAL(2*LA-1)*PIGAPS
      Y2=Y*Y
      Y4=Y2*Y2
C     SOLUTION USING   HQR  ROUTINE
      CALL COEFFS(WRR)
C     LOOP FOR TWO CLASSES   LSA=1 SYM    LSA=2 ANTISYM
      DO 101 LSA=1,1
      DO 110 LC=1,NHI
      TABA(LA,LC,2+LSA)=WRR(LC)
  110 CONTINUE
  101 CONTINUE
  100 CONTINUE
C     WRITE OUT RESULTS FOR THIS LZ,LY SET
      WRITE(8,206)  THETLD, THETHD
  206 FORMAT(/'  OM FOR PANELS (TIMES 10**-4) (RAD/SEC)'/
     1 '   THETLD = ', F7.2,'   THETAH = ',F7.2/
     2 '   M  N        MVD-CP      LEISSA      MVD-TP    ')
C     IN THIS VERSION NOT USING RAT NOR LEISSA NONDIM VALUES
```

```
      DO 210 M=1,MHI
      DO 220 N=1,5
      NN=2*N-1
      DONCS=TABA(M,N,1)/10000.
      DONCA=TABA(M,N,2)/10000.
      DONTS=TABA(M,N,3)/10000.
  220 WRITE(8,216) M,N,DONCS,DONCA,DONTS
  216 FORMAT(1X,2I3,1X,4F12.4)
  210 WRITE(8,226)
  226 FORMAT(' ')
 1000 CONTINUE
      RETURN
      END
C-----------------------------------------------------------------------
      SUBROUTINE COEFFS(WRR)
C     DEFINE LHS OF EQUIL EQNS FOR THIS MS - SYM MODES IN THETA
      IMPLICIT DOUBLE PRECISION (A-H,O-Z)
      COMMON/ZZZ/RS,RR,PSI,TOR,THIC,RO,POIS,EY,PL,PH,RL,RH,MHI,NHI,NDM
      COMMON/DDD/TO,PI,WFACT,AKFAC,DEER4,ONER3,EHR4,R4D,RAT,AKLI
      COMMON/HHH/X,X2,Y,Y2,Y4,EM,THETAL,THETAH
      DIMENSION F(5),G(5),WRR(21)
      DIMENSION BB(21,21),DD(21,21),BD(21,21),DB(21,21)
      DIMENSION BBI(21,21),BBZ(21,21),STOR(21,21)
      DIMENSION AA(21,21),BS(21,21),WR(21),WI(21),III(21)
      THETL=THETAL
      THETH=THETAH
      FAC=AKFAC
      THETAO=TOR
      MEQ=NHI
C     SET UP EQUATION SET FOR THIS MS  DEFINE AA MATRIX
C     MATRIX SET UP BY COLUMNS
      BOT1=-ONER3/(2.*WFACT)
      BOT2= DEER4/(2.*WFACT)
      DO 100 N=1,MEQ
      IN=N*2-1
      EN=REAL(IN)*AKFAC
      CALL COFFS(EN,F)
      CALL COFGS(EN,G)
      DO 101 L=1,MEQ
      IL=L*2-1
      CALL STMNLS(F,G,IL,IN,FAC,THETL,THETH,COFB,COFH,COFT)
C     ADD OMS TERM TO 1ST DIAG COEFFT
      IF(N.EQ.L) COFTT=COFT
      BB(L,N) = EHR4*COFB
      BD(L,N) = ONER3*COFH
      DB(L,N) = BOT1*COFH/COFTT
      DD(L,N) = BOT2*COFB/COFTT
  101 CONTINUE
  100 CONTINUE
C     CONSTRUCT FINAL MATRIX
C     INVERSE OF BB => BBI
```

```
      N8=NHI
      DO 110 I=1,N8
      DO 111 J=1,N8
      BBZ(I,J)=BB(I,J)
  111 BBI(I,J)=BB(I,J)
  110 CONTINUE
      CALL GAUSSJ(BBI,N8,N8,BBZ,N8,N8)
C     PRODUCT OF BBI WITH BD => STOR
      NX38=21
      DO 120 I=1,N8
      DO 120 J=1,NX38
      STOR(I,J)=.0
      DO 120 K=1,N8
      STOR(I,J)=STOR(I,J)+BBI(I,K)*BD(K,J)
  120 CONTINUE
C     DD - PRODUCT OF DB WITH STOR => AK
      DO 130 I=1,NX38
      DO 130 J=1,NX38
      SUM=.0
      DO 132 K=1,N8
  132 SUM=SUM+DB(I,K)*STOR(K,J)
      AA(I,J)=DD(I,J)-SUM
  130 CONTINUE
C     CALCULATE THE EIGENVALUES
      N=NX38
      EPS=1.D-10
      BETA=1.D-20
      CALL QRMET(N,AA,EPS,BETA,WR,WI,BS,KODE)
C     SORT BY SIZE AND TRANSFER THE RESULTS INTO ARRAY  WRR
      DO 400 I=1,N8
      WR(I)=DSQRT(WR(I))
  400 III(I)=1
      DO 700 I=1,N8
      TEMP=2.D9
      DO 720 J=1,N8
      IF(III(J).EQ.0) GO TO 710
      IF(WR(J).GE.TEMP) GO TO 710
      TEMP=WR(J)
      ITEMP=J
  710 CONTINUE
  720 CONTINUE
      III(ITEMP)=0
      WRR(I)=TEMP
  700 CONTINUE
      RETURN
      END
C-----------------------------------------------------------------------
      SUBROUTINE COFFS(EN,F)
C     ROUTINE TO GENERATE ONE  F  COEFFT
C     EN IS ACTUALLY KAPPA_N    X IS GAMMA    Y IS MUM
      IMPLICIT DOUBLE PRECISION (A-H,O-Z)
```

```
      DOUBLE PRECISION N2,N3,N4
      COMMON/HHH/X,X2,Y,Y2,Y4,EM,THETAL,THETAH
      DIMENSION F(5)
      N2=EN*EN
      N3=N2*EN
      N4=N3*EN
C     CALCULATE THE  FIVE    F    VALUES
      F(1)=(N3+3.*N2*Y2-3.*EN*Y2+5.*Y4)*X2
      F(2)=2.*(-N3-2.*N2*Y2+EN*Y2-2.*Y4)*X
      F(3)=2.*(N4+2.*N2*Y2+Y4)+(6.*N2*Y2+10.*Y4)*X2
      F(4)=2.*(N3-2.*N2*Y2-EN*Y2-2.*Y4)*X
      F(5)=(-N3+3.*N2*Y2+3.*EN*Y2+5.*Y4)*X2
      RETURN
      END
C-----------------------------------------------------------------------
      SUBROUTINE COFGS(EN,G)
C     ROUTINE TO GENERATE     G     COEFFTS
C     EN IS ACTUALLY KAPPA_N   X IS GAMMA   Y IS MUM
      IMPLICIT DOUBLE PRECISION (A-H,O-Z)
      DOUBLE PRECISION N2
      COMMON/HHH/X,X2,Y,Y2,Y4,EM,THETAL,THETAH
      DIMENSION G(5)
      N2=EN*EN
      G(1)=.5*(N2-EN-3.*Y2)*X2
      G(2)=(-N2+EN+2.*Y2)*X
      G(3)=-2.*Y2+(N2-3.*Y2)*X2
      G(4)=(-N2-EN+2.*Y2)*X
      G(5)=.5*(N2+EN-3.*Y2)*X2
      RETURN
      END
C-----------------------------------------------------------------
      SUBROUTINE STMNLS(F,G,L,N,FAC,THETAL,THETAH,COFB,COFH,COFT)
C     CALCULATE THREE COEFFTS  -  SMNL BAR, SMNL HAT,  COFT
      IMPLICIT DOUBLE PRECISION (A-H,O-Z)
      DIMENSION F(5),G(5),TMN(5)
      COFB=.0
      COFH=.0
      DO 10 I=1,5
      FACS=FAC*REAL(N+L)+REAL(I-3)
      FACD=FAC*REAL(N-L)+REAL(I-3)
      ANGSL=FACS*THETAL
      ANGSH=FACS*THETAH
      ANGDL=FACD*THETAL
      ANGDH=FACD*THETAH
      SINS=SIN(ANGSH)-SIN(ANGSL)
      SIND=SIN(ANGDH)-SIN(ANGDL)
      IF(L.EQ.N.AND.I.EQ.3) FACD=1.DO
      IF(L.EQ.N.AND.I.EQ.3) SIND=THETAH-THETAL
      TMN(I)=(SIND/FACD + SINS/FACS)
      COFB=COFB+F(I)*TMN(I)
   10 COFH=COFH+G(I)*TMN(I)
```

```
      COFT=TMN(3)
      RETURN
      END
C************************ START QREIG.FOR ****************************
C     LAST MODIFICATION   -   APRIL 2, 1995
C     QREIG FORTRAN - GENERAL EIGENVALUE EXTRACTION ROUTINE
C     SOLVING STANDARD EIGENVALUE PROBLEM - SYM OR NON-SYM MATRIX
C     REF. ALGORITHM 343 COMM ACM 11 DEC 1968
      SUBROUTINE QRMET(N,A,EPS,BETA,WR,WI,VECT,KFAIL)
 IMPLICIT DOUBLE PRECISION(A-H,O-Z)
 DIMENSION A(N,N),VECT(N,N),WR(N),WI(N)
 CALL QRTHES(N,BETA,A,VECT)
 CALL HQR2S(N,EPS,A,VECT,WR,WI,KFAIL)
 RETURN
 END
C---------------------------------------------------------------------
      SUBROUTINE HQR2S(N,EP,H,VECS,WR,WI,KFAIL)
C        USING THE QR ROUTINE FOR EIGENVALUES FROM GENERAL MATRIX
      IMPLICIT DOUBLE PRECISION(A-H,O-Z)
 DIMENSION H(N,N),VECS(N,N),WR(N),WI(N)
 KFAIL=0
 NN=N
 T=.0
   10 ITS=0
      NA=NN-1
 IF(NA) 220,51,20
   20 DO 30 L1=2,NN
      L=NN-L1+2
 IF(ABS(H(L,L-1)).LE.EP*(ABS(H(L-1,L-1))+ABS(H(L,L)))) GO TO 40
   30 CONTINUE
   51 L=1
   40 X=H(NN,NN)
      IF(L.EQ.NN) GO TO 50
      Y=H(NA,NA)
 W=H(NN,NA)*H(NA,NN)
 IF(L.EQ.NA) GO TO 60
 IF(ITS.EQ.30) GO TO 70
 IF(ITS.EQ.20) GO TO 80
 IF(ITS.EQ.10) GO TO 80
   41 ITS=ITS+1
      M1=NN-2
 DO 90 M2=L,M1
 M=M1-M2+L
 Z=H(M,M)
 R=X-Z
 S=Y-Z
 P=(R*S-W)/H(M+1,M)+H(M,M+1)
 Q=H(M+1,M+1)-Z-R-S
 R=H(M+2,M+1)
 S=ABS(P)+ABS(Q)+ABS(R)
 P=P/S
```

```
Q=Q/S
R=R/S
IF(M.EQ.L) GO TO 100
IF(ABS(H(M,M-1))*(ABS(Q)+ABS(R)).LE.EP*ABS(P)
    1  *(ABS(H(M-1,M-1))+ABS(Z)+ABS(H(M+1,M+1)))) GO TO 100
  90 CONTINUE
 100 I1=M+2
     I2=M+3
DO 110 I=I1,NN
 110 H(I,I-2)=.0
     IF(I2.GT.NN) GO TO 121
DO 120 I=I2,NN
 120 H(I,I-3)=.0
 121 DO 130 K=M,NA
     IF(K.EQ.M) GO TO 140
P=H(K,K-1)
     Q=H(K+1,K-1)
R=.0
IF(K.NE.NA) R=H(K+2,K-1)
X=ABS(P)+ABS(Q)+ABS(R)
IF(X.EQ..0) GO TO 130
P=P/X
Q=Q/X
R=R/X
 140 S=SQRT(P*P+Q*Q+R*R)
     IF(P.LT..0) S=-S
IF(K.EQ.M) GO TO 150
H(K,K-1)=-S*X
GO TO 160
 150 IF(L.NE.M) H(K,K-1)=-H(K,K-1)
 160 P=P+S
     X=P/S
     Y=Q/S
Z=R/S
Q=Q/P
R=R/P
DO 170 J=K,N
P=H(K,J)+Q*H(K+1,J)
IF(K.EQ.NA) GO TO 180
P=P+R*H(K+2,J)
H(K+2,J)=H(K+2,J)-P*Z
 180 H(K+1,J)=H(K+1,J)-P*Y
 170 H(K,J)=H(K,J)-P*X
     J=NN
     IF(K+3.LT.NN) J=K+3
DO 190 I=1,J
P=X*H(I,K)+Y*H(I,K+1)
IF(K.EQ.NA) GO TO 200
P=P+Z*H(I,K+2)
H(I,K+2)=H(I,K+2)-P*R
 200 H(I,K+1)=H(I,K+1)-P*Q
```

```
 190 H(I,K)=H(I,K)-P
     DO 210 I=1,N
P=X*VECS(I,K)+Y*VECS(I,K+1)
IF(K.EQ.NA) GO TO 211
P=P+Z*VECS(I,K+2)
VECS(I,K+2)=VECS(I,K+2)-P*R
 211 VECS(I,K+1)=VECS(I,K+1)-P*Q
 210 VECS(I,K)=VECS(I,K)-P
 130 CONTINUE
     GO TO 20
  50 WR(NN)=X+T
     H(NN,NN)=X+T
WI(NN)=0.
NN=NA
GO TO 10
  60 P=(Y-X)/2.
     Q=P*P+W
Z=SQRT(ABS(Q))
X=X+T
H(NN,NN)=X
H(NA,NA)=Y+T
IF(Q.LE..0) GO TO 65
IF(P.LT..0) Z=-Z
Z=Z+P
WR(NA)=X+Z
WR(NN)=X-W/Z
WI(NA)=.0
WI(NN)=.0
X=H(NN,NA)
R=SQRT(X**2+Z**2)
P=X/R
Q=Z/R
DO 62 J=NA,N
Z=H(NA,J)
H(NA,J)=Q*Z+P*H(NN,J)
  62 H(NN,J)=Q*H(NN,J)-P*Z
     DO 63 I=1,NN
Z=H(I,NA)
H(I,NA)=Q*Z+P*H(I,NN)
  63 H(I,NN)=Q*H(I,NN)-P*Z
     DO 64 I=1,N
Z=VECS(I,NA)
VECS(I,NA)=Q*Z+P*VECS(I,NN)
  64 VECS(I,NN)=Q*VECS(I,NN)-P*Z
     GO TO 66
  65 WR(NA)=X+P
     WR(NN)=X+P
WI(NA)=Z
WI(NN)=-Z
  66 NN=NN-2
     GO TO 10
```

```
  70 KFAIL=1
     RETURN
  80 T=T+X
     DO 81 I=1,NN
  81 H(I,I)=H(I,I)-X
S=ABS(H(NN,NA))+ABS(H(NA,NN-2))
X=.75*S
Y=X
W=-.4375*S*S
GO TO 41
 220 ANORM=0.
     K=1
DO 230 I=1,N
DO 240 J=K,N
 240 ANORM=ANORM+ABS(H(I,J))
 230 K=I
     DO 250 NM=1,N
NN=N-NM+1
P=WR(NN)
Q=WI(NN)
NA=NN-1
IF(Q) 320, 260,250
 260 M=NN
     H(NN,NN)=1.
DO 310 I1=1,NA
IF(NA.LE.0) GO TO 310
I=NA-I1+1
W=H(I,I)-P
R=H(I,NN)
IF(M.GT.NA) GO TO 271
DO 270 J=M,NA
 270 R=R+H(I,J)*H(J,NN)
 271 IF(WI(I)) 280,290,300
 280 Z=W
     S=R
GO TO 310
 290 M=I
     H(I,NN)=EP*ANORM
IF(W.NE.0.) H(I,NN)=W
H(I,NN)=-R/H(I,NN)
GO TO 310
 300 M=I
     X=H(I,I+1)
     Y=H(I+1,I)
Q=(WR(I)-P)**2+WI(I)**2
T=(X*S-Z*R)/Q
H(I,NN)=T
H(I+1,NN)=-(S+Y*T)/Z
IF(ABS(X).GT.ABS(Z)) H(I+1,NN)=-(R+W*T)/X
 310 CONTINUE
     GO TO 250
```

```
 320 M=NA
     IF(ABS(H(NN,NA)).LE.ABS(H(NA,NN))) GO TO 330
H(NA,NA)=-(H(NN,NN)-P)/H(NN,NA)
H(NA,NN)=-Q/H(NN,NA)
     GO TO 340
 330 CALL CDIVS(-H(NA,NN),.0D0,H(NA,NA)-P,Q,H(NA,NA),H(NA,NN))
 340 H(NN,NA)=1.
     H(NN,NN)=0.
NB=NA-1
DO 350 I1=1,NB
IF(NB.LE.0) GO TO 350
I=NB-I1+1
W=H(I,I)-P
RA=H(I,NN)
SA=0.
IF(M.GT.NA) GO TO 361
DO 360 J=M,NA
RA=RA+H(I,J)*H(J,NA)
 360 SA=SA+H(I,J)*H(J,NN)
 361 IF(WI(I)) 370,380,390
 370 Z=W
     R=RA
S=SA
GO TO 420
 380 M=I
     CALL CDIVS(-RA,-SA,W,Q,H(I,NA),H(I,NN))
GO TO 420
 390 M=I
     X=H(I,I+1)
Y=H(I+1,I)
VR=(WR(I)-P)**2+WI(I)**2-Q**2
VI=(WR(I)-P)*2.0*Q
IF(VR.NE.0.) GO TO 400
IF(VI.NE.0.) GO TO 400
VR=EP*ANORM*(ABS(W)+ABS(Q)+ABS(X)+ABS(Y)+ABS(Z))
 400 CALL CDIVS(X*R-Z*RA+Q*SA,X*S-Z*SA-Q*RA,VR,VI,H(I,NA),H(I,NN))
     IF(ABS(X).LE.ABS(Z)+ABS(Q)) GO TO 410
H(I+1,NA)=(-RA-W*H(I,NA)+Q*H(I,NN))/X
H(I+1,NN)=(-SA-W*H(I,NN)-Q*H(I,NA))/X
GO TO 420
 410 CALL CDIVS(-R-Y*H(I,NA),-S-Y*H(I,NN),Z,Q,H(I+1,NA),H(I+1,NN))
 420 CONTINUE
 350 CONTINUE
 250 CONTINUE
     DO 430 J1=1,N
J=N-J1+1
M=J
L=J-1
IF(WI(J)) 440,490,430
 440 DO 450 I=1,N
     Y=0.
```

```
      Z=0.
      DO 460 K=1,M
      Y=Y+VECS(I,K)*H(K,L)
  460 Z=Z+VECS(I,K)*H(K,J)
          VECS(I,L)=Y
  450 VECS(I,J)=Z
          GO TO 430
  490 DO 470 I=1,N
          Z=0.
      DO 480 K=1,M
  480 Z=Z+VECS(I,K)*H(K,J)
          VECS(I,J)=Z
  470 CONTINUE
  430 CONTINUE
          RETURN
      END
C-----------------------------------------------------------------------
      SUBROUTINE QRTHES(N,BETA,A,V)
      IMPLICIT DOUBLE PRECISION(A-H,O-Z)
              DIMENSION A(N,N),V(N,N),D(250)
      DO 100 I=1,N
      DO 100 J=1,N
      V(I,J)=0.
  100 V(I,I)=1.
          NA=N-1
      DO 10 M=2,NA
      H=0.
      DO 20 I1=M,N
      I=N-I1+M
      F=A(I,M-1)
      D(I)=F
   20 H=H+F**2
          IF(H.GT.BETA) GO TO 30
      G=0.
      GO TO 40
   30 G=SQRT(H)
          IF(F.GE.0.) G=-G
          H=H-F*G
      D(M)=F-G
      DO 60 J=M,N
      F=0.
      DO 50 I1=M,N
      I=N-I1+M
   50 F=F+D(I)*A(I,J)
          F=F/H
      DO 60 I=M,N
   60 A(I,J)=A(I,J)-F*D(I)
          DO 70 I=1,N
      E=0.
      F=0.
      DO 80 J1=M,N
```

```
      J=N-J1+M
      E=E+D(J)*V(I,J)
   80 F=F+D(J)*A(I,J)
      F=F/H
      E=E/H
      DO 90 J=M,N
      V(I,J)=V(I,J)-E*D(J)
   90 A(I,J)=A(I,J)-F*D(J)
   70 CONTINUE
   40 A(M,M-1)=G
   10 CONTINUE
      RETURN
      END
C-----------------------------------------------------------------------
      SUBROUTINE CDIVS(A,B,C,D,E,F)
      IMPLICIT DOUBLE PRECISION(A-H,O-Z)
      IF(ABS(C).LT.ABS(D)) GO TO 1
      R=D/C
      DEN=C+R*D
      E=(A+B*R)/DEN
      F=(B-A*R)/DEN
      GO TO 2
    1 R=C/D
      DEN=D+R*C
      E=(A*R+B)/DEN
      F=(B*R-A)/DEN
    2 RETURN
      END
C********************* END QREIG.FOR *********************************
      SUBROUTINE gaussj(a,n,np,b,m,mp)
C     ROUTINE TO DETERMINE INVERSE OF MATRIX  'A'
      IMPLICIT DOUBLE PRECISION (A-H,O-Z)
      INTEGER m,mp,n,np,NMAX
      DIMENSION A(21,21),B(NP,MP)
      PARAMETER (NMAX=50)
      INTEGER i,icol,irow,j,k,l,ll,indxc(NMAX),indxr(NMAX),ipiv(NMAX)
      REAL big,dum,pivinv
      do 11 j=1,n
        ipiv(j)=0
11    continue
      do 22 i=1,n
        big=0.
        do 13 j=1,n
          if(ipiv(j).ne.1)then
            do 12 k=1,n
              if (ipiv(k).eq.0) then
                if (abs(a(j,k)).ge.big)then
                  big=abs(a(j,k))
                  irow=j
                  icol=k
                endif
```

```
            else if (ipiv(k).gt.1) then
              pause 'singular matrix in gaussj'
            endif
12        continue
        endif
13    continue
      ipiv(icol)=ipiv(icol)+1
      if (irow.ne.icol) then
        do 14 l=1,n
          dum=a(irow,l)
          a(irow,l)=a(icol,l)
          a(icol,l)=dum
14      continue
        do 15 l=1,m
          dum=b(irow,l)
          b(irow,l)=b(icol,l)
          b(icol,l)=dum
15      continue
      endif
      indxr(i)=irow
      indxc(i)=icol
      if (a(icol,icol).eq.0.) pause 'singular matrix in gaussj'
      pivinv=1./a(icol,icol)
      a(icol,icol)=1.
      do 16 l=1,n
        a(icol,l)=a(icol,l)*pivinv
16    continue
      do 17 l=1,m
        b(icol,l)=b(icol,l)*pivinv
17    continue
      do 21 ll=1,n
        if(ll.ne.icol)then
          dum=a(ll,icol)
          a(ll,icol)=0.
          do 18 l=1,n
            a(ll,l)=a(ll,l)-a(icol,l)*dum
18        continue
          do 19 l=1,m
            b(ll,l)=b(ll,l)-b(icol,l)*dum
19        continue
        endif
21    continue
22  continue
    do 24 l=n,1,-1
      if(indxr(l).ne.indxc(l))then
        do 23 k=1,n
          dum=a(k,indxr(l))
          a(k,indxr(l))=a(k,indxc(l))
          a(k,indxc(l))=dum
23      continue
      endif
```

```
24    continue
      return
      END
C********************** END DQMHQR.FOR ********************************
C*************************** D A T A ***********************************
      BLOCK DATA
      IMPLICIT DOUBLE PRECISION (A-H,O-Z)
      COMMON/ZZZ/RS,RR,PSI,TOR,THIC,RO,POIS,EY,PL,PH,RL,RH,MHI,NHI,NDM
      COMMON/TTT/NMCASE,ATLO(16),ATHI(16)
C     PL PH RL RH:PANEL LENGTH,PANEL HEIGHT,RATIO LENGTH,RATIO HEIGHT
C     ZZZ BLOCK DATA
      DATA RS/-1./, RR/-1./, PSI/-1./, TOR/-1./, THIC/-1./
      DATA RO/7770./, POIS/.3/, EY/.207D+12/
      DATA PL/-1./, PH/-1./, RL/-1./, RH/-1./
      DATA MHI/  3/, NHI/ 21/, NDM/  2/
C
      DATA ATLO(1)/-90./, ATLO(2)/90./
      DATA ATHI(1)/ 90./, ATHI(2)/270./
C
      DATA ATLO(3)/.0/, ATLO(4)/90./
      DATA ATHI(3)/ 90./, ATHI(4)/180./
C
      DATA ATLO(5)/.0/, ATLO(6)/45./, ATLO(7)/90./, ATLO(8)/135./
      DATA ATHI(5)/45./, ATHI(6)/ 90./, ATHI(7)/135./, ATHI(8)/180./
C
      DATA ATLO(9)/.0/, ATLO(10)/22.5/
      DATA ATLO(11)/45./, ATLO(12)/67.5/, ATLO(13)/90./
      DATA ATLO(14)/112.5/, ATLO(15)/135./, ATLO(16)/157.5/
C
      DATA ATHI(9)/22.5/, ATHI(10)/45./
      DATA ATHI(11)/67.5/, ATHI(12)/90./, ATHI(13)/112.5/
      DATA ATHI(14)/135./, ATHI(15)/157.5/, ATHI(16)/180./
      END
C     NDM = NUMBER OF PANELS IN FULL MERID DIRECTION (NDM=16 ARC=22.5)
C          NOTE IN PAPER  N_D MEANS PANELS PER 180 DEG  I.E. NDM=2*ND
C     NMCASE = WHICH OF THE MERID PANELS IS TO BE ANALYZED (1 AT EXTRAD)
C     ENLR = ARC LENGTH MERID / ARC LENGTH CIRCUM AT TOR CENTRE-LINE RAD
C     RARR=RR/RS     RATHIC=THIC/RS
C     RS=RADIUS OF CROSSECTION  (METRES)
C NDM NMCASE    ENLR      RARR    RATHIC        RS
C  16   16      .928 4.1813043  .0252978  .4953000
C******************** END PROGRAM ***************************************
C$DATA
    8
    4    3        1.     5.714      .005       .56
    4    4        1.     5.714      .005       .56
    8    5        1.     5.714      .005       .56
    8    6        1.     5.714      .005       .56
    8    8        1.     5.714      .005       .56
   16    9        1.     5.714      .005       .56
   16   12        1.     5.714      .005       .56
```

16	16	1.	5.714	.005	.56
4	3	1.	5.714	.01	.56
4	4	1.	5.714	.01	.56
8	5	1.	5.714	.01	.56
8	6	1.	5.714	.01	.56
8	8	1.	5.714	.01	.56
16	9	1.	5.714	.01	.56
16	12	1.	5.714	.01	.56
16	16	1.	5.714	.01	.56

Program Tordqm.m

```
% tordqm.m  last modification - may 27, 1998
% natural frequency of a toroidal shell panel using the dqm
% mvd theory using three governing eqns thin walled struct '92 223-239
% translated the fortran version of tordqm dqm module
%
% ndm=no of panels in semi-merid, nmcase=panel case for analysis
% enlr=ratio of panel circum panel length/meridional panel length
% m = no of sampling points, lwave=longitudinal wave number
% ibc = bound cond code for theta: ibc=1 diaphragm ibc=2 clamped
%                                                  ibc=3 free
% rho=density, pr=poisson ratio, ey=youngs modulus
% rs=x-sect radius, rarr=torus radius/rs, rathic=shell thick/rs
% psi=panel angular span in phi direction
% atlo,athi=set of low,high angles of panel (theta low, theta high)
%
% data arrays for the eight cases
storndm(1)=4;       stornm(1)=3;
storndm(2)=4;       stornm(2)=4;
storndm(3)=8;       stornm(3)=5;
storndm(4)=8;       stornm(4)=6;
storndm(5)=8;       stornm(5)=8;
storndm(6)=16;      stornm(6)=9;
storndm(7)=16;      stornm(7)=12;
storndm(8)=16;      stornm(8)=16;
atlo(1)=-90.;     athi(1)= 90.;
atlo(2)= 90.;     athi(2)=270.;
atlo(3)=  .0;     athi(3)= 90.;
atlo(4)= 90.;     athi(4)=180.;
atlo(5)=  .0;      athi(5)= 45.;
atlo(6)= 45.;      athi(6)= 90.;
atlo(7)= 90.;      athi(7)=135.;
atlo(8)=135.;      athi(8)=180.;
atlo(9)=  0.;       athi(9)= 22.5;
atlo(10)= 22.5;     athi(10)= 45.;
atlo(11)= 45.0;     athi(11)= 67.5;
atlo(12)= 67.5;     athi(12)= 90.;
atlo(13)= 90.0;     athi(13)=112.5;
atlo(14)=112.5;     athi(14)=135.;
atlo(15)=135.0;     athi(15)=157.5;
atlo(16)=157.5;     athi(16)=180.;
%
% would like to have a loop here over  8  cases
iloop=5;
ndm=storndm(iloop)
nmcase=stornm(iloop)
%
m=20;
m1=m-1; m2=m-2; m4=m-4;
```

```
lwave=1;
%
rho=7770.;
pr=.3;
ey=.207e+12;
gee=.5*ey/(1+pr);
%
rs=.56;
rs2=rs*rs;
enlr=1;
rarr=5.714;
rathic=.01;
thic=rs*rathic;
dee=ey*thic*thic*thic/(12*(1-pr*pr));
deep=ey*thic*thic*thic/(12*(1+pr));
%
rad=pi/180.;
psi=2.*pi/(ndm*rarr*enlr);
anglo=atlo(nmcase)
anghi=athi(nmcase)
tolo=anglo*rad;
tohi=anghi*rad;
%-----------------------------------------------------------------
% this subroutine finds the weighting coeffts for meridional direct
% use unequal spacing with one delta point at each end
% inputs - no. of samp points "m" ,initial,final angles 'tolo tohi'
% outputs- a1(i.j), a2(i,j),a3(i,j),a4(i,j) for 1st to 4th derivats
x(1)=0;
x(2)=.00001;
x(m1)=.99999;
x(m)=1;
%
for i=3:m2
tt=(pi*(i-2))/(m-3);
x(i)=(1-cos(tt))/2;
end
%
teedif=tohi-tolo;
for i=1:m
x(i)=tolo+x(i)*teedif;
end
%
for i=1:m
pai(i)=1;
for j=1:m
if i~=j
        pai(i)=(x(i)-x(j))*pai(i);
end
end;end
%
for i=1:m
```

```
for j=1:m
if i~=j
   a1(i,j)=pai(i)/((x(i)-x(j))*pai(j));
end
end;end
%
for i=1:m
a1(i,i)=0;
for j=1:m
if i~=j
    a1(i,i)=a1(i,i)-a1(i,j);
end
end;end
%
for i=1:m
for j=1:m
if i~=j
  a2(i,j)=2*(a1(i,i)*a1(i,j)-a1(i,j)/(x(i)-x(j)));
end
end;end
%
for i=1:m
a2(i,i)=0;
for j=1:m
if i~=j
    a2(i,i)=a2(i,i)-a2(i,j);
end
end;end
%
for i=1:m
for j=1:m
if i~=j
  a3(i,j)=3*(a2(i,i)*a1(i,j)-a2(i,j)/(x(i)-x(j)));
end
end;end
%
for i=1:m
a3(i,i)=0;
for j=1:m
if i~=j
    a3(i,i)=a3(i,i)-a3(i,j);
end
end;end
%
for i=1:m
for j=1:m
if i~=j
  a4(i,j)=4*(a3(i,i)*a1(i,j)-a3(i,j)/(x(i)-x(j)));
end
end;end
%
```

```
for i=1:m
a4(i,i)=0;
for j=1:m
if i~=j
    a4(i,i)=a4(i,i)-a4(i,j);
end
end;end
%-----------------------------------------------------------------
% this subroutine finds the aii,aim,...,ann matrices for the gov eqns
% the ai* series are for 1st, am* for 2nd and an* for the 3rd eqns
% a*i is for U component, a*m for V and a*n for W displacements
% input - m, and a1,...,a4 matrices
% output - aii,aim,...,ann matrices
%
%  aii  aim  ain     u             u
%  ami  amm  amn     v  =   w^2    v
%  ani  amn  ann     w             w
%
fact=ey/((1-pr*pr)*rs*rs*rho);
pkhat=rathic*rathic/12.;
an1=(1.-pr)/2.;
an2=(1.+pr)/2.;
an3=(3.-pr)/2.;
gam=1./rarr;
gam2=gam*gam;
pigap=gam*pi/psi;
%
aii(:,:)=zeros(m);aim(:,:)=zeros(m);ain(:,:)=zeros(m);
ami(:,:)=zeros(m);amm(:,:)=zeros(m);amn(:,:)=zeros(m);
ani(:,:)=zeros(m);anm(:,:)=zeros(m);ann(:,:)=zeros(m);
%
amu=(2*lwave-1)*pigap;
amu2=amu*amu;
amu4=amu2*amu2;
% loop over stations
for i=1:m
tee=x(i);
ct=cos(tee);
st=sin(tee);
z=1.+gam*ct;
zm2=1./(z*z);
zm1=1./z;
z2=z*z;
z3=z2*z;
z4=z2*z2;
ct2=ct*ct;
st2=st*st;
c2t=cos(2.*tee);
umc2t=1.-c2t;
%
aii(i,i)=-zm2*(an1*amu2+pr*gam*z*ct+gam2*st2);
```

```
aim(i,i)=-zm2*an3*gam*st*amu;
ain(i,i)=-zm2*gam*st;
%
ami(i,i)=-zm2*an3*gam*amu*st;
amm(i,i)=-zm2*(amu2-an1*gam*z*ct+an1*gam2*st2);
amn(i,i)= zm2*amu*(gam*ct+pr*z);
%
ani(i,i)= zm2*gam*st*(gam*ct+pr*z);
anm(i,i)= zm2*amu*(gam*ct+pr*z);
ann(i,i)=-(1.+2.*zm1*pr*gam*ct+zm2*gam2*ct2);
zm4=zm2*zm2;
ann(i,i)=ann(i,i)-pkhat*zm4*(amu4-amu2*(2.*gam2*umc2t+2.*gam*z*ct));
% loop over terms in series
for ii=1:m
aii(i,ii)=aii(i,ii)+a2(i,ii)-gam*zm1*st*a1(i,ii);
aim(i,ii)=aim(i,ii)-an2*zm1*amu*a1(i,ii);
ain(i,ii)=ain(i,ii)+(1.+pr*gam*zm1*ct)*a1(i,ii);
%
ami(i,ii)=ami(i,ii)+an2*zm1*amu*a1(i,ii);
amm(i,ii)=amm(i,ii)+an1*a2(i,ii)-an1*gam*zm1*st*a1(i,ii);
%
ani(i,ii)=ani(i,ii)-(1.+pr*gam*zm1*ct)*a1(i,ii);
sub1=z4*a4(i,ii)-(2.*gam*z3*st)*a3(i,ii);
sub2=-(.5*gam2*z2*umc2t+2.*gam*z3*ct)*a2(i,ii);
sub3=-(.5*gam2*z*umc2t+2.*gam2*z2*ct-gam*z3)*st*a1(i,ii);
sub4=-amu2*(2.*gam*z*st)*a1(i,ii)-amu2*2.*z2*a2(i,ii);
ann(i,ii)=ann(i,ii)-pkhat*zm2*zm2*(sub1+sub2+sub3+sub4);
end;end
%-----------------------------------------------------------------
% in this subroutine the coeffts are placed in their final positions
% input - m,n,a**,d**.
% output - db, dd matrices
dd=zeros(3*m-8);db=zeros((3*m-8),8);
%
for i=1:m2
ni=1+i;
db(i,1)=aii(ni,1);      db(i,5)=ain(ni,1);
db(i,2)=aii(ni,m);      db(i,6)=ain(ni,2);
db(i,3)=aim(ni,1);      db(i,7)=ain(ni,m-1);
db(i,4)=aim(ni,m);      db(i,8)=ain(ni,m);
%
db(i+m2,1)=ami(ni,1);   db(i+m2,5)=amn(ni,1);
db(i+m2,2)=ami(ni,m);   db(i+m2,6)=amn(ni,2);
db(i+m2,3)=amm(ni,1);   db(i+m2,7)=amn(ni,m-1);
db(i+m2,4)=amm(ni,m);   db(i+m2,8)=amn(ni,m);
end;end
%
for i=1:m4
n2i=2+i;
db(i+2*m2,1)=ani(n2i,1);   db(i+2*m2,5)=ann(n2i,1);
db(i+2*m2,2)=ani(n2i,m);   db(i+2*m2,6)=ann(n2i,2);
```

```
db(i+2*m2,3)=anm(n2i,1);   db(i+2*m2,7)=ann(n2i,m-1);
db(i+2*m2,4)=anm(n2i,m);   db(i+2*m2,8)=ann(n2i,m);
end;end
%
for i=1:m2
for j=1:m2
ni=1+i;nj=1+j;
dd(i,j)      =aii(ni,nj);
dd(i,m2+j)   =aim(ni,nj);
dd(m2+i,j)   =ami(ni,nj);
dd(m2+i,m2+j)=amm(ni,nj);
end;end
%
for i=1:m2
for j=1:m4
ni=1+i;n2j=2+j;
dd(i,2*m2+j)   =ain(ni,n2j);
dd(m2+i,2*m2+j)=amn(ni,n2j);
dd(2*m2+j,i)   =ani(n2j,ni);
dd(2*m2+j,m2+i)=anm(n2j,ni);
end;end
%
for i=1:m4
for j=1:m4
dd(2*m2+i,2*m2+j)=ann(2+i,2+j);
end;end
%-----------------------------------------------------------------------
% in this subroutine enforce diaphragm-diaphragm boundary conditions
ibc = 1
bb=zeros(8,8);bd=zeros(8,(3*m-8));
for i=1:8
bb(i,i)=1;
end
% conditions at tee=teelo
tee=x(1);
st=sin(tee);
ct=cos(tee);
z=1.+gam*ct;
% eqn n_theta = 0
bb(1,1)=a1(1,1)-pr*gam*st/z;
bb(1,2)=a1(1,m);
bb(1,3)=-pr*amu/z;
bb(1,5)=1+pr*gam*ct/z;
% special eqn at station 2
tee=x(2);
st=sin(tee);
ct=cos(tee);
z=1.+gam*ct;
% eqn m_theta = 0
bb(6,1)=a1(2,1)-pr*gam*st/z;
bb(6,2)=a1(2,m);
```

```
bb(6,3)=-pr*amu*gam*ct/(z*z);
bb(6,5)=-a2(2,1)   +pr*gam*(st/z)*a1(2,1)+pr*amu2/(z*z);
bb(6,6)=-a2(2,2)   +pr*gam*(st/z)*a1(2,2);
bb(6,7)=-a2(2,m1) +pr*gam*(st/z)*a1(2,m1);
bb(6,8)=-a2(2,m)   +pr*gam*(st/z)*a1(2,m);
% eqn n_theta= 0 and then m_theta=0  - u for both  w for last
for i=2:m1
bd(1,(i-1))=a1(1,i);
bd(6,(i-1))=a1(2,i);
end
for i=3:m2
bd(6,(2*m-6+i))=-a2(2,i)+pr*gam*(st/z)*a1(2,i);
end
%
% conditions at tee=teehi
tee=x(m);
st=sin(tee);
ct=cos(tee);
z=1+gam*ct;
% eqn n_theta = 0
bb(2,1)=a1(m,1);
bb(2,2)=a1(m,m)-pr*gam*st/z;
bb(2,4)=-pr*amu/z;
bb(2,8)=1+pr*gam*ct/z;
% special eqn at station m1
tee=x(m1);
st=sin(tee);
ct=cos(tee);
z=1+gam*ct;
% eqn m_theta = 0
bb(7,1)=a1(m1,1);
bb(7,2)=a1(m1,m)-pr*gam*st/z;
bb(7,4)=-pr*amu*gam*ct/(z*z);
bb(7,5)=-a2(m1,1)   +pr*gam*(st/z)*a1(m1,1);
bb(7,6)=-a2(m1,2)   +pr*gam*(st/z)*a1(m1,2);
bb(7,7)=-a2(m1,m1) +pr*gam*(st/z)*a1(m1,m-1);
bb(7,8)=-a2(m1,m)   +pr*gam*(st/z)*a1(m1,m)+pr*amu2/(z*z);
% eqn  n_theta=0  and then  m_theta=0  - u for both  w for last
for i=2:m1
bd(2,(i-1))=a1(m,i);
bd(7,(i-1))=a1(m1,i);
end
for i=3:m2
bd(7,(2*m-6+i))=-a2(m1,i)+pr*gam*(st/z)*a1(m1,i);
end
%-----------------------------------------------------------------------
% subroutine eigen for diaphragm support
l1=inv(bb);
l2=l1*bd;
l3=db*l2;
l4=dd-l3;
```

```
l5=-l4;
e=eig(l5);
%
mm=0;
for i=1:(3*m-8);
if imag(e(i)) == 0
if e(i)> 0
   mm=mm+1;
   l(mm)=e(i);
   end
   end
end
% output the smallest eigenvalue
k=min(l);
freq=sqrt(fact*k)
%-----------------------------------------------------------------
% in this subroutine enforce clamped-clamped boundary conditions
ibc = 2
clear bb; clear bd; clear l1; clear l2; clear l3; clear l4, clear l5;
clear e; clear l; clear k; clear freq;
bb=zeros(8,8);bd=zeros(8,(3*m-8));
for i=1:8
bb(i,i)=1;
end
% eqns 6 7 for slope condition
bb(6,1)=-1;
bb(6,5)=a1(2,1);    bb(7,5)=a1(m1,1);
bb(6,6)=a1(2,2);    bb(7,6)=a1(m1,2);
bb(6,7)=a1(2,m1);  bb(7,7)=a1(m1,m1);
bb(6,8)=a1(2,m);    bb(7,8)=a1(m1,m);
bb(7,2)=-1;
%
for i=1:m4
bd(6,2*m-4+i)=a1(2,i+2);
bd(7,2*m-4+i)=a1(m1,i+2);
end
%-----------------------------------------------------------------
% subroutine eigen for clamped boundary conditions
l1=inv(bb);
l2=l1*bd;
l3=db*l2;
l4=dd-l3;
l5=-l4;
e=eig(l5);
%
mm=0;
for i=1:(3*m-8);
if imag(e(i)) == 0
if e(i)> 0
   mm=mm+1;
   l(mm)=e(i);
```

```
   end
   end
end
% output the smallest eigenvalue
k=min(l);
freq=sqrt(fact*k)
%-----------------------------------------------------------------
% in this subroutine enforce free-free boundary conditions
ibc = 3
clear bb; clear bd; clear l1; clear l2; clear l3; clear l4, clear l5;
clear e; clear l; clear k; clear freq;
bb=zeros(8,8);bd=zeros(8,(3*m-8));
% ******************** ****************** ****
% the following is for free boundary conditions
% eqns 1 2  N_theta=0,   eqns 6 7  M_theta = 0
% eqns 3 4  T_theta=0,   eqns 5 8  V_theta = 0  New wrt ss
% conditions at tee=teelo
tee=x(1);
st=sin(tee);
ct=cos(tee);
ct2=ct*ct;
z=1.+gam*ct;
zm1=1/z;
zm2=1/(z*z);
zm3=zm1*zm2;
% eqn n_theta = 0
bb(1,1)=a1(1,1)-pr*gam*st/z;
bb(1,2)=a1(1,m);
bb(1,3)=-pr*amu/z;
bb(1,5)=1+pr*gam*ct/z;
% eqn t_theta = 0
bb(3,1)=amu*(gee*thic*rs2*zm1+deep*gam*zm2*ct);
bb(3,3)=(gee*thic*rs2+deep*gam2*zm2*ct2)*a1(1,1);
bb(3,3)=bb(3,3)+gee*thic*gam*rs2*zm1*st;
bb(3,4)=(gee*thic*rs2+deep*gam2*zm2*ct2)*a1(1,m);
bb(3,5)=-amu*deep*gam*zm2*ct*a1(1,1)-amu*deep*gam*zm3*st*ct;
bb(3,6)=-amu*deep*gam*zm2*ct*a1(1,2);
bb(3,7)=-amu*deep*gam*zm2*ct*a1(1,m1);
bb(3,8)=-amu*deep*gam*zm2*ct*a1(1,m);
% eqn v_theta = 0
bb(5,1)=-amu2*deep*zm2;
bb(5,3)=-amu*deep*gam*zm2*ct*a1(1,1);
bb(5,4)=-amu*deep*gam*zm2*ct*a1(1,m);
var1=dee+deep;
bb(5,5)=-dee*a3(1,1) +dee*gam*zm1*st*a2(1,1) +amu2*zm2*var1*a1(1,1);
bb(5,5)=bb(5,5)+amu2*zm3*(2*gam*dee+deep)*st;
bb(5,6)=-dee*a3(1,2) +dee*gam*zm1*st*a2(1,2) +amu2*zm2*var1*a1(1,2);
bb(5,7)=-dee*a3(1,m1)+dee*gam*zm1*st*a2(1,m1)+amu2*zm2*var1*a1(1,m1);
bb(5,8)=-dee*a3(1,m) +dee*gam*zm1*st*a2(1,m) +amu2*zm2*var1*a1(1,m);
% bd array
for i=2:m1
```

```
bd(1,(i-1))=a1(1,i);
bd(3,(m-3+i))=(gee*thic*rs2+deep*gam2*zm2*ct2)*a1(1,i);
bd(5,(m-3+i))=-amu*deep*gam*zm2*ct*a1(1,i);
end
for i=3:m2
bd(3,2*m-6+i)=-amu*deep*gam*zm2*ct*a1(1,i);
bd(5,2*m-6+i)=-dee*a3(1,i)+dee*gam*zm1*st*a2(1,i)+amu2*zm2*var1*a1(1,i);
end
% special equation at station 2
tee=x(2);
st=sin(tee);
ct=cos(tee);
ct2=ct*ct;
z=1.+gam*ct;
zm1=1/z;
% eqn m_theta = 0
bb(6,1)=a1(2,1)-pr*gam*st*zm1;
bb(6,2)=a1(2,m);
bb(6,3)=-pr*amu*gam*ct*zm2;
bb(6,5)=-a2(2,1)   +pr*gam*(st/z)*a1(2,1)+pr*amu2*zm2;
bb(6,6)=-a2(2,2)   +pr*gam*(st/z)*a1(2,2);
bb(6,7)=-a2(2,m1)  +pr*gam*(st/z)*a1(2,m1);
bb(6,8)=-a2(2,m)   +pr*gam*(st/z)*a1(2,m);
% bd array
for i=2:m1
bd(6,(i-1))=a1(2,i);
end
for i=3:m2
bd(6,(2*m-6+i))=-a2(2,i)+pr*gam*(st/z)*a1(2,i);
end
% conditions at tee=teehi
tee=x(m);
st=sin(tee);
ct=cos(tee);
ct2=ct*ct;
z=1+gam*ct;
zm1=1/z;
zm2=zm1*zm1;
zm3=zm2*zm1;
% eqn n_theta = 0
bb(2,1)=a1(m,1);
bb(2,2)=a1(m,m)-pr*gam*st/z;
bb(2,4)=-pr*amu/z;
bb(2,8)=1+pr*gam*ct/z;
% eqn t_theta = 0
bb(4,2)=amu*(gee*thic*rs2*zm1+deep*gam*zm2*ct);
bb(4,3)=(gee*thic*rs2+deep*gam2*zm2*ct2)*a1(m,1);
bb(4,4)=(gee*thic*rs2+deep*gam2*zm2*ct2)*a1(m,m);
bb(4,4)=bb(4,4)+gee*thic*gam*rs2*zm1*st;
bb(4,5)=-amu*deep*gam*zm2*ct*a1(m,1);
bb(4,6)=-amu*deep*gam*zm2*ct*a1(m,2);
```

```
bb(4,7)=-amu*deep*gam*zm2*ct*a1(m,m1);
bb(4,8)=-amu*deep*gam*zm2*ct*a1(m,m)-amu*deep*gam*zm3*st*ct;
% eqn v_theta = 0
bb(8,2)=-amu2*deep*zm2;
bb(8,3)=-amu*deep*gam*zm2*ct*a1(m,1);
bb(8,4)=-amu*deep*gam*zm2*ct*a1(m,m);
var1=dee+deep;
bb(8,5)=-dee*a3(m,1) +dee*gam*zm1*st*a2(m,1) +amu2*zm2*var1*a1(m,1);
bb(8,6)=-dee*a3(m,2) +dee*gam*zm1*st*a2(m,2) +amu2*zm2*var1*a1(m,2);
bb(8,7)=-dee*a3(m,m1)+dee*gam*zm1*st*a2(m,m1)+amu2*zm2*var1*a1(m,m1);
bb(8,8)=-dee*a3(m,m) +dee*gam*zm1*st*a2(m,m) +amu2*zm2*var1*a1(m,m);
bb(8,8)=bb(8,8)+amu2*zm3*(2*gam*dee+deep)*st;
% bd array
for i=2:m1
bd(2,(i-1))=a1(m,i);
bd(4,(m-3+i))=(gee*thic*rs2+deep*gam2*zm2*ct2)*a1(m,i);
bd(8,(m-3+i))=-amu*deep*gam*zm2*ct*a1(m,i);
end
for i=3:m2
bd(4,2*m-6+i)=-amu*deep*gam*zm2*ct*a1(m,i);
bd(8,2*m-6+i)=-dee*a3(m,i)+dee*gam*zm1*st*a2(m,i)+amu2*zm2*var1*a1(m,i);
end
% special equation at station m1
tee=x(m1);
st=sin(tee);
ct=cos(tee);
ct2=ct*ct;
z=1+gam*ct;
zm1=1/z;
zm2=zm1*zm1;
zm3=zm2*zm1;
% eqn m_theta = 0
bb(7,1)=a1(m1,1);
bb(7,2)=a1(m1,m)-pr*gam*st/z;
bb(7,4)=-pr*amu*gam*ct/(z*z);
bb(7,5)=-a2(m1,1)   +pr*gam*(st/z)*a1(m1,1);
bb(7,6)=-a2(m1,2)   +pr*gam*(st/z)*a1(m1,2);
bb(7,7)=-a2(m1,m1)  +pr*gam*(st/z)*a1(m1,m1);
bb(7,8)=-a2(m1,m)   +pr*gam*(st/z)*a1(m1,m)+pr*amu2/(z*z);
% bd array
for i=2:m1
bd(7,(i-1))=a1(m1,i);
end
for i=3:m2
bd(7,(2*m-6+i))=-a2(m1,i)+pr*gam*(st/z)*a1(m1,i);
end
%-----------------------------------------------------------------
% subroutine eigen for free boundary conditions
l1=inv(bb);
l2=l1*bd;
l3=db*l2;
```

```
l4=dd-l3;
l5=-l4;
e=eig(l5);
%
mm=0;
for i=1:(3*m-8);
if imag(e(i)) == 0
if e(i)> 0
   mm=mm+1;
   l(mm)=e(i);
   end
   end
end
% output the smallest eigenvalue
k=min(l);
freq=sqrt(fact*k)
```

Tables

Table 3.1: Description of panel cases

Case	*Divisions*	*Location*	θ_L	θ_H	ψ^{deg}
1	2	*Extrados*	0^o	90^o	15.75^o
2	2	*Intrados*	90^o	180^o	15.75^o
3	4	*Extrados*	0^o	45^o	7.875^o
4	4	*Crown*	45^o	90^o	7.875^o
5	4	*Intrados*	135^o	180^o	7.875^o
6	8	*Extrados*	0^o	22.5^o	3.938^o
7	8	*Crown*	67.50^o	90^o	3.938^o
8	8	*Intrados*	157.5^o	180^o	3.938^o

Table 3.2: Convergence study - fundamental frequencies (premultiplied by 10^{-4})

	Terms in series			*Sampling points in DQM*			*Leissa*
Case	$m = 5$	$m = 15$	$m = 21$	$N = 10$	$N = 15$	$N = 20$	*&Kadi*
1	0.1931	0.1931	0.1931	0.1876	0.1854	0.1854	-
2	0.1150	0.1150	0.1150	0.1160	0.1116	0.1116	-
3	0.4727	0.4727	0.4727	0.3265	0.3264	0.3264	-
4	0.4609	0.4609	0.4609	0.3025	0.3024	0.3024	0.4592
5	0.4639	0.4639	0.4639	0.2635	0.2633	0.2633	-
6	0.5614	0.5614	0.5614	0.5567	0.5567	0.5567	-
7	0.5767	0.5767	0.5767	0.5729	0.5729	0.5729	0.5754
8	0.6363	0.6363	0.6363	0.6379	0.6379	0.6379	-

Table 3.3: Effect of varying δ - fundamental frequencies (premultiplied by 10^{-4})

	Diaphragm (δ *power*)				*Free* (δ *power*)				
Case	-3	-5	-7	-9	-3	-5	-6	-7	-9
1	0.1855	0.1854	0.1854	0.1854	0.0314	0.0314	0.0411	0.2288	0.0141
2	0.1118	0.1116	0.1116	0.1116	0.0531	0.0531	0.0520	0.1040	0.1072
3	0.3266	0.3264	0.3264	0.3264	0.0861	0.0860	0.0774	0.4771	0.3015
4	0.3026	0.3024	0.3024	0.3024	0.0944	0.0945	0.1063	0.3833	0.3138
5	0.2635	0.2633	0.2633	0.2633	0.1473	0.1473	0.1455	0.1622	0.3528
6	0.5568	0.5567	0.5567	0.5567	0.2205	0.2208	0.2009	1.0774	0.3384
7	0.5730	0.5729	0.5729	0.5729	0.2684	0.2686	0.2685	0.7069	0.2722
8	0.6380	0.6379	0.6379	0.6379	0.3953	0.4005	0.7628	0.2121	0.3681

Table 3.4: Convergence of FEM solution - fundamental frequencies (premultiplied by 10^{-4})

Case	10×10	15×15	20×20	30×30	40×40
1	0.2271	0.1877	0.1845	0.1822	0.1814
2	0.1221	-	0.1109	-	0.1080

Table 3.5: Effect of boundary conditions - fundamental frequencies (premultiplied by 10^{-4})

	Diaphragm			*Clamped*		*Free*	
Case	*FS*	*FEM*	*DQM*	*FEM*	*DQM*	*FEM*	*DQM*
1	0.1931	0.1814	0.1854	0.2321	0.2343	0.0761	0.0314
2	0.1150	0.1080	0.1116	0.1808	0.1845	0.0577	0.0531
3	0.4727*	0.3196	0.3264	0.4573	0.4660	0.1221	0.0860
4	0.4609*	0.2956	0.3024	0.4511	0.4601	0.1101	0.0945
5	0.4639*	0.2567	0.2633	0.4651	0.4740	0.1559	0.1473
6	0.5614	0.5459	0.5567	0.9346	0.9506	0.3077	0.2208
7	0.5767	0.5613	0.5729	0.9327	0.9504	0.2713	0.2686
8	0.6363	0.6258	0.6379	0.9589	0.9777	0.4457	0.4005

Table 3.6: Effect of panel thickness - fundamental frequencies (premultiplied by 10^{-4})

	$h/r = 0.005$			$h/r = 0.01$			$h/r = 0.02$		
Case	*FS*	*FEM*	*DQM*	*FS*	*FEM*	*DQM*	*FS*	*FEM*	*DQM*
1	0.1667	0.1395	0.1415	0.1931	0.1814	0.1854	0.2711	0.2397	0.2462
2	0.0583	0.0570	0.0592	0.1150	0.1080	0.1116	0.2291	0.1622	0.1684
3	0.2856	0.2660	0.2705	0.4727*	0.3196	0.3264	0.4924	0.4722	0.4822
4	0.2575	0.2314	0.2355	0.4609*	0.2956	0.3024	0.4929	0.4643	0.4772
5	0.2328	0.1592	0.1624	0.4639*	0.2567	0.2633	0.5113	0.4743	0.4899
6	0.4909	0.4809	0.4892	0.5614	0.5459	0.5567	0.7823	0.7485	0.7695
7	0.4927	0.4730	0.4819	0.5767	0.5613	0.5729	0.8317	0.8023	0.8259
8	0.5155	0.4883	0.4970	0.6363	0.6258	0.6379	0.9805	0.9594	0.9888

Table 3.7: First four natural frequencies for eight panel cases (premultiplied by 10^{-4})

	Mode number			
Case	1	2	3	4
1	0.1931	-	-	-
2	0.1080	0.1391	0.1962	0.2038
3	0.3196	0.4561	0.4624	0.5845
4	0.2956	0.4500	0.4515	0.5579
5	0.2567	0.4540	0.4584	0.6205
6	0.5459	0.8604	0.9840	1.2890
7	0.5614	0.8806	1.0964	1.4218
8	0.6258	0.9542	1.4035	1.7666

Table 4.1: Comparison of results for buckling load - FEM vs shell theory (const. press.)

Case	h	r	R	*Elements* - $\phi \times \theta$	$\lambda - FEM$	$\lambda - Sobel$
A	1	100	400	60x36	46.8	
B	1	100	400	60x48	52.8	50.6
C	1	100	400	60x60	52.3	
D	2	200	400	30x60	74.1	
E	2	200	400	36x60	88.0	81.6
F	2	200	400	60x120	89.6	

Table 4.2: Convergence of FEM results for platform shell

Mesh	*Elements* - $\phi \times \theta$	λ
i	40x24	1.447
ii	60x36	1.363
iii	80x48	1.325

Table 4.3: Effect of loading area and shell thickness on buckling load

Case	h	r	R	*Loaded elements*	$\lambda - FEM$	*React.press.*
1	0.4	80	400	6x6	0.234	1.0
2	0.8	80	400	6x6	1.36	1.0
3	1.6	80	400	6x6	8.15	1.0
4	4.0	80	400	6x6	93.3	1.0
5	0.8	80	400	4x4	0.106	1.0
6	0.8	80	400	2x2	0.0765	1.0
7	4.0	80	400	4x4	8.128	1.0
8	4.0	80	400	2x2	6.912	1.0

Table 4.4: First four buckling loads for eight shell cases

	Buckling load number			
Case	1	2	3	4
1	0.2335	0.2591	0.2898	0.4314
2	-	-	-	-
3	8.154	8.817	13.21	14.51
4	93.31	100.4	13.86	16.81
5	1.058	1.105	1.736	1.849
6	0.7653	0.8085	1.1691	-
7	81.27	83.97	123.2	144.0
8	69.12	6.17	119.21	-

Figures

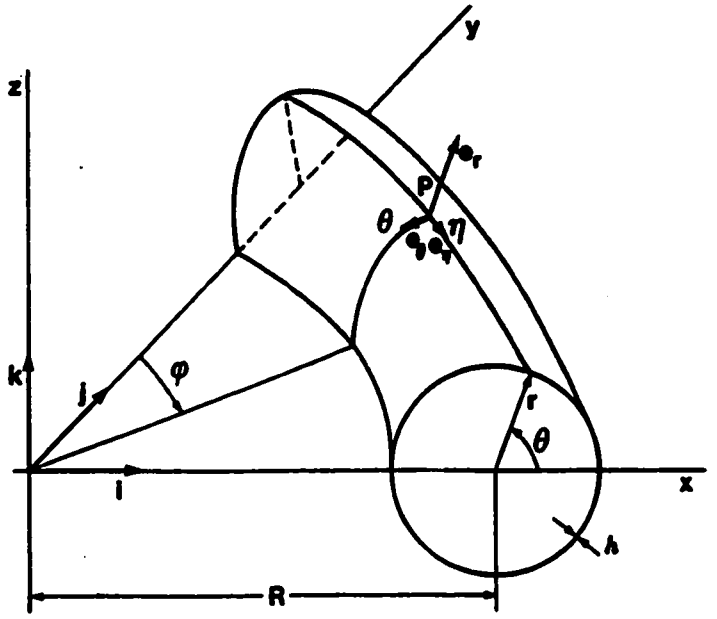

Figure 1.1: Toroidal coordinate system

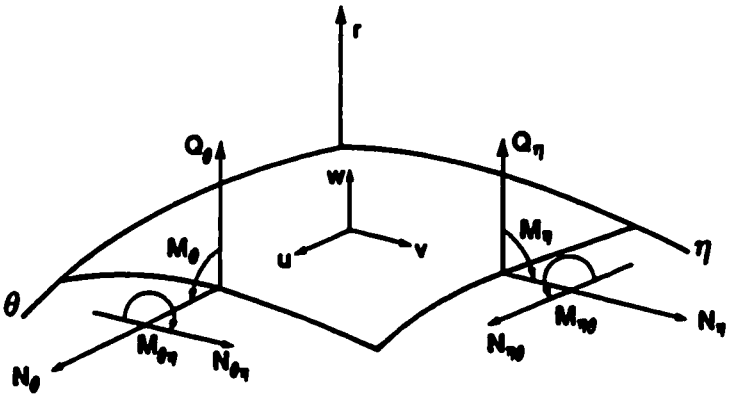

Figure 1.2: Displacement components and stress resultants

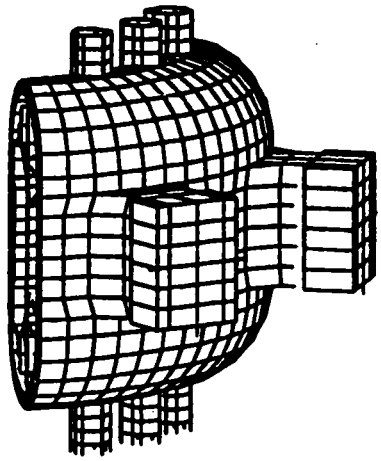

Figure 1.3: TOKAMAK breeder reactor

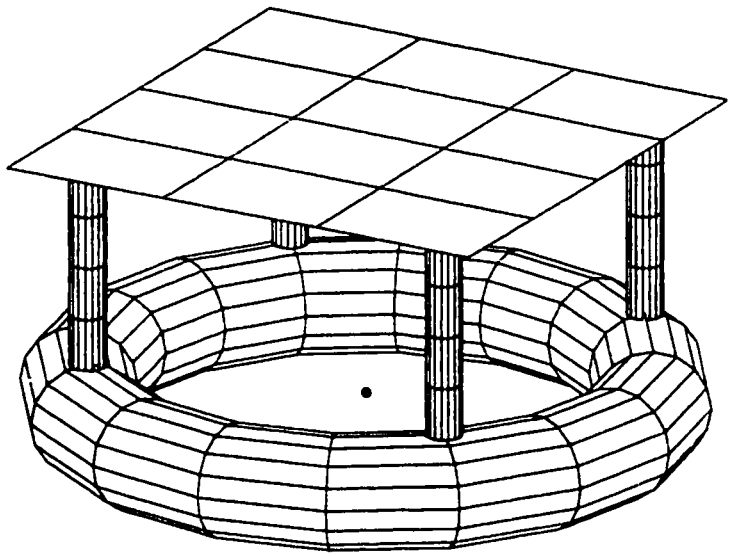

Figure 1.4: Floating toroidal shell with platform

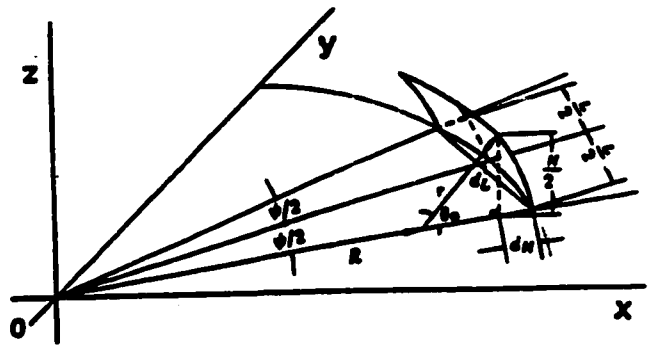

Figure 3.1: Geometry for toroidal panel

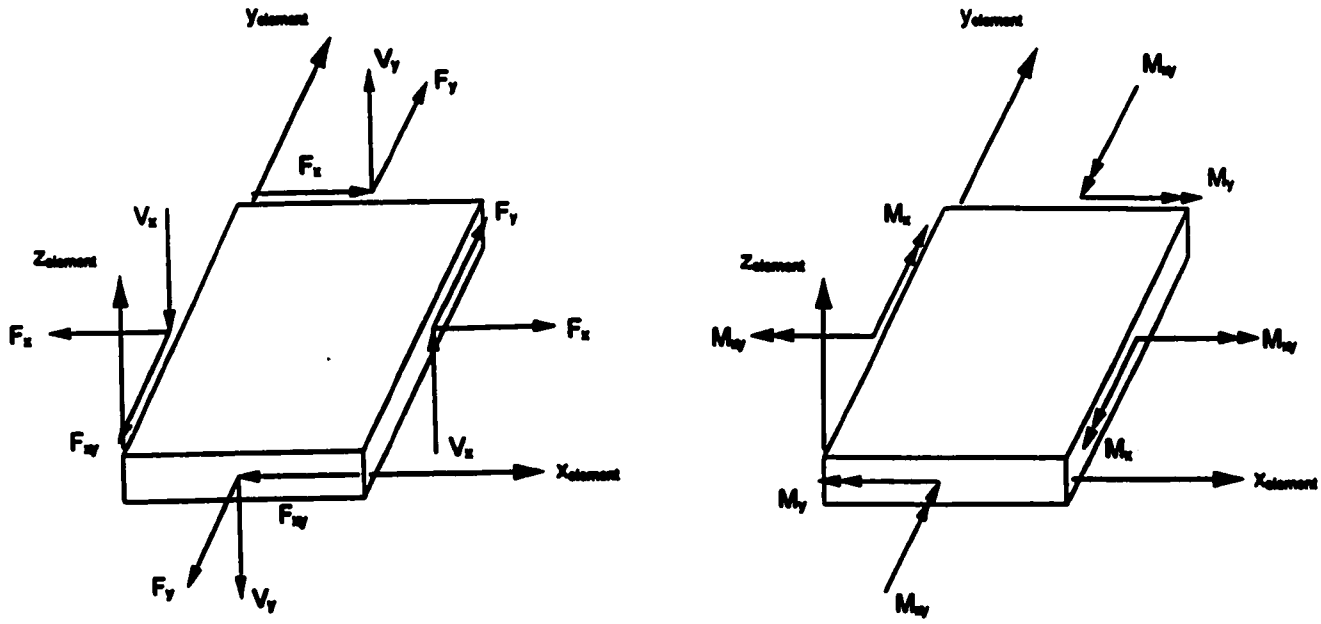

Figure 3.2: Forces and moments in CQUADR element

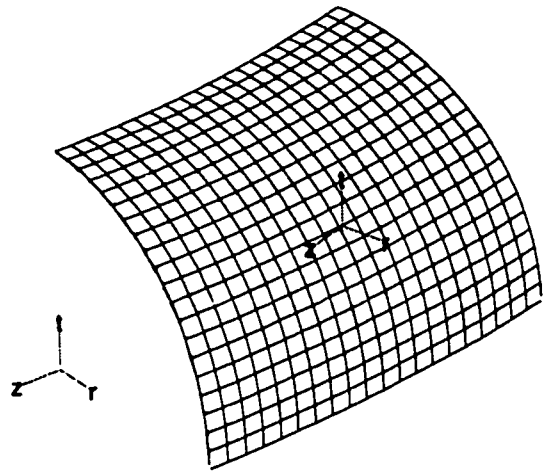

Figure 3.3: Sample coarse FEM mesh for panel at extrados

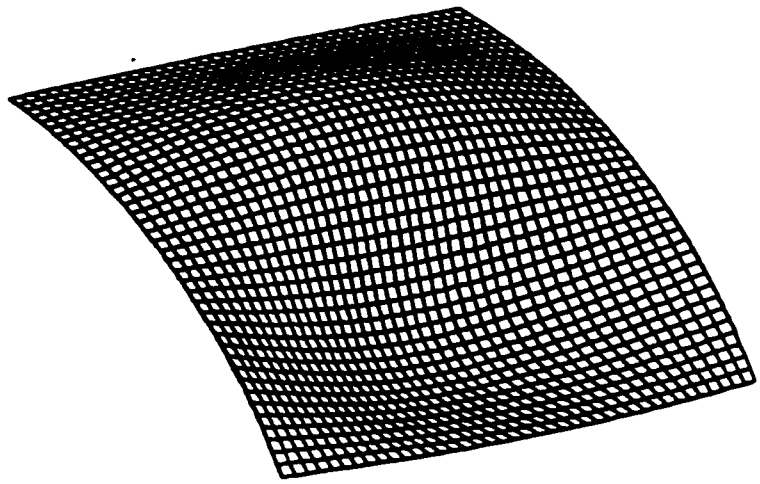

Figure 3.4: Sample fine FEM mesh for panel at crown

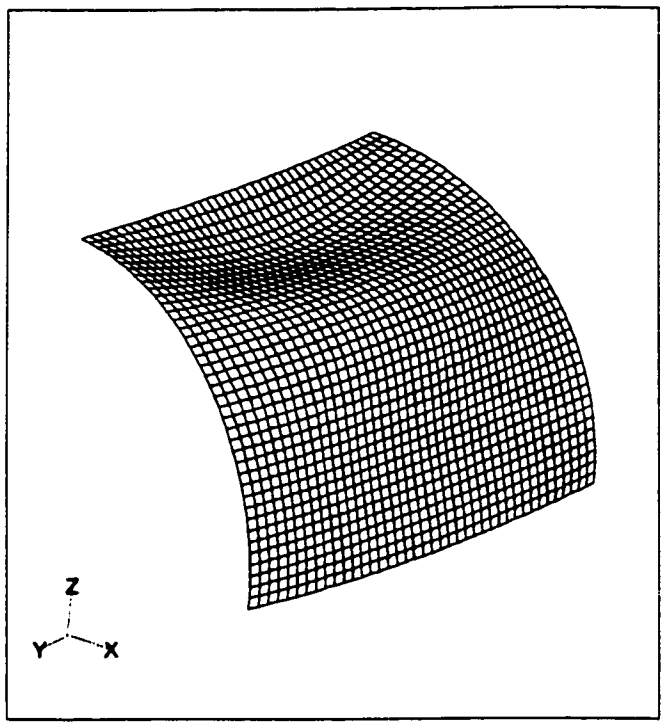

Figure 3.5a: Case1 - mode shape 1

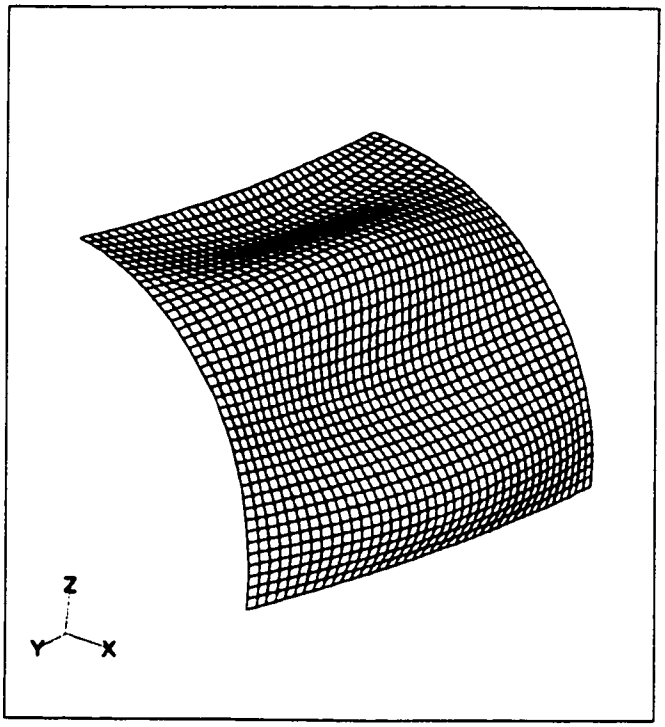

Figure 3.5b: Case1 - mode shape 2

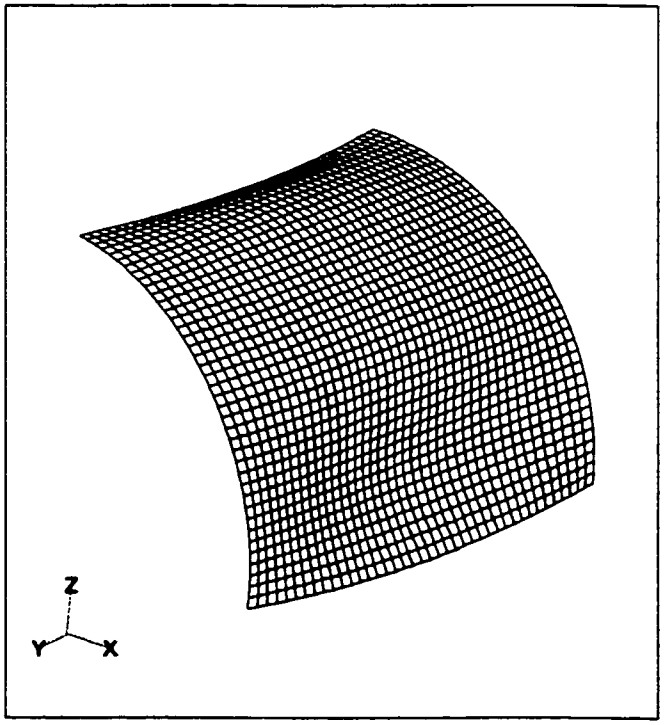

Figure 3.5c: Case1 - mode shape 3

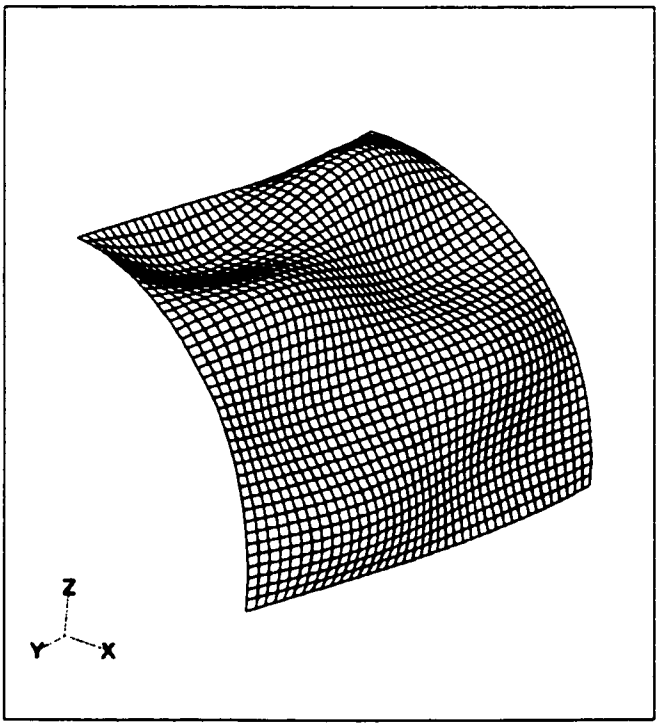

Figure 3.5d: Case1 - mode shape 4

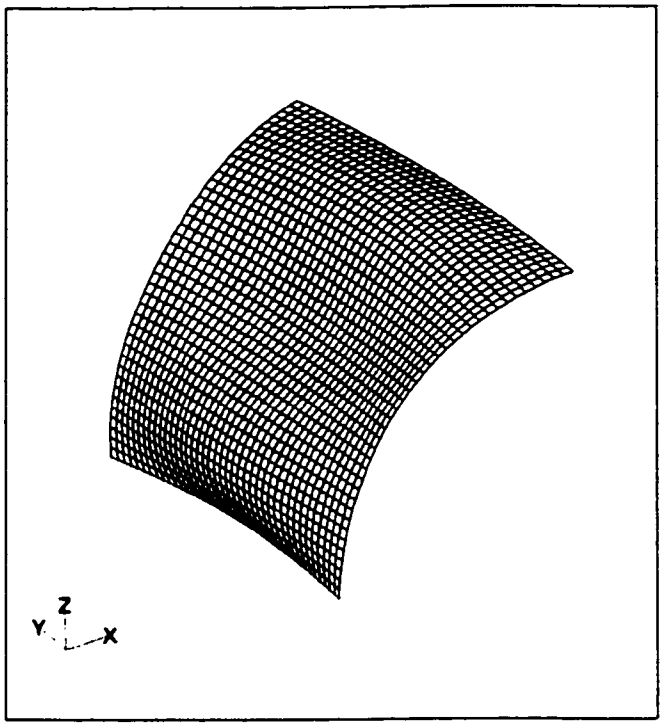

Figure 3.6a: Case2 - mode shape 1

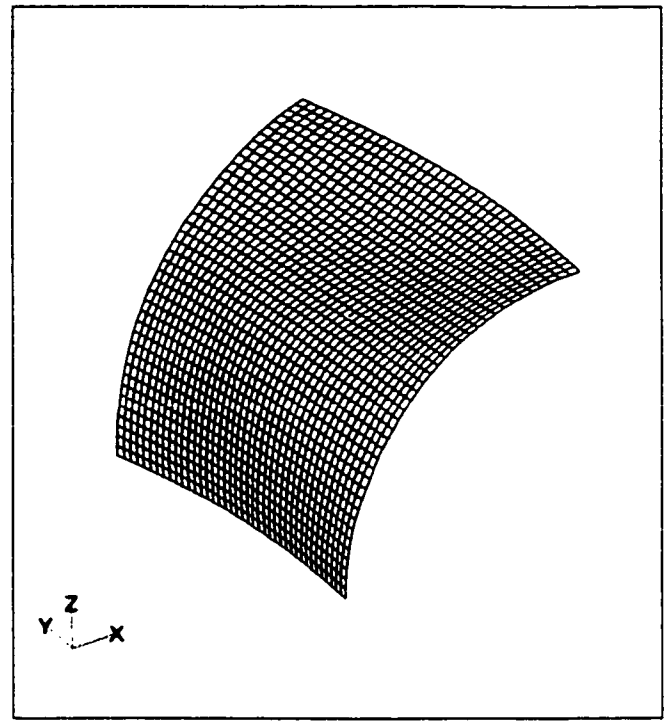

Figure 3.6b: Case2 - mode shape 2

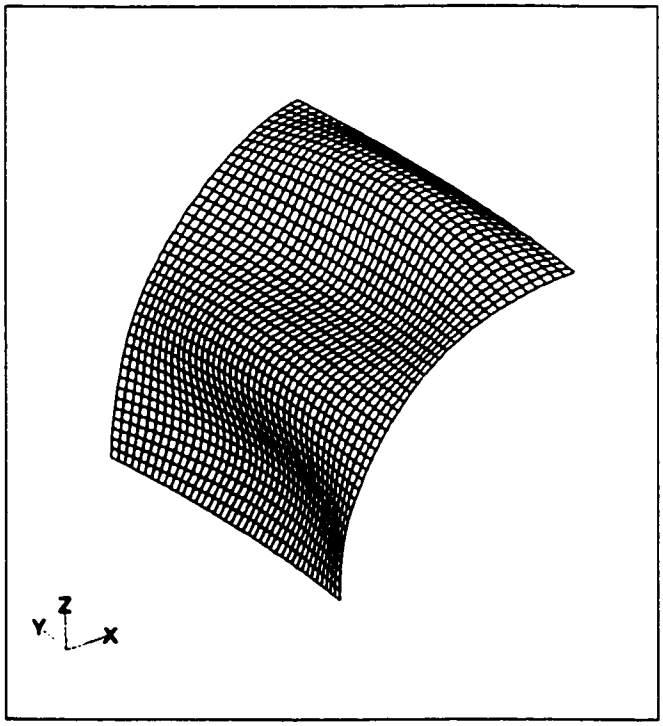

Figure 3.6c: Case2 - mode shape 3

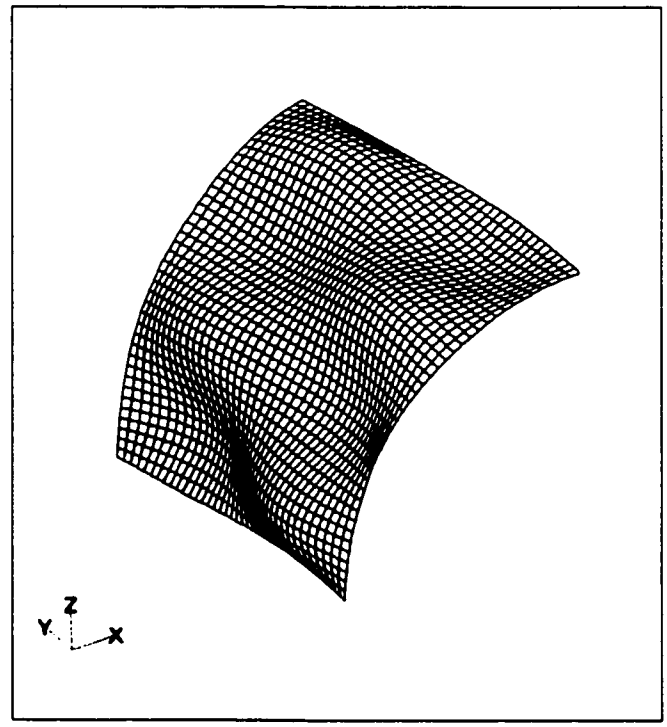

Figure 3.6d: Case2 - mode shape 4

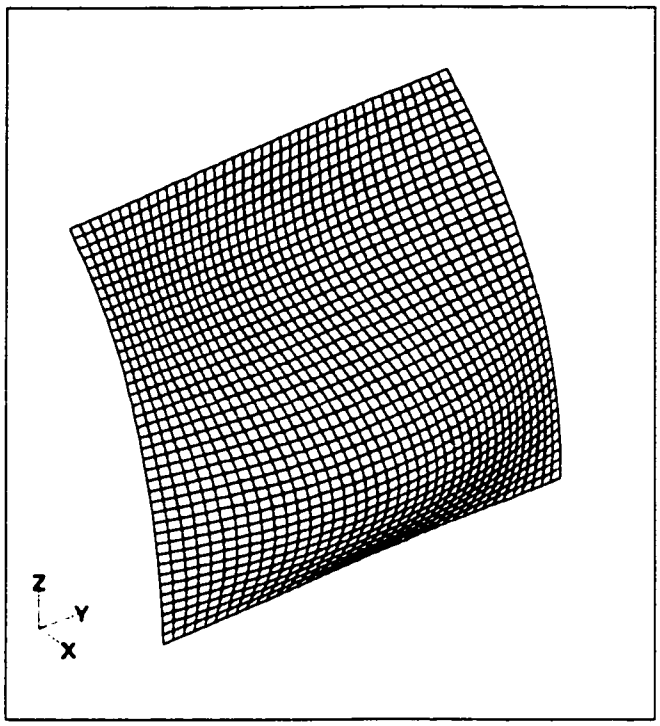

Figure 3.7a: Case 3 - mode shape 1

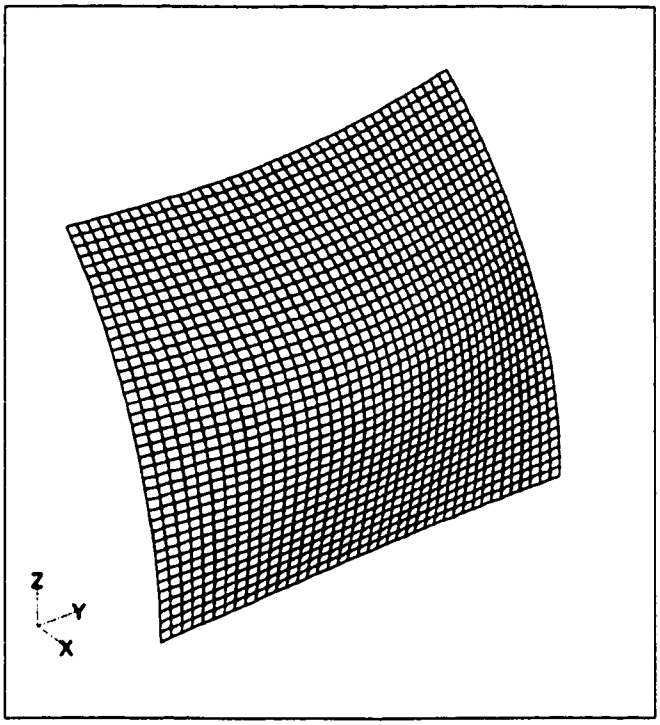

Figure 3.7b: Case 3 - mode shape 2

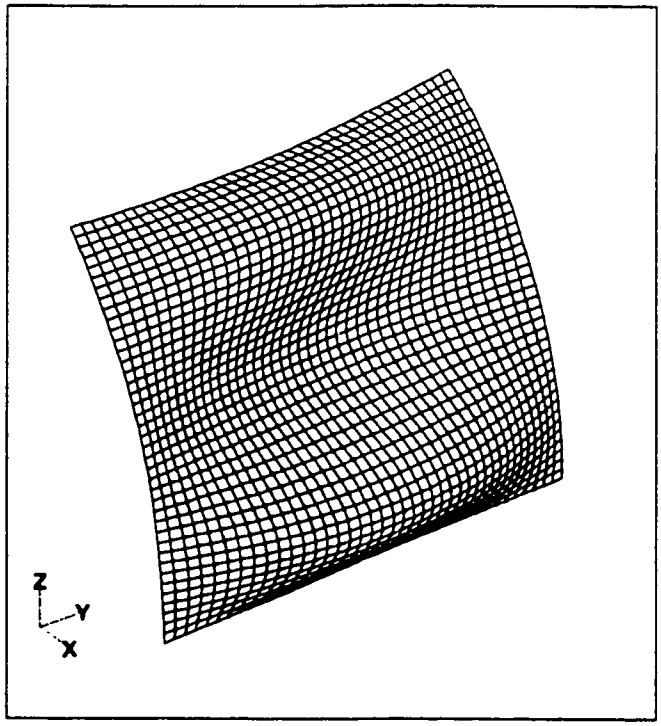

Figure 3.7c: Case 3 - mode shape 3

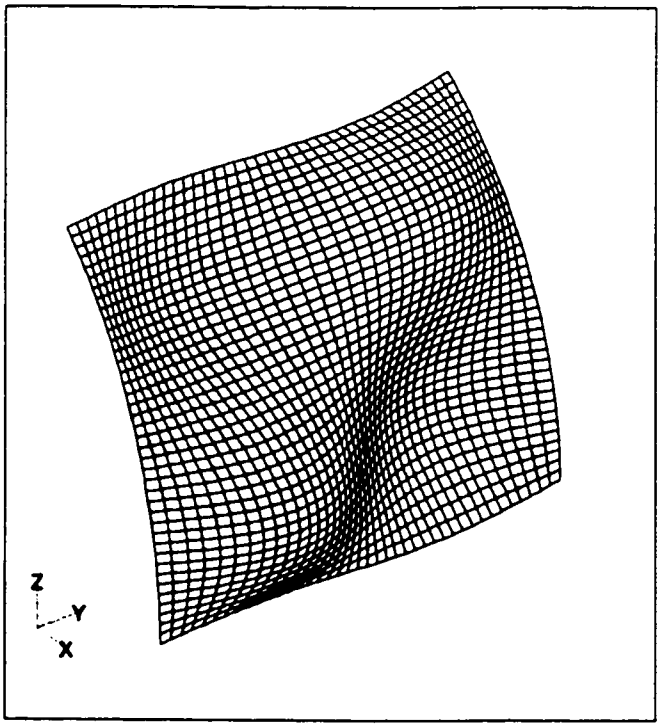

Figure 3.7d: Case 3 - mode shape 4

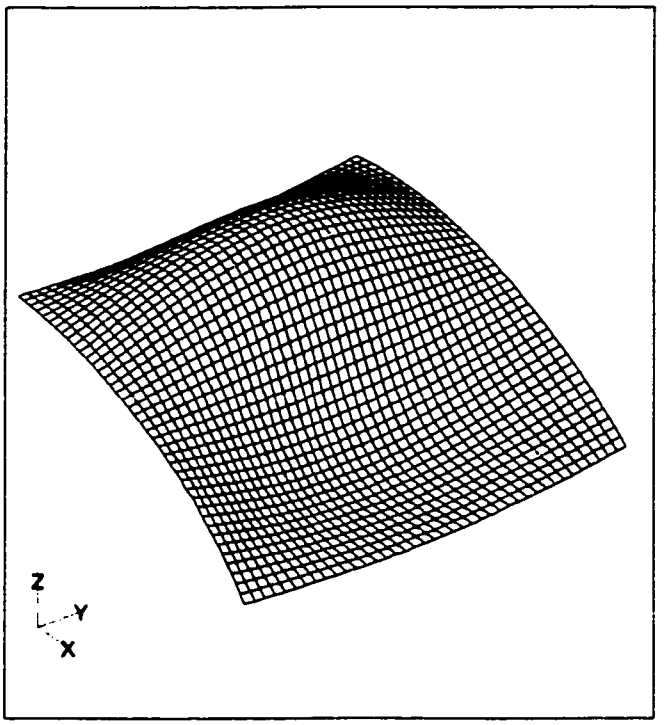

Figure 3.8a: Case 4 - mode shape 1

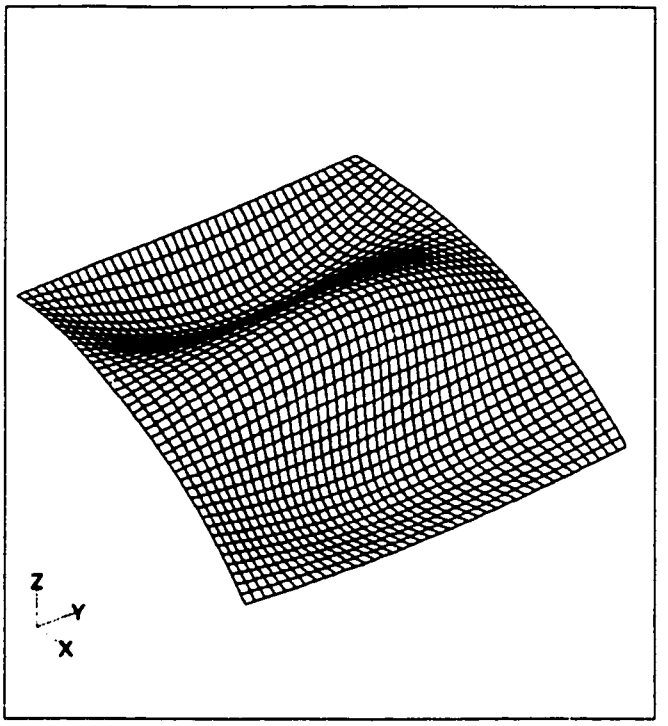

Figure 3.8b: Case 4 - mode shape 2

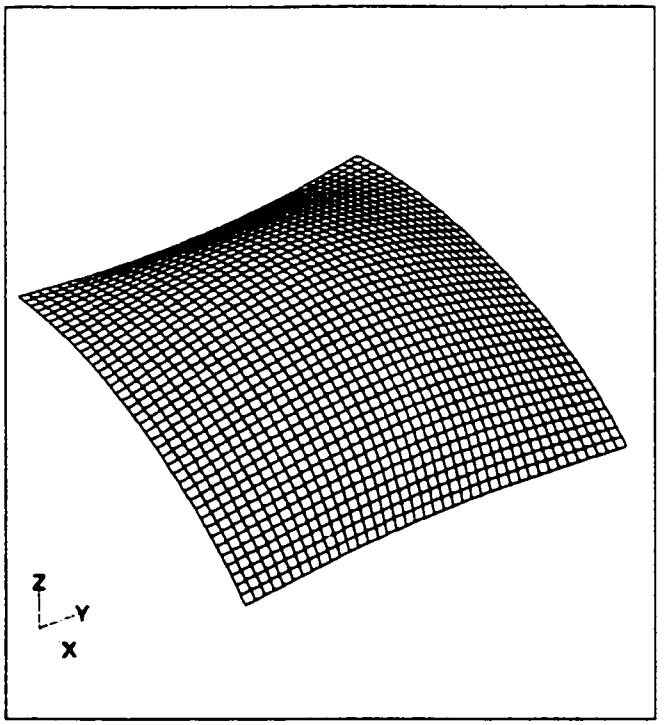

Figure 3.8c: Case 4 - mode shape 3

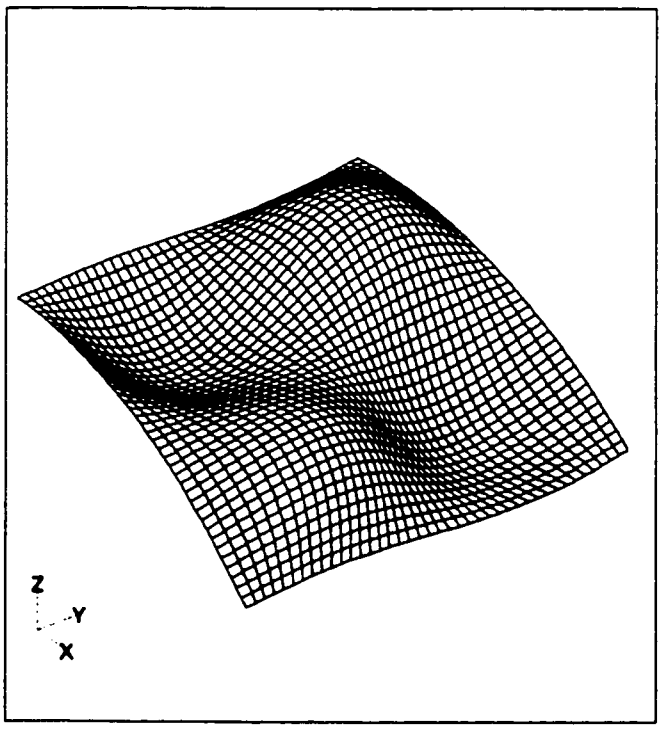

Figure 3.8d: Case 4 - mode shape 4

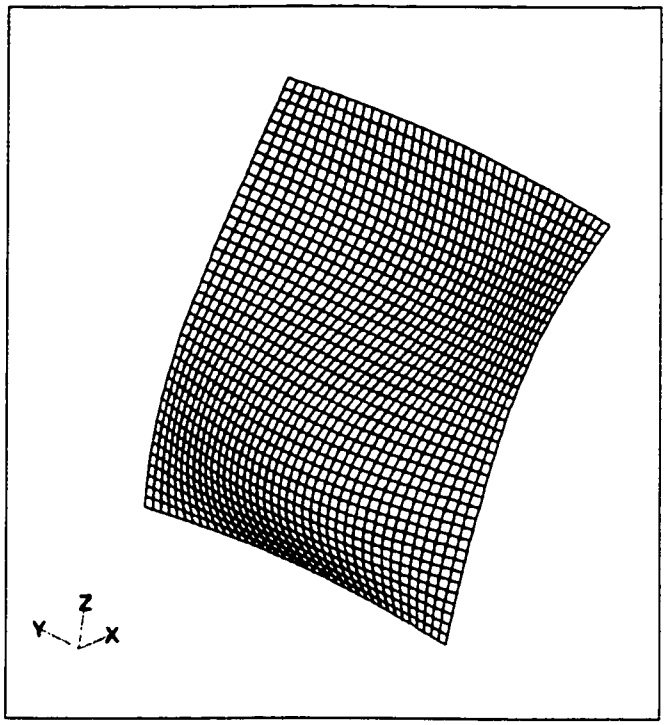

Figure 3.9a: Case 5 - mode shape 1

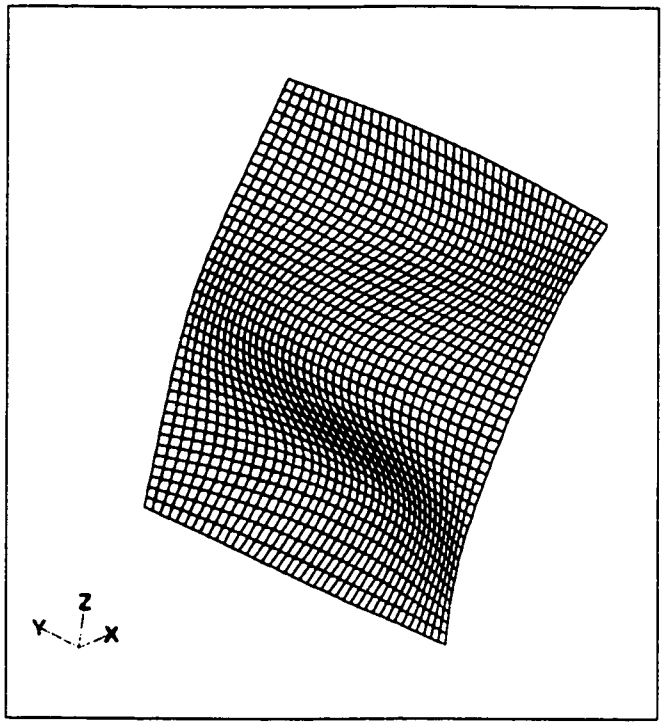

Figure 3.9b: Case 5 - mode shape 2

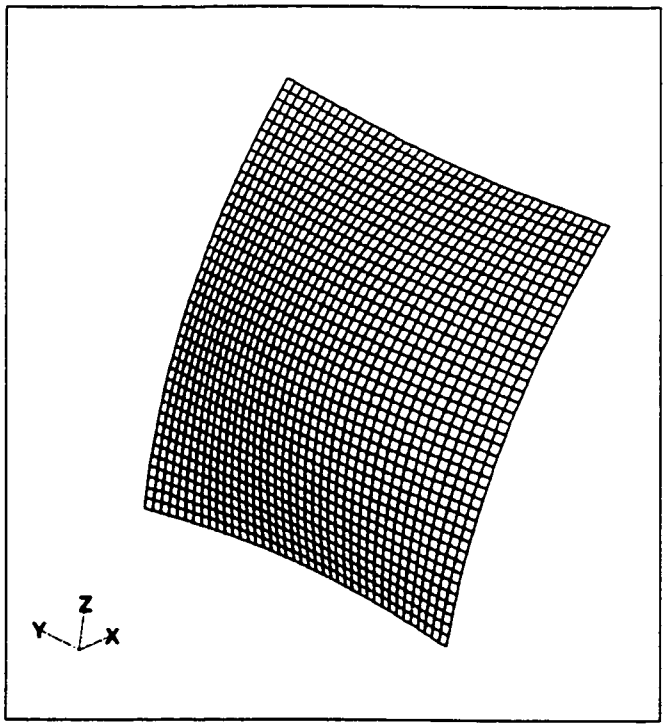

Figure 3.9c: Case 5 - mode shape 3

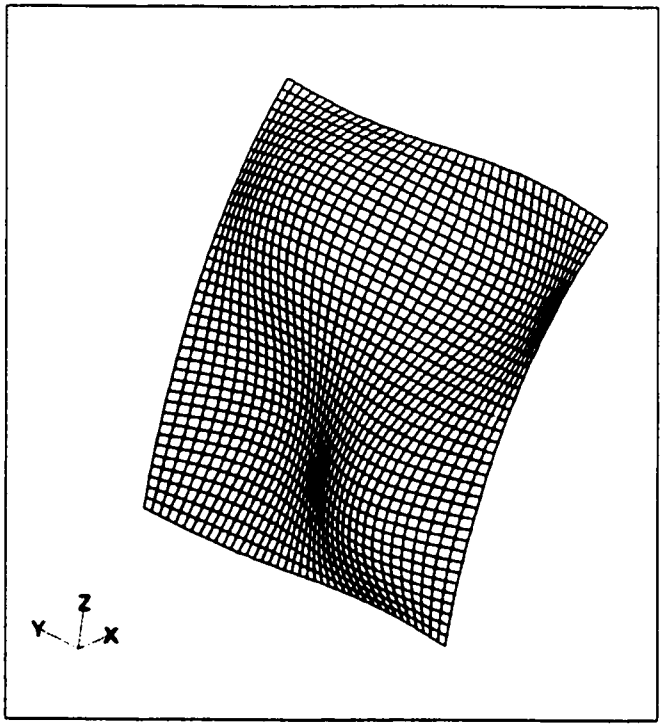

Figure 3.9d: Case 5 - mode shape 4

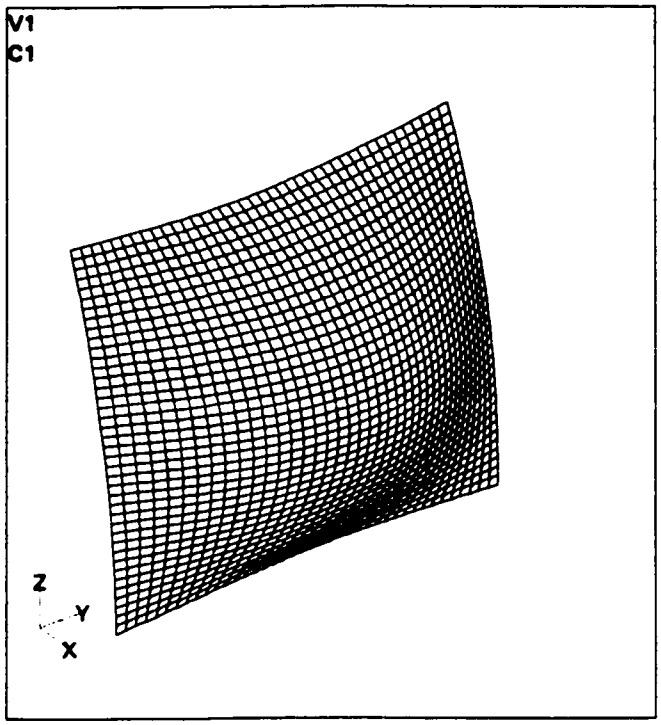

Figure 3.10a: Case 6 - mode shape 1

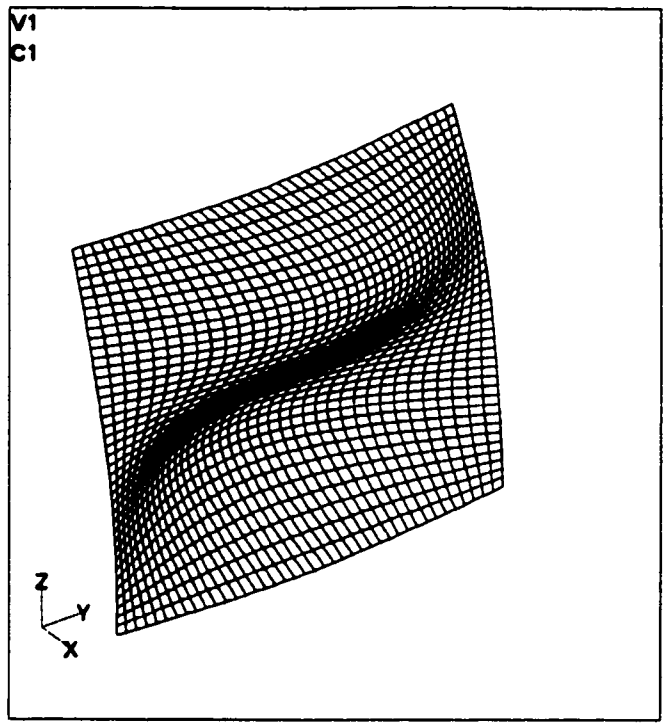

Figure 3.10b: Case 6 - mode shape 2

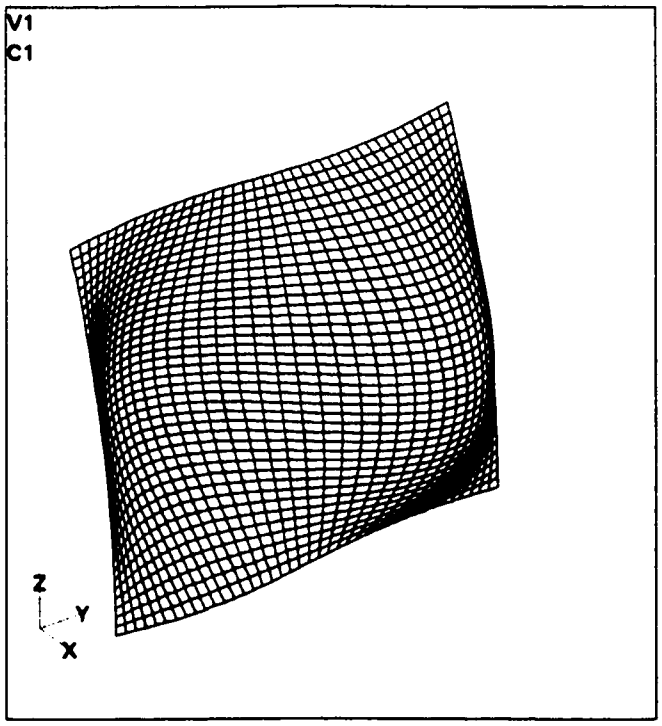

Figure 3.10c: Case 6 - mode shape 3

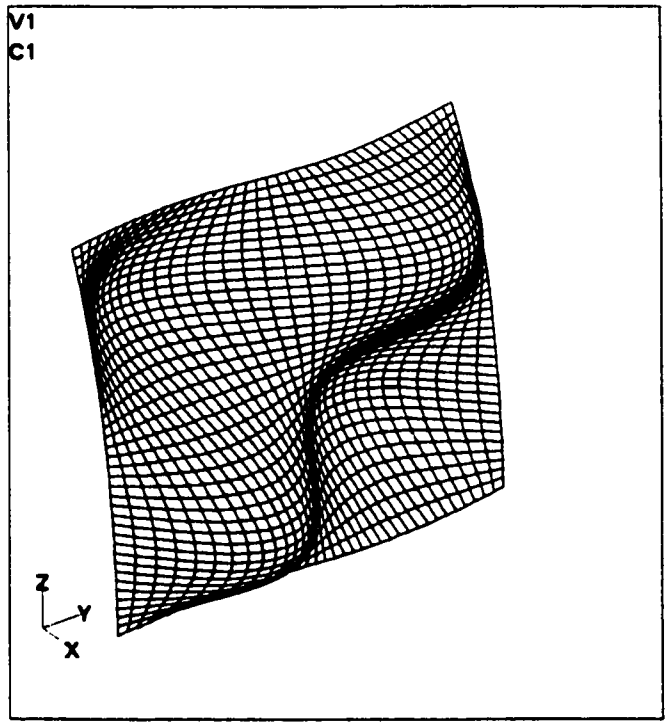

Figure 3.10d: Case 6 - mode shape 4

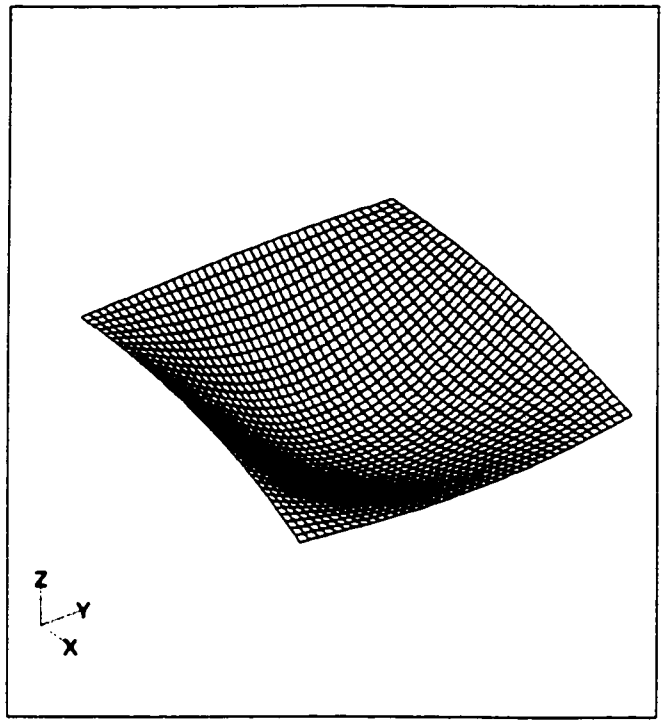

Figure 3.11a: Case 7 - mode shape 1

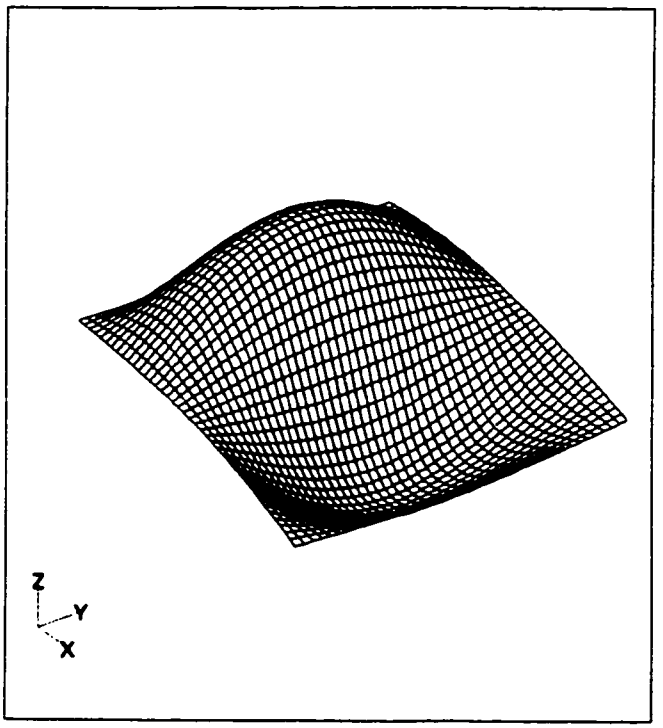

Figure 3.11b: Case 7 - mode shape 2

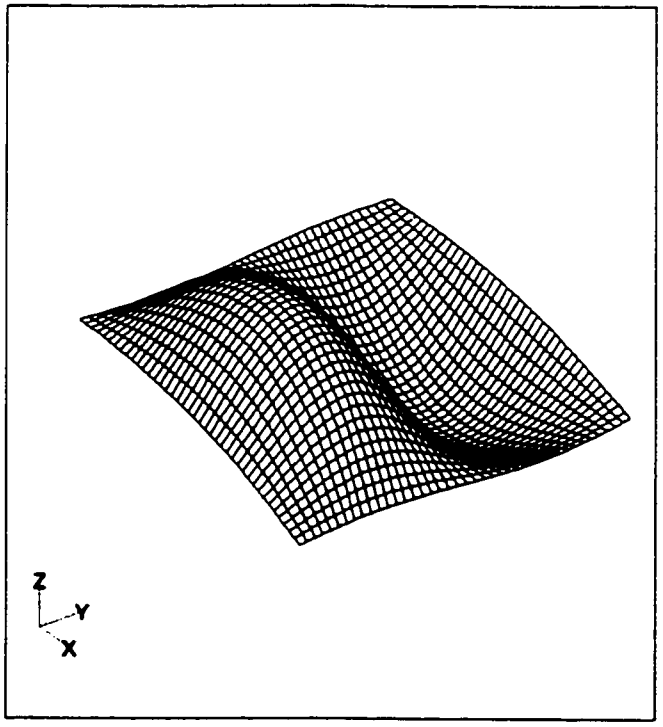

Figure 3.11c: Case 7 - mode shape 3

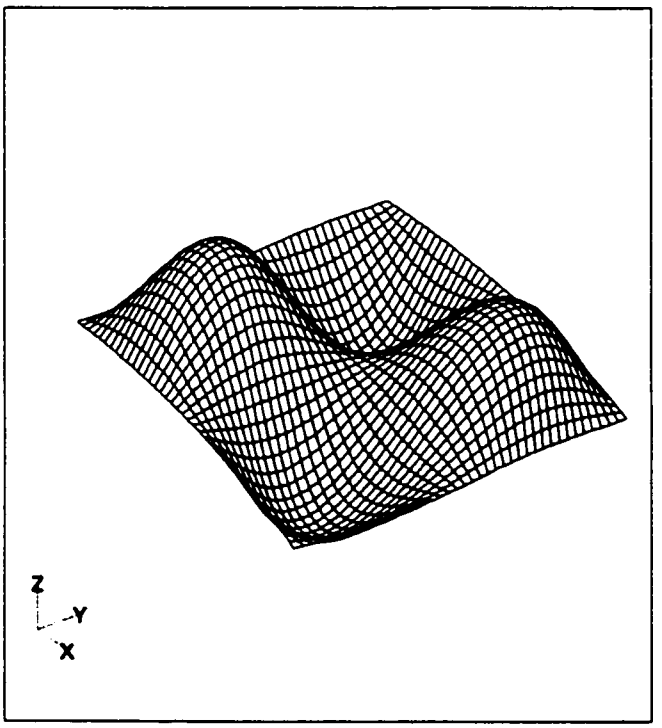

Figure 3.11d: Case 7 - mode shape 4

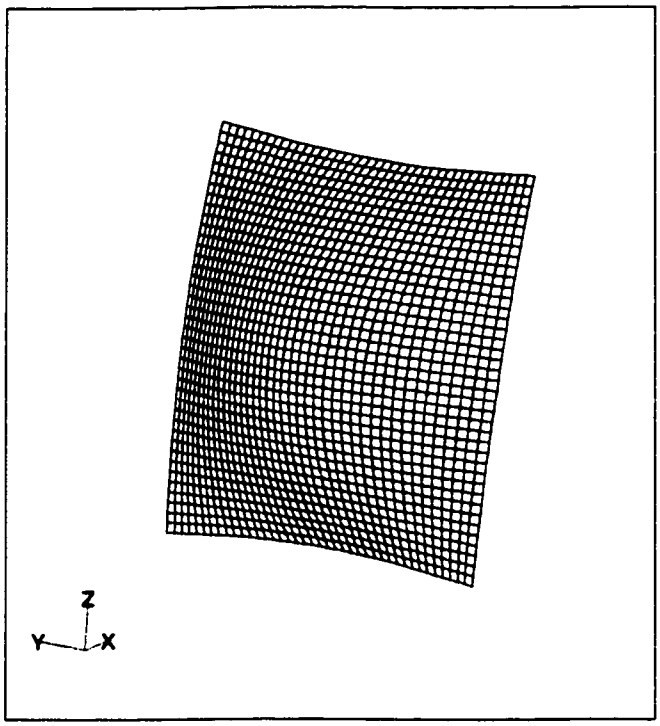

Figure 3.12a: Case 8 - mode shape 1

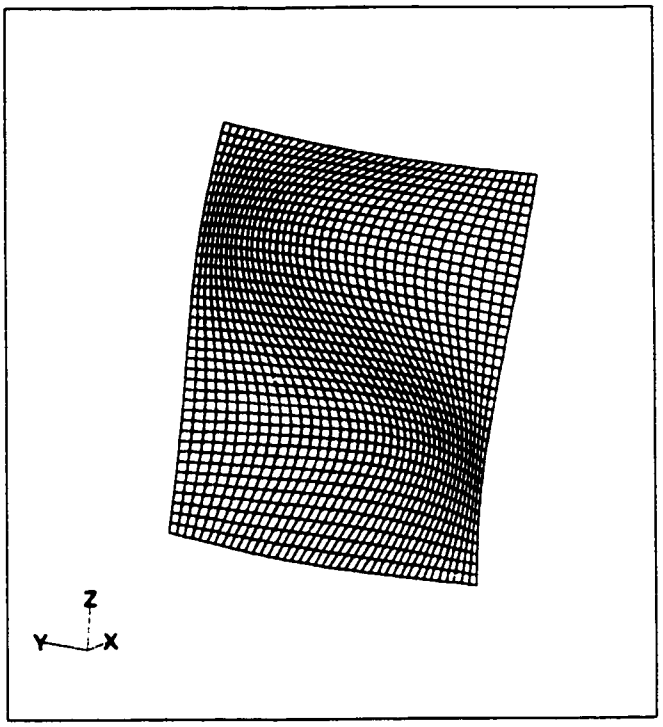

Figure 3.12b: Case 8 - mode shape 2

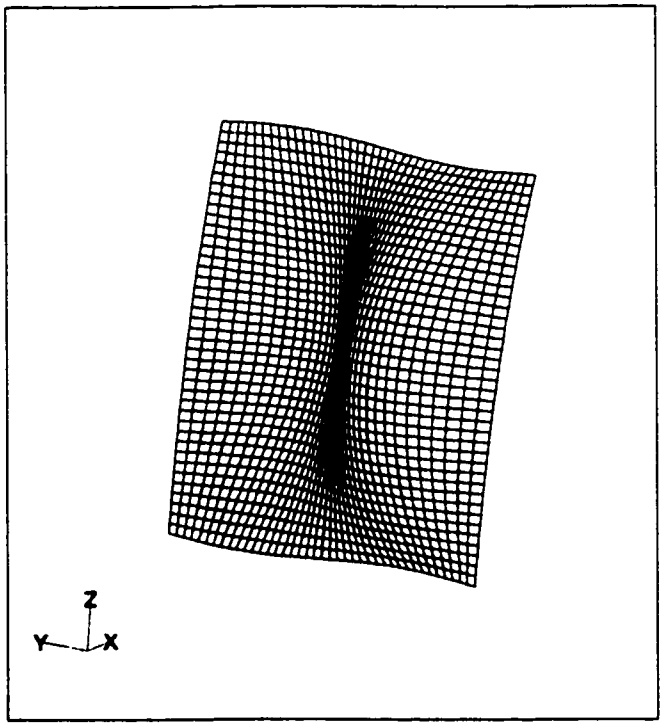

Figure 3.12c: Case 8 - mode shape 3

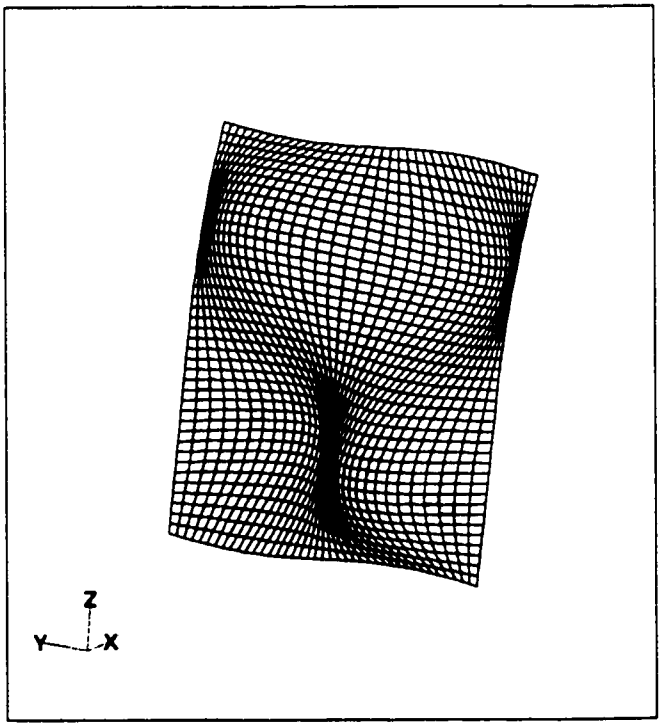

Figure 3.12d: Case 8 - mode shape 4

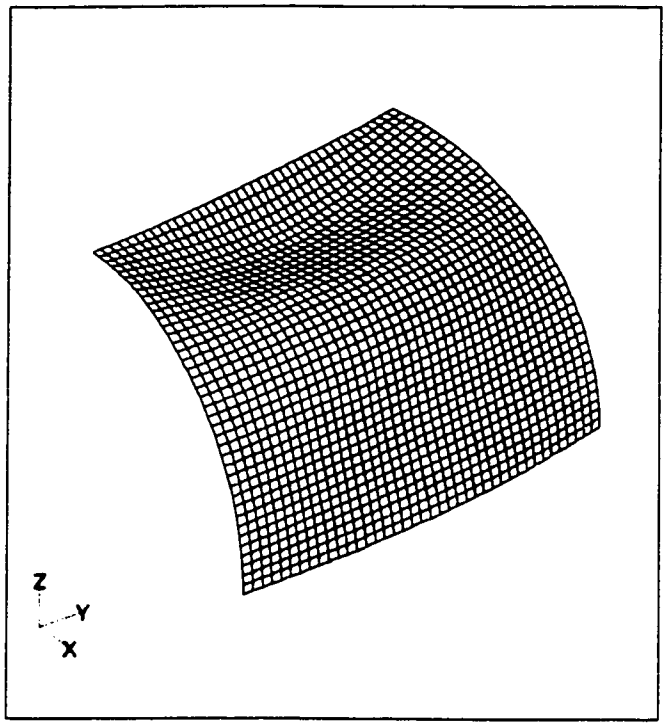

Figure 3.13a: Case 1 - diaphragm meridional support

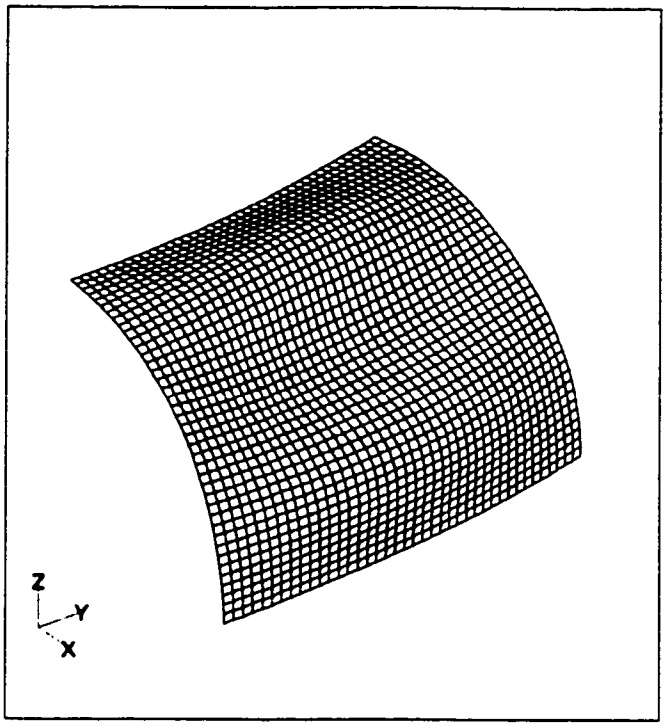

Figure 3.13b: Case 1 - clamped meridional support

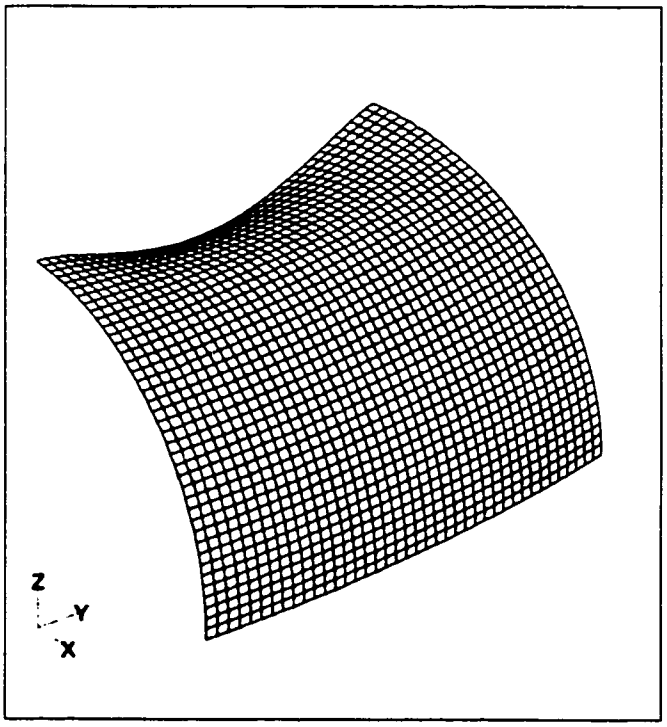

Figure 3.13c: Case 1 - free meridional support

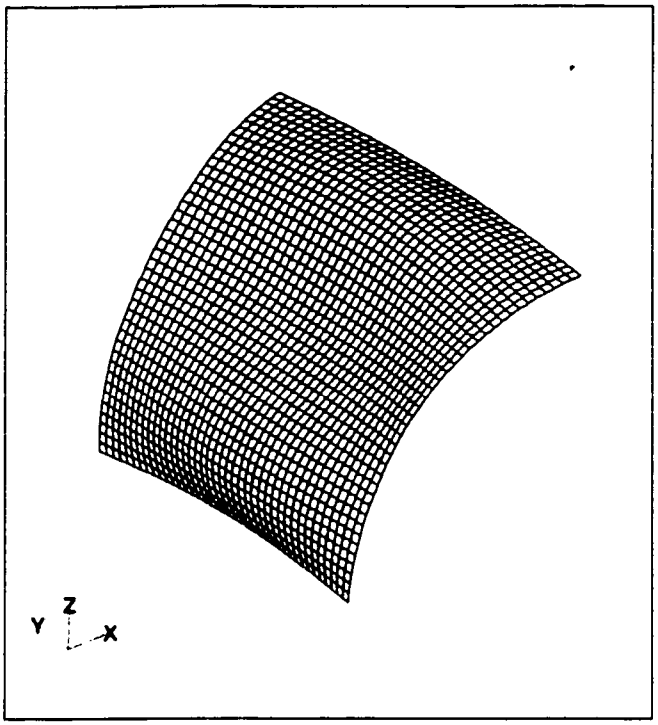

Figure 3.14a: Case 2 - diaphragm meridional support

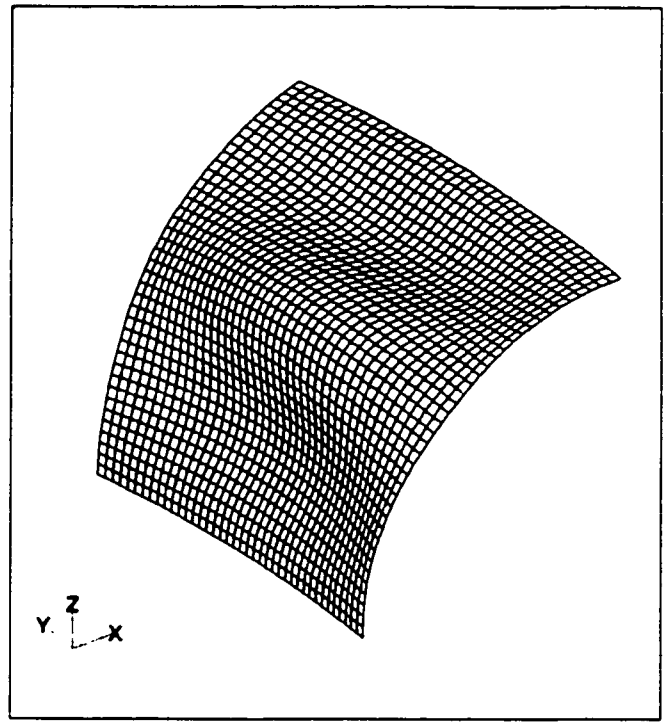

Figure 3.14b: Case 2 - clamped meridional support

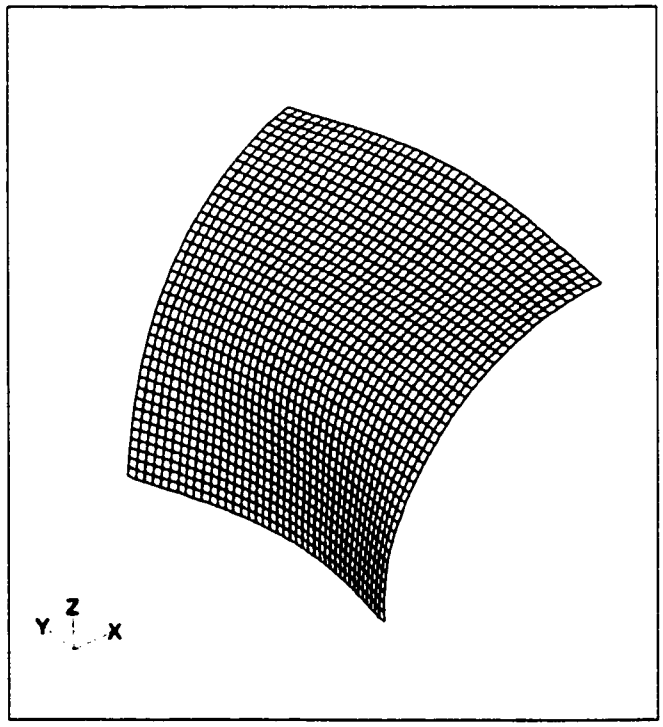

Figure 3.14c: Case 2 - free meridional support

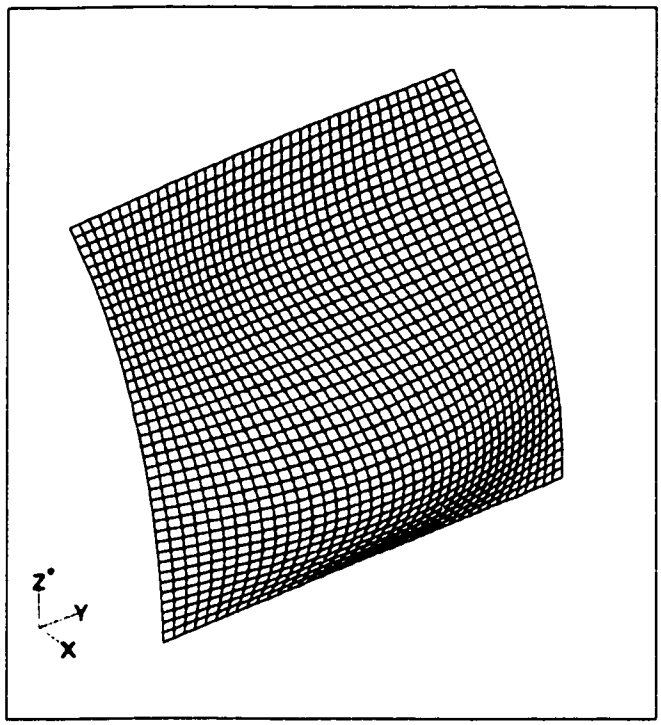

Figure 3.15a: Case 3 - diaphragm meridional support

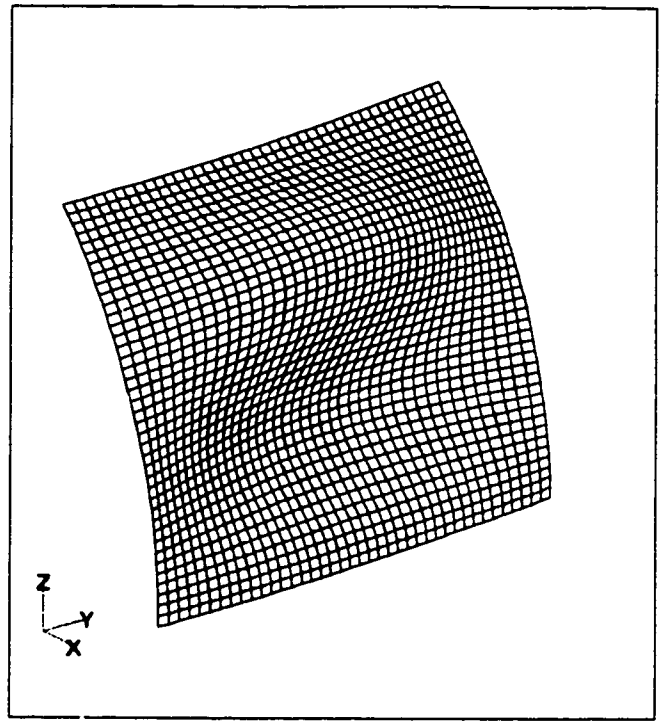

Figure 3.15b: Case 3 - clamped meridional support

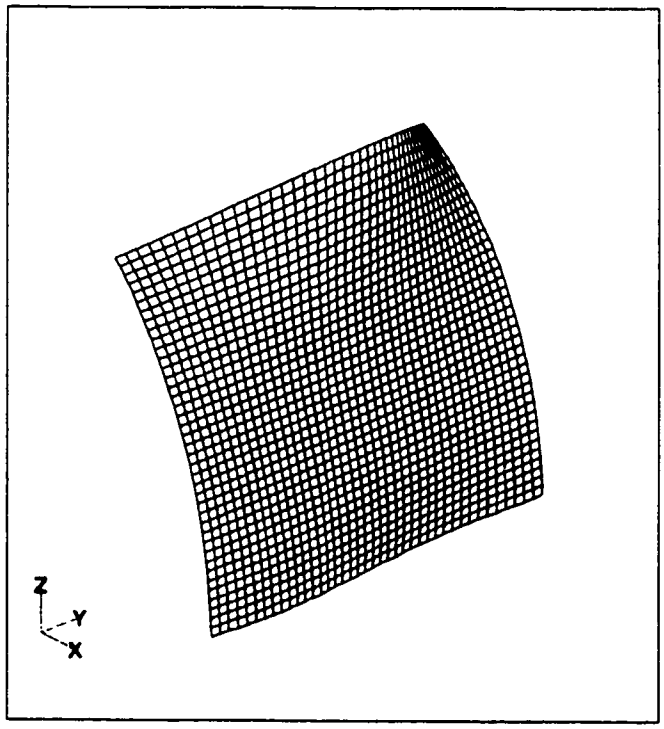

Figure 3.15c: Case 3 - free meridional support

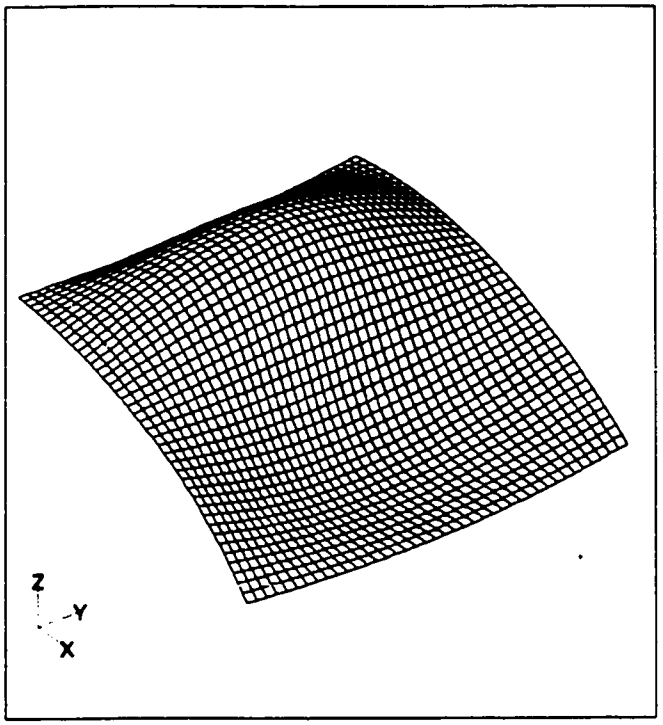

Figure 3.16a: Case 4 - diaphragm meridional support

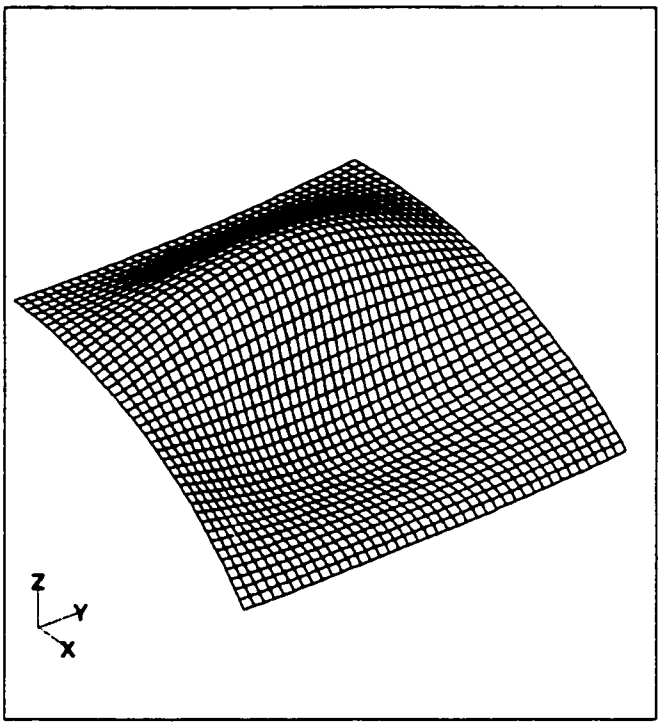

Figure 3.16b: Case 4 - clamped meridional support

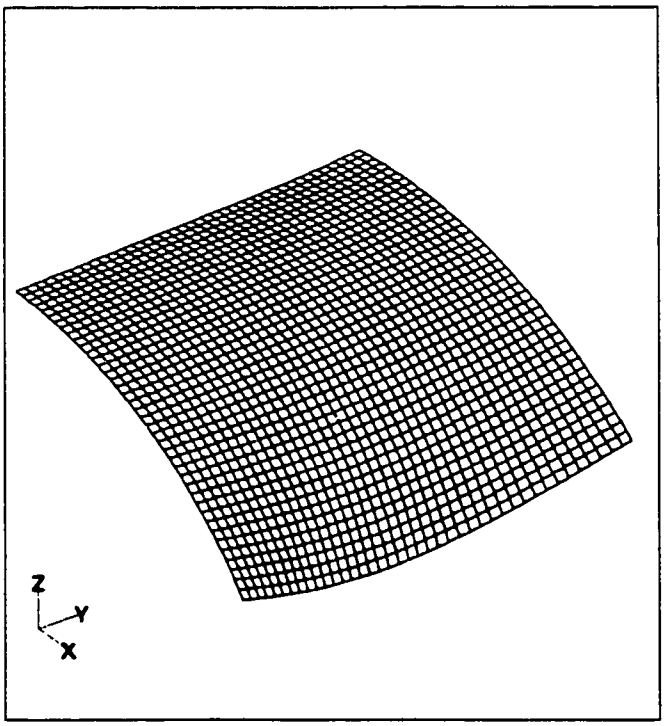

Figure 3.16c: Case 4 - free meridional support

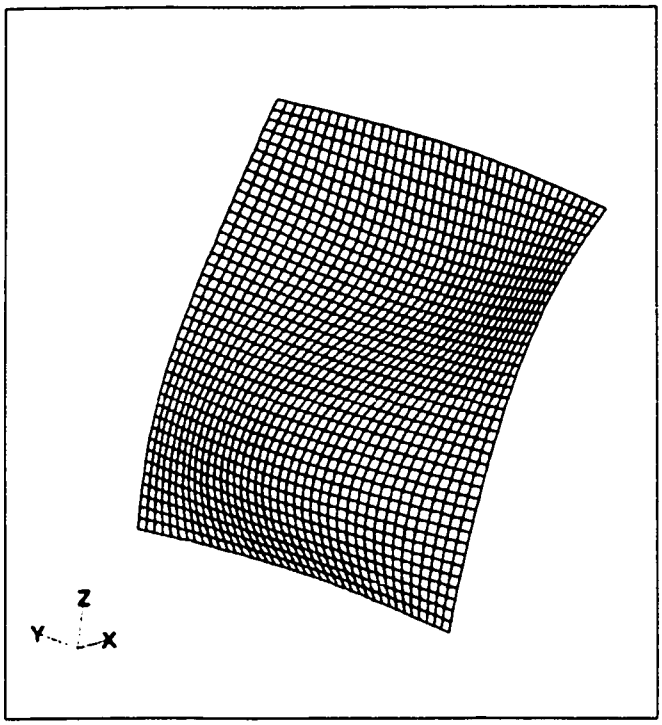

Figure 3.17a: Case 5 - diagragm meridional support

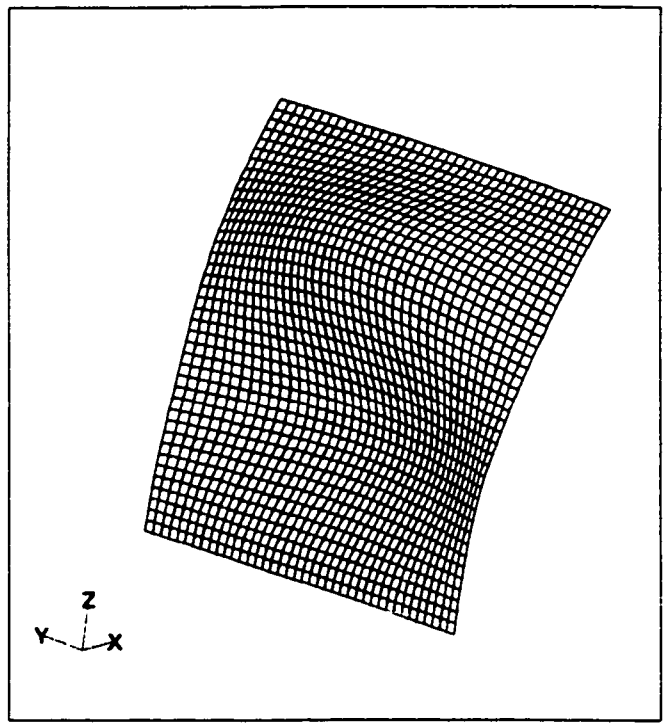

Figure 3.17b: Case 5 - clamped meridional support

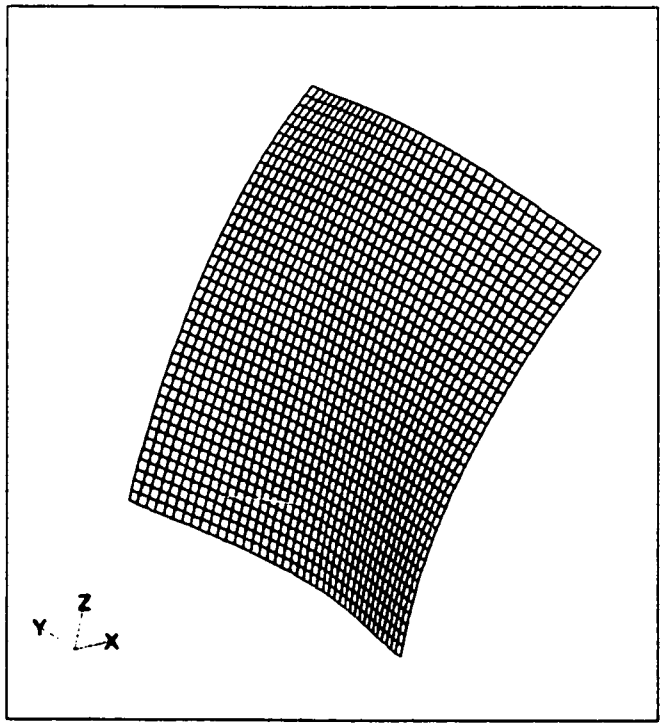

Figure 3.17c: Case 5 - free meridional support

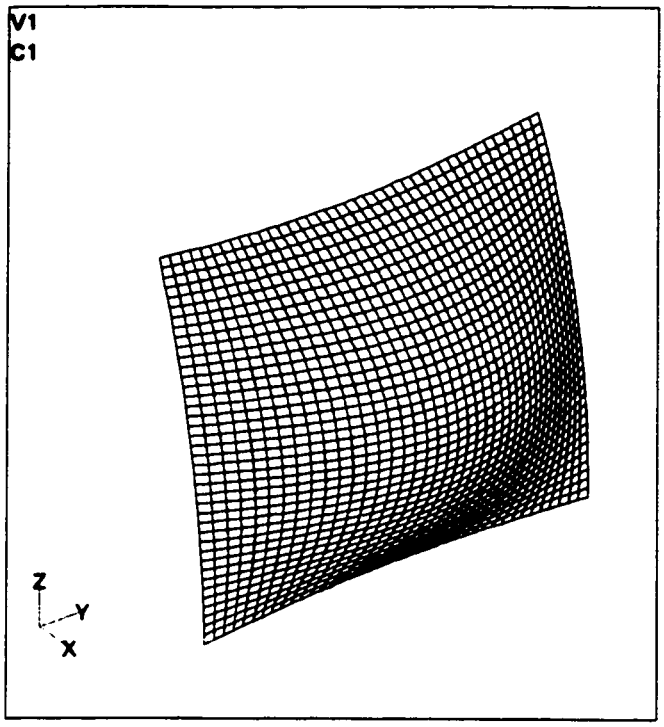

Figure 3.18a: Case 6 - diaphragm meridional support

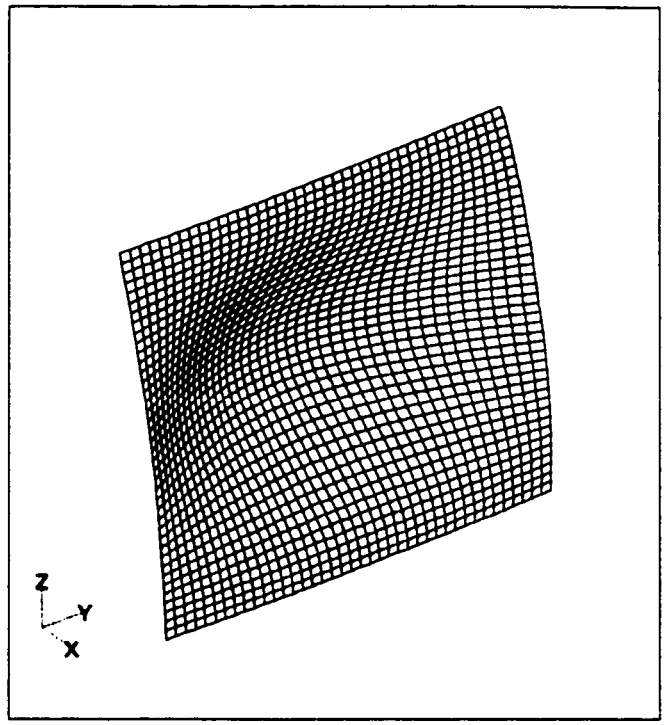

Figure 3.18b: Case 6 - clamped meridional support

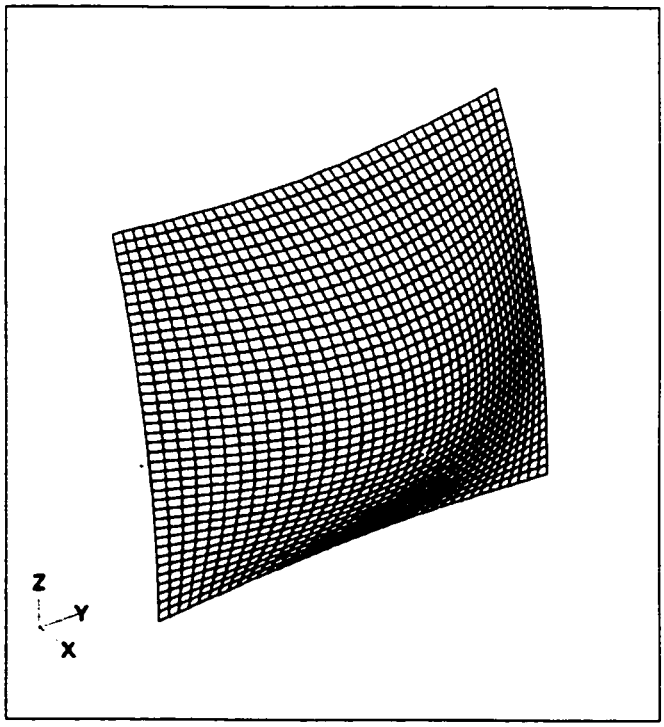

Figure 3.18c: Case 6 - free meridional support

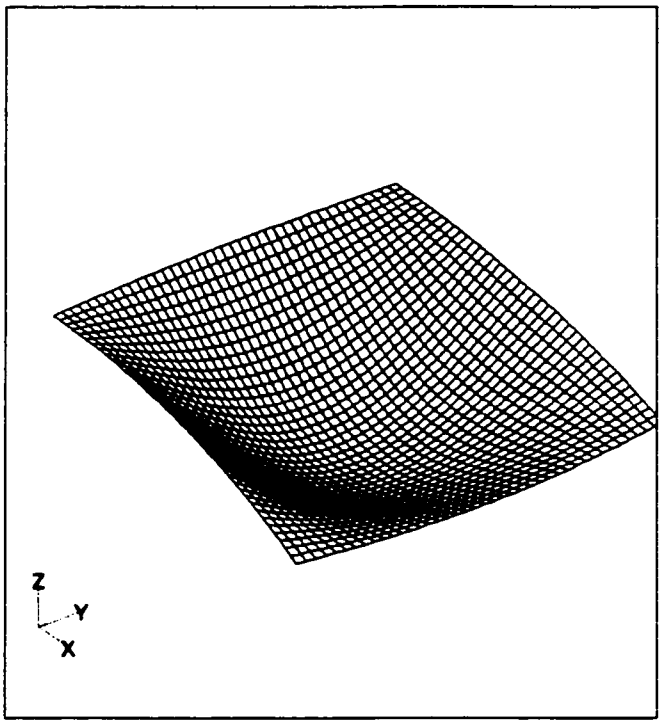

Figure 3.19a; Case 7 - diaphragm meridional support

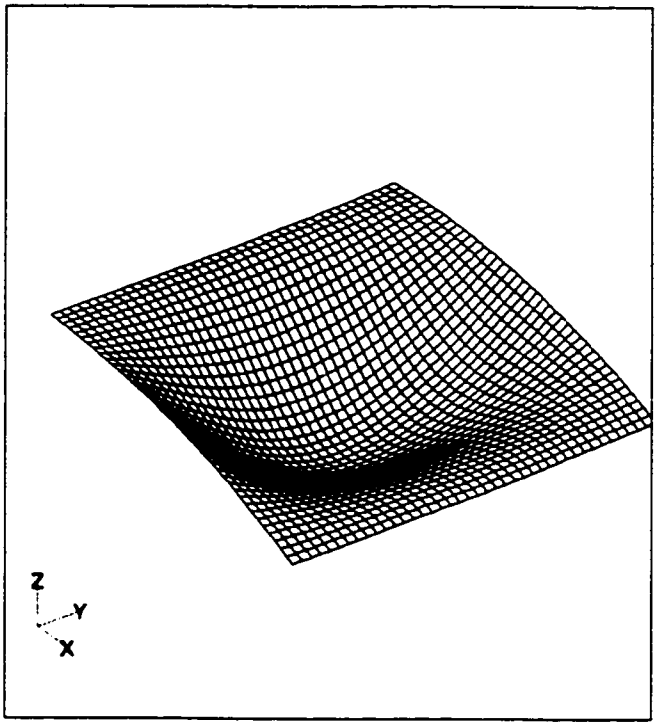

Figure 3.19b: Case 7 - clamped meridional support

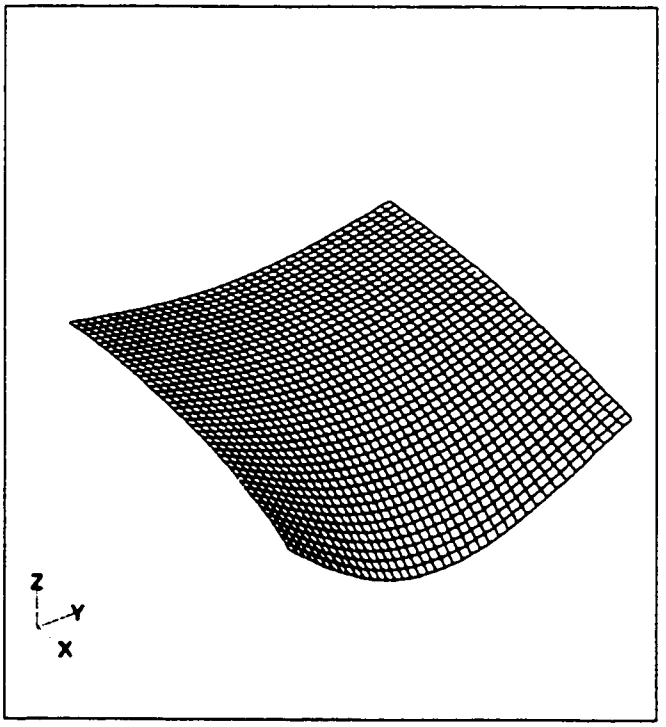

Figure 3.19c: Case 7 - free meridional support

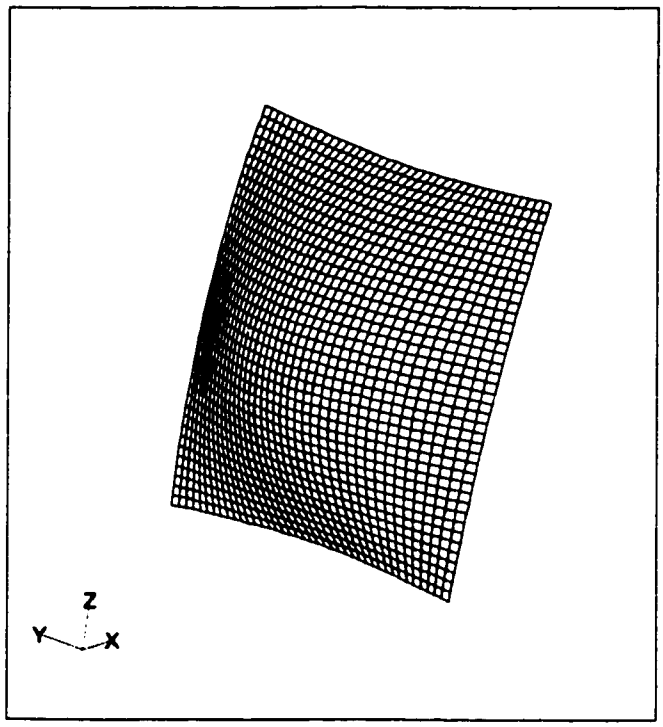

Figure 3.20a: Case 8 - diaphragm meridional support

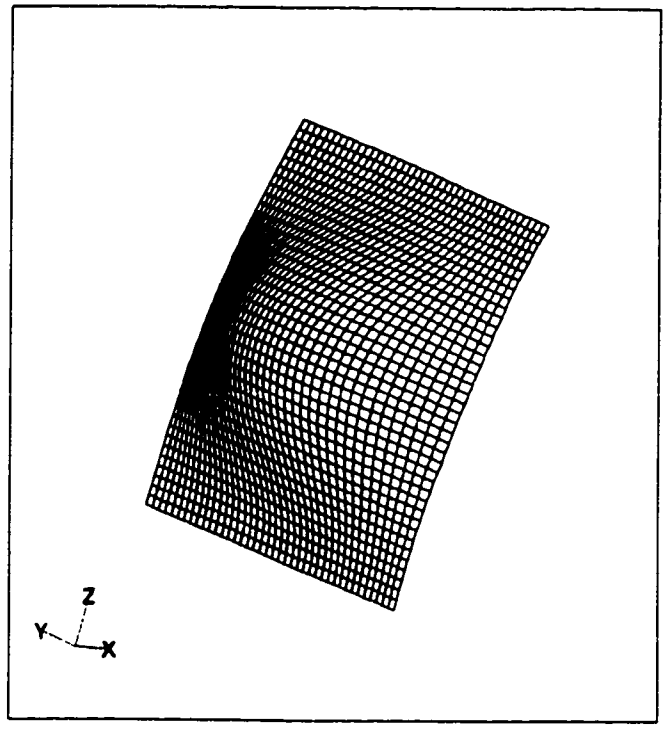

Figure 3.20b: Case 8 - clamped meridional support

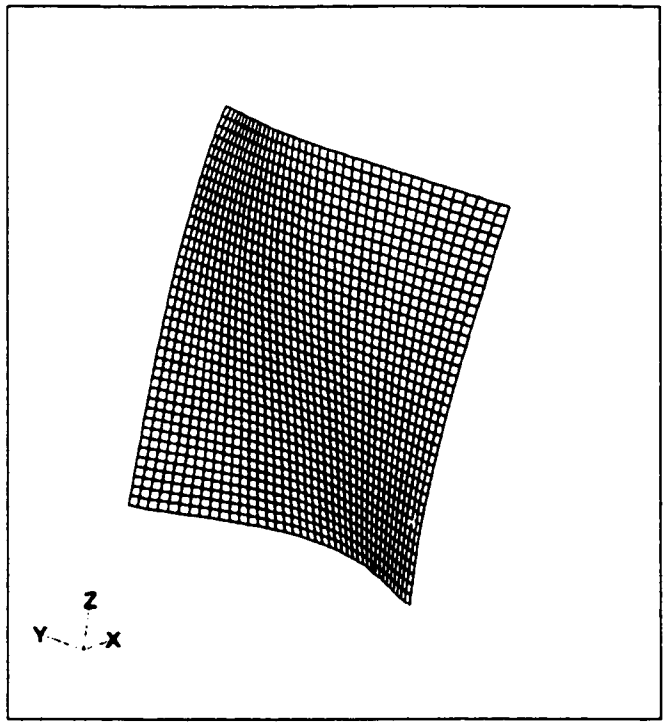

Figure 3.20c: Case 8 - free meridional support

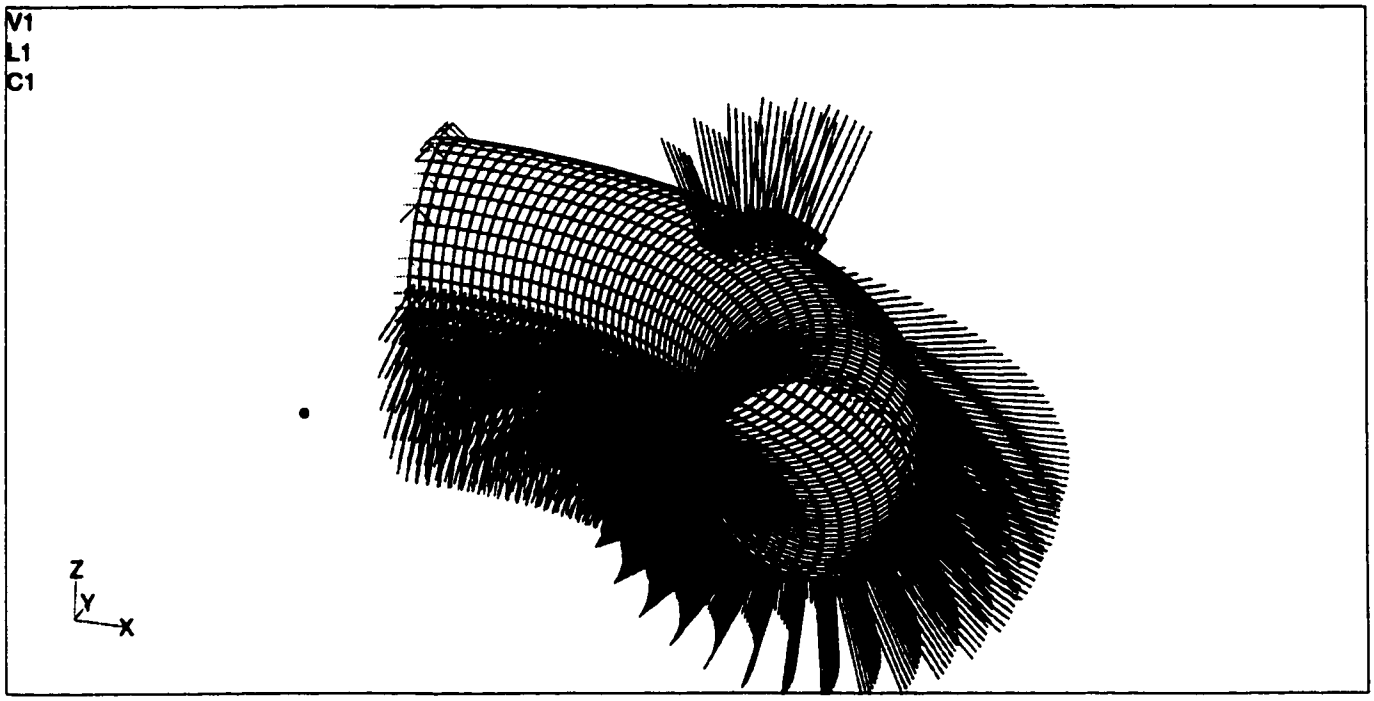

Figure 4.1: FEM mesh of platform shell with loading

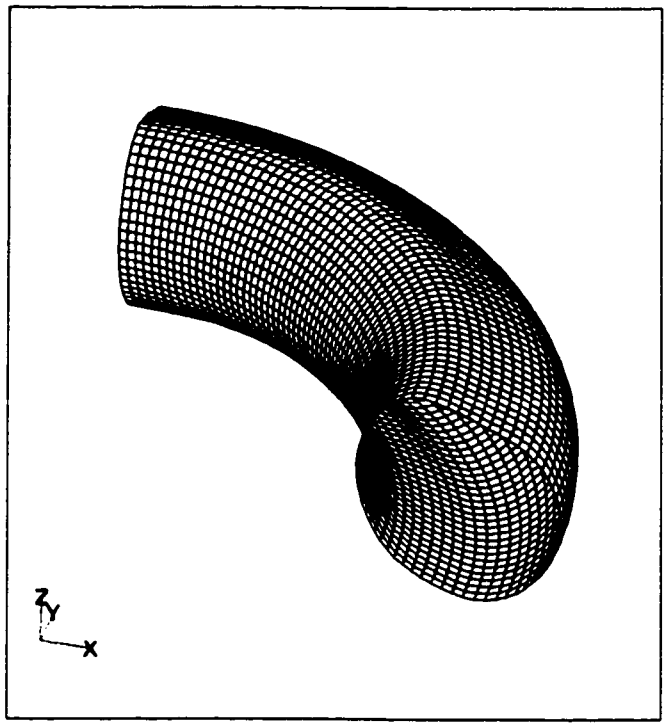

Figure 4.2a: Case C - mode shape 1

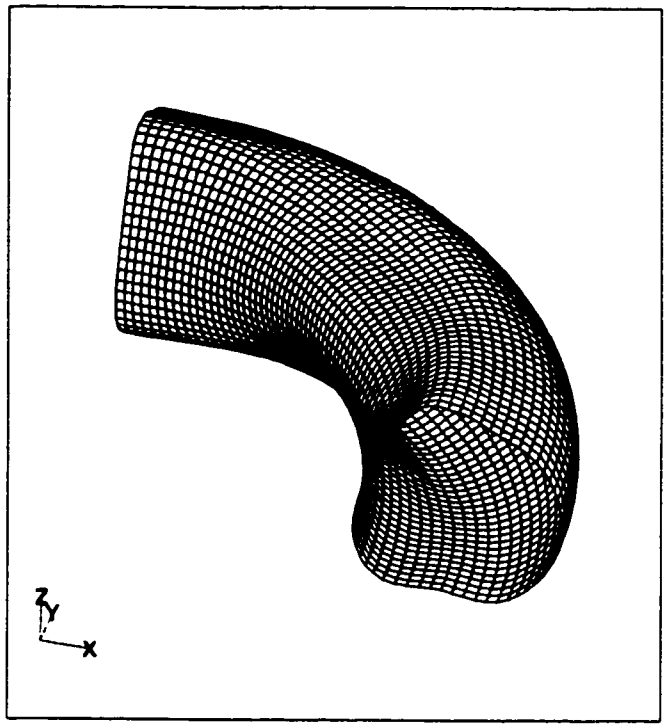

Figure 4.2b: Case C - mode shape 2

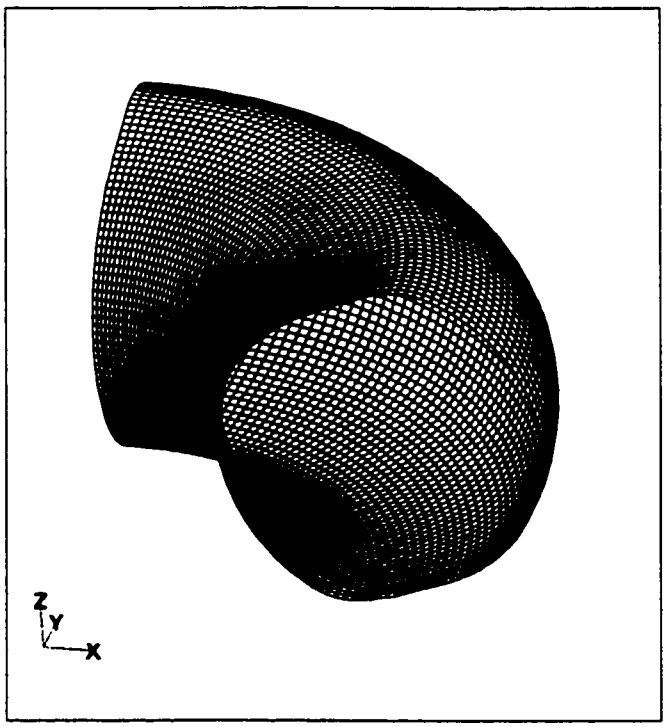

Figure 4.2 c: Case F - mode shape 1

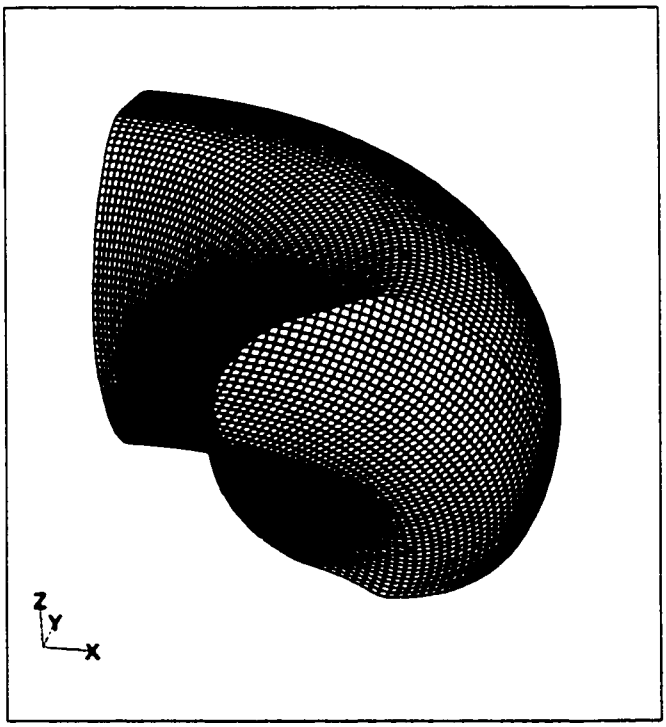

Figure 4.2d: Case F - mode shape 2

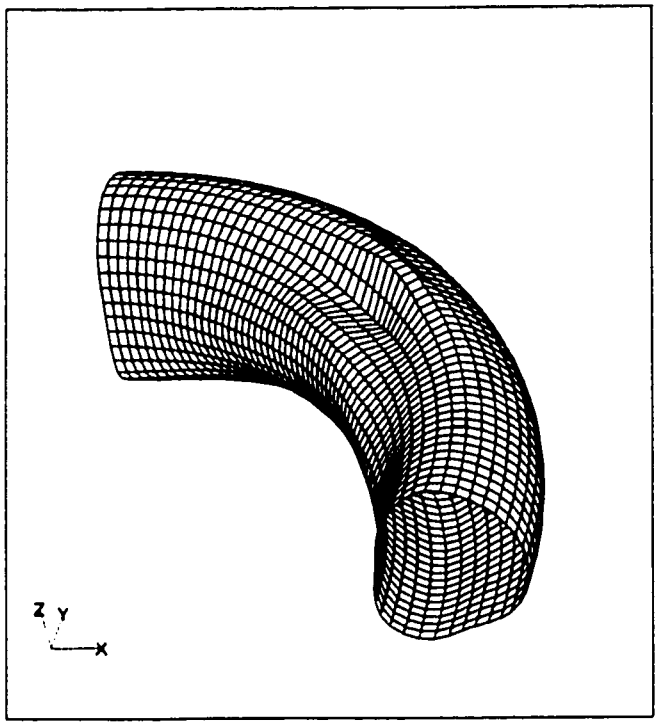

Figure 4.3a: Case 1 - mode shape 1

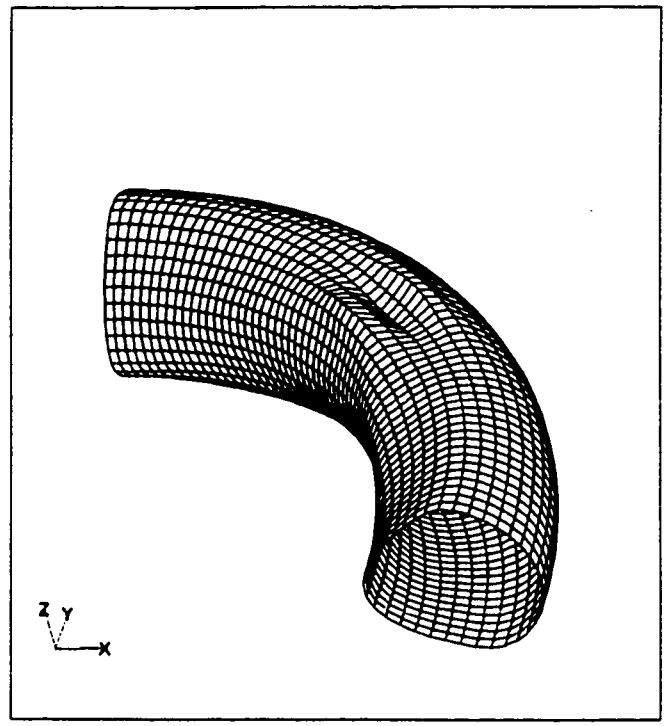

Figure 4.3b: Case 1 - mode shape 2

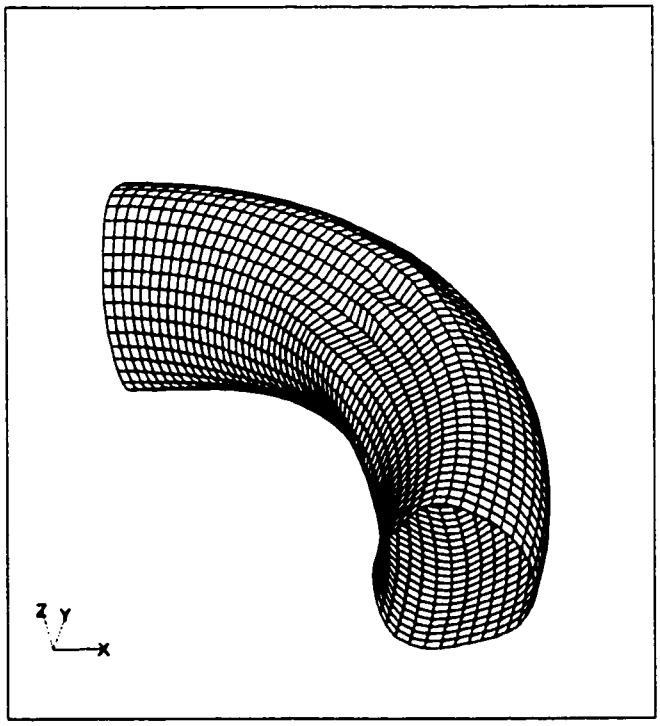

Figure 4.3c: Case 1 - mode shape 3

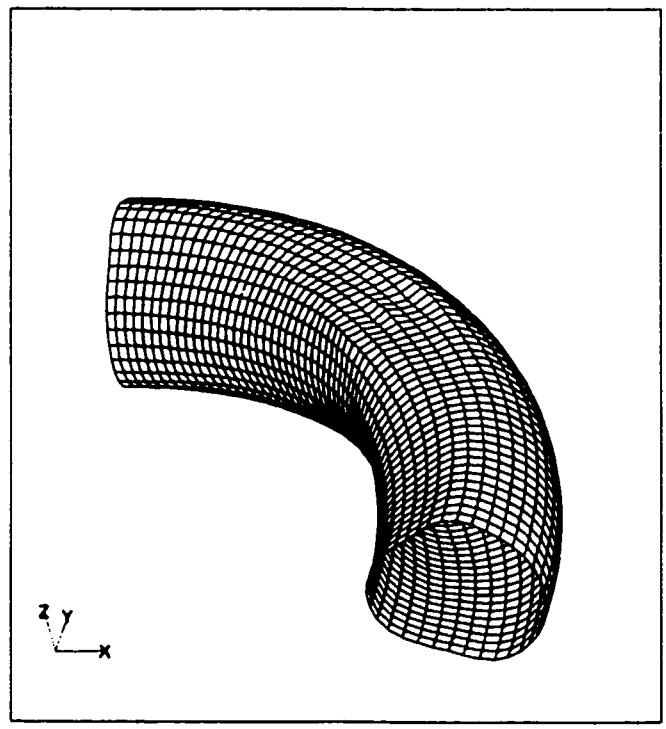

Figure 4.3d: Case 1 - mode shape 4

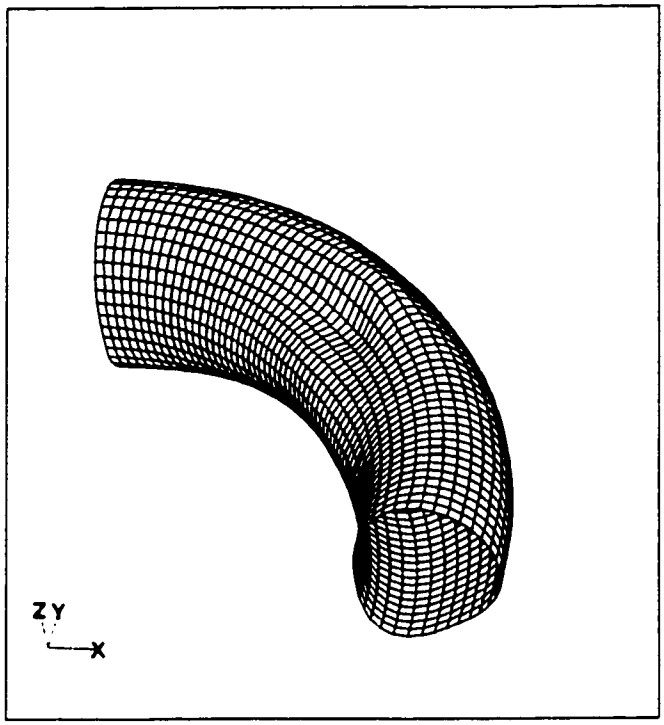

Figure 4.5a: Case 3 - mode shape 1

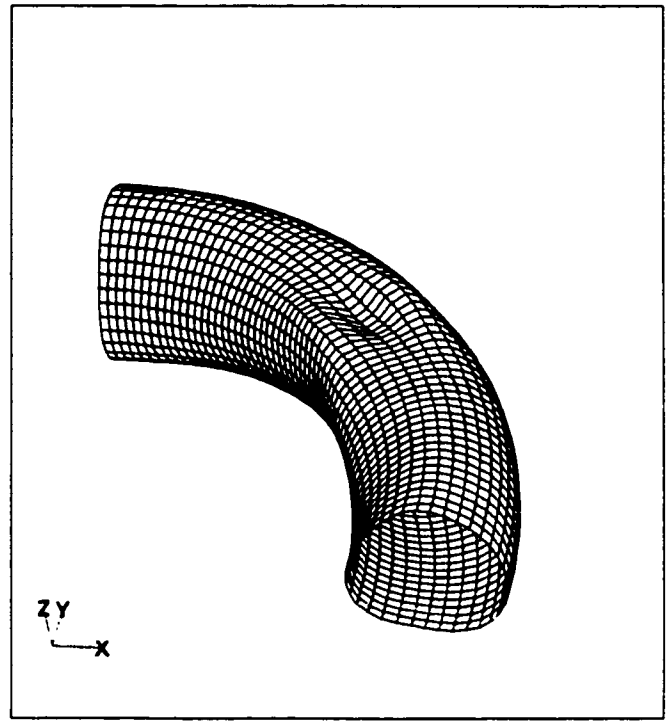

Figure 4.5b: Case 3 - mode shape 2

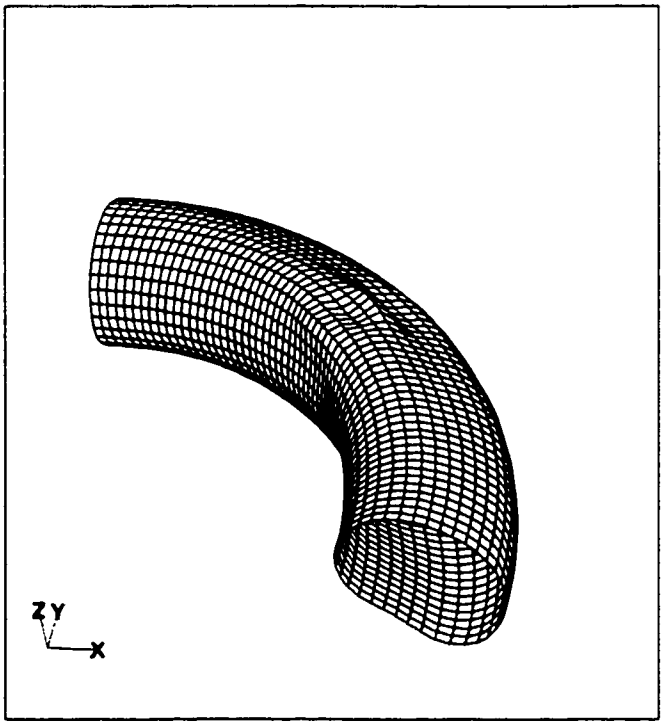

Figure 4.5c: Case 3 - mode shape 3

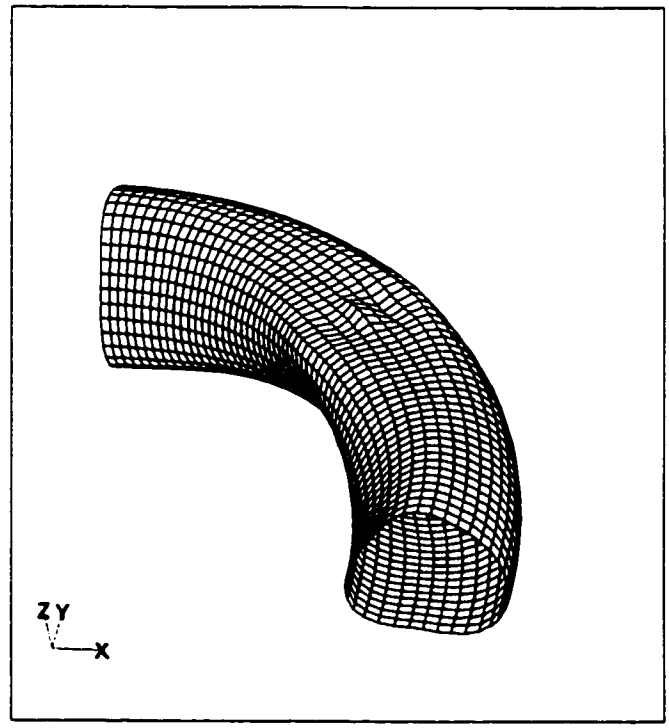

Figure 4.5d: Case 3 - mode shape 4

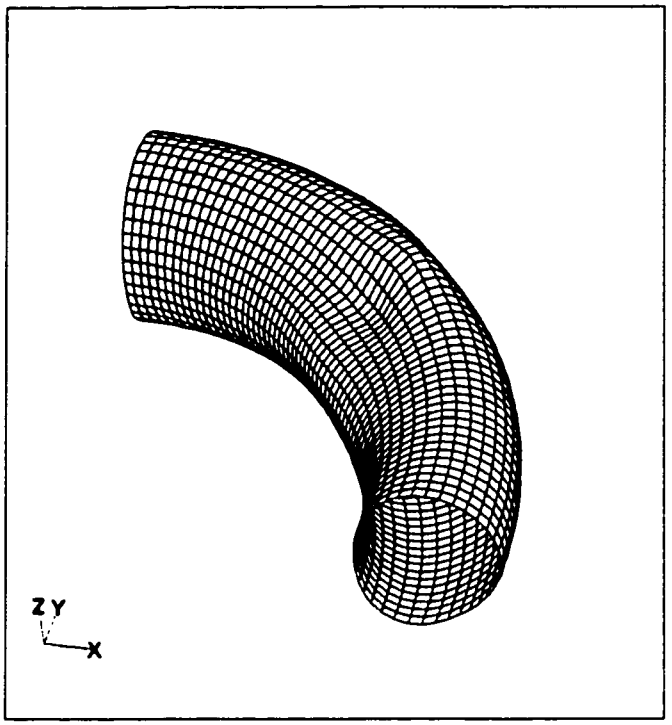

Figure 4.6a: Case 4 - mode shape 1

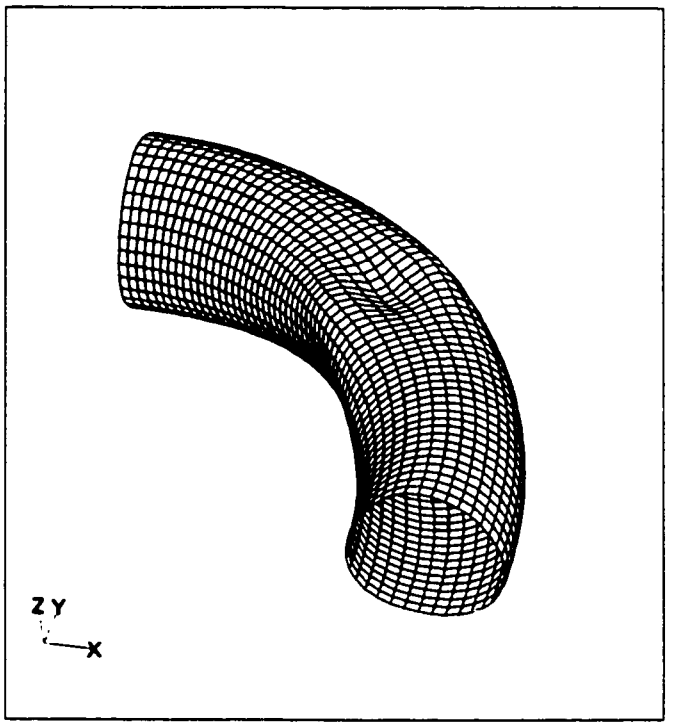

Figure 4.6b: Case 4 - mode shape 2

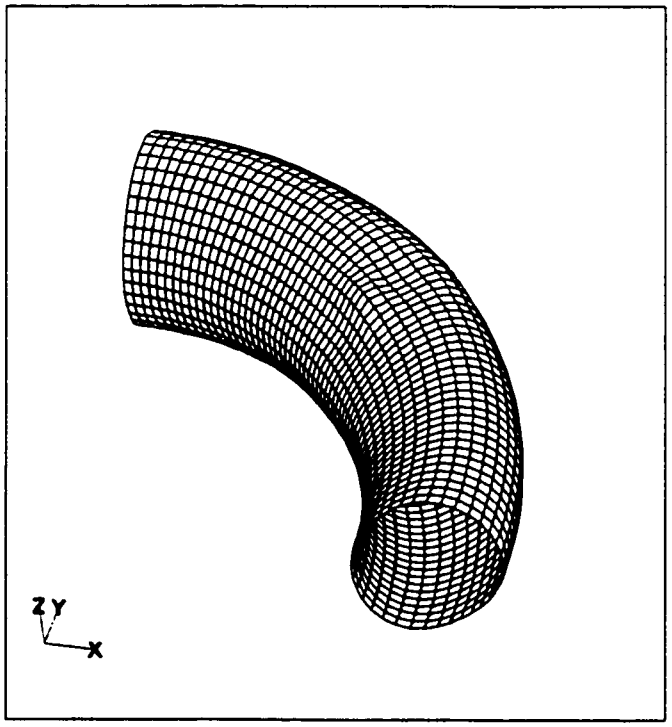

Figure 4.6c: Case 4 - mode shape 3

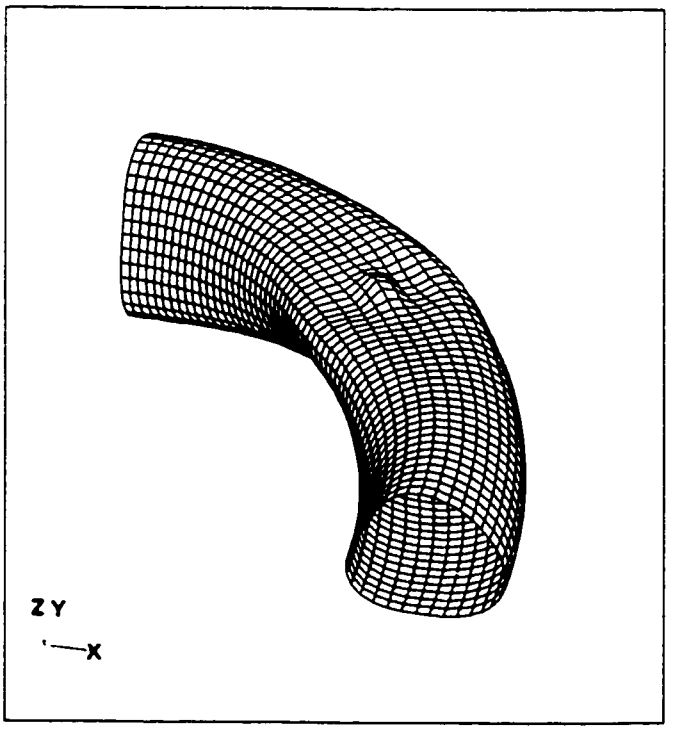

Figure 4.6d: Case 4 - mode shape 4

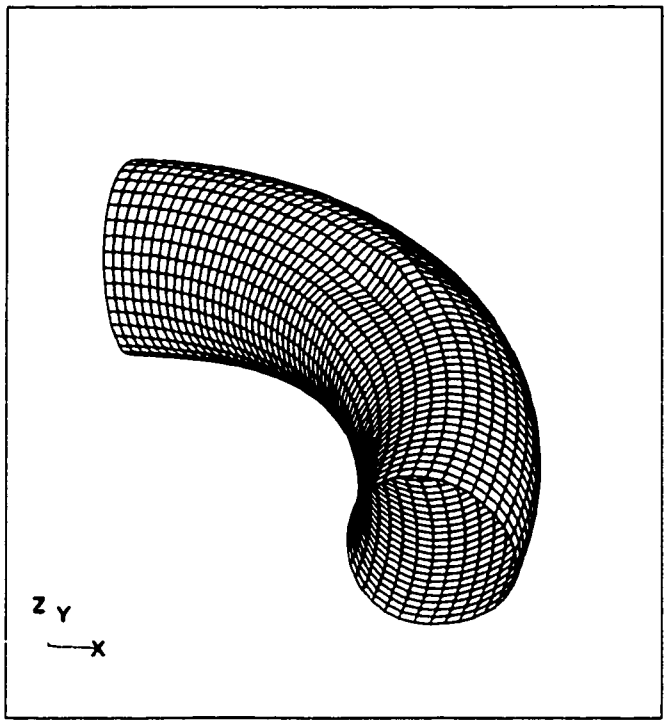

Figure 4.7a: Case 5 - mode shape 1

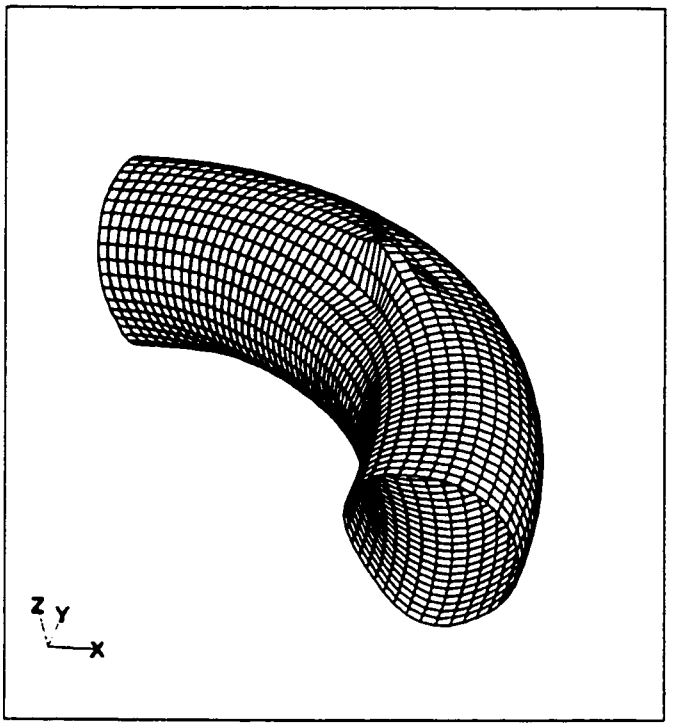

Figure 4.7b: Case 5 - mode shape 2

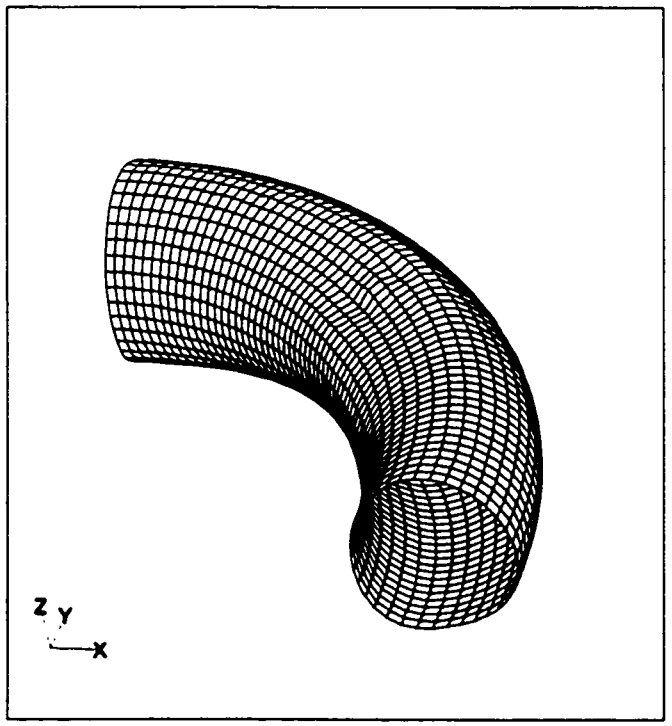

Figure 4.7c: Case 5 - mode shape 3

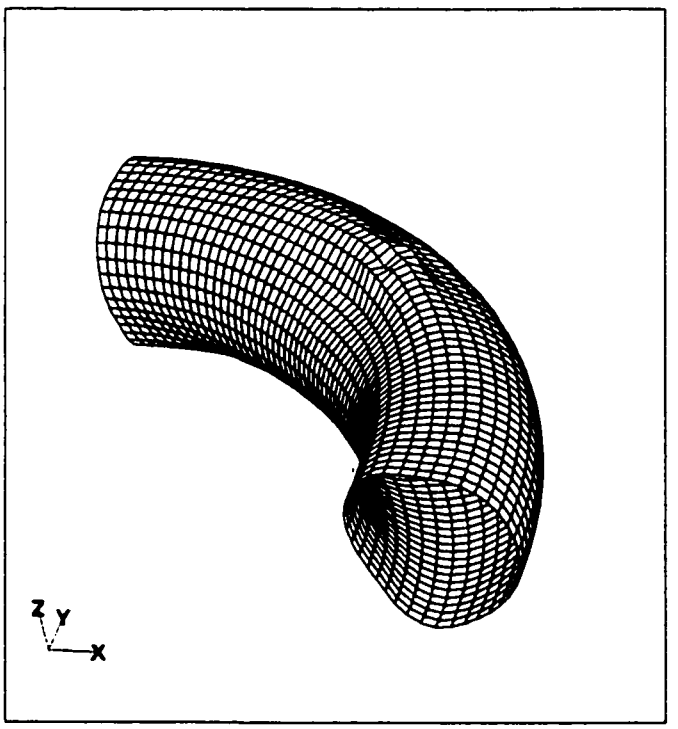

Figure 4.7d: Case 5 - mode shape 4

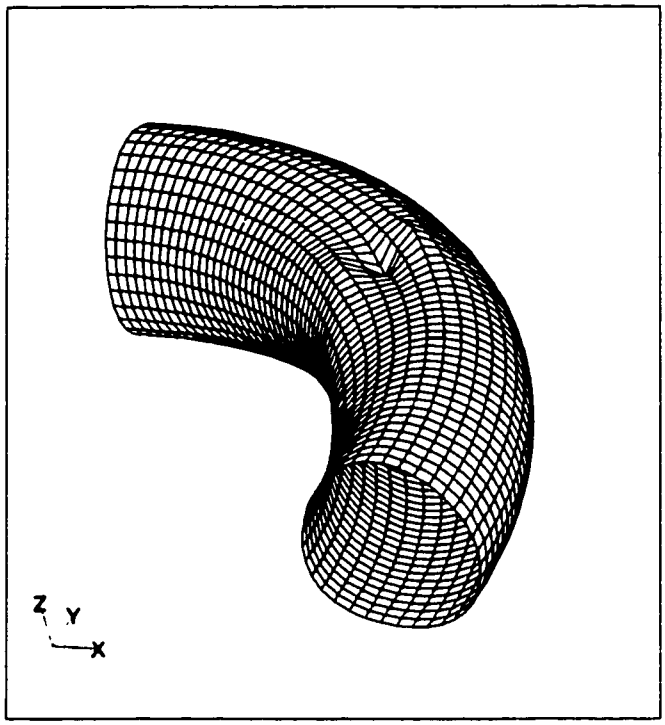

Figure 4.8a: Case 6 - mode shape 1

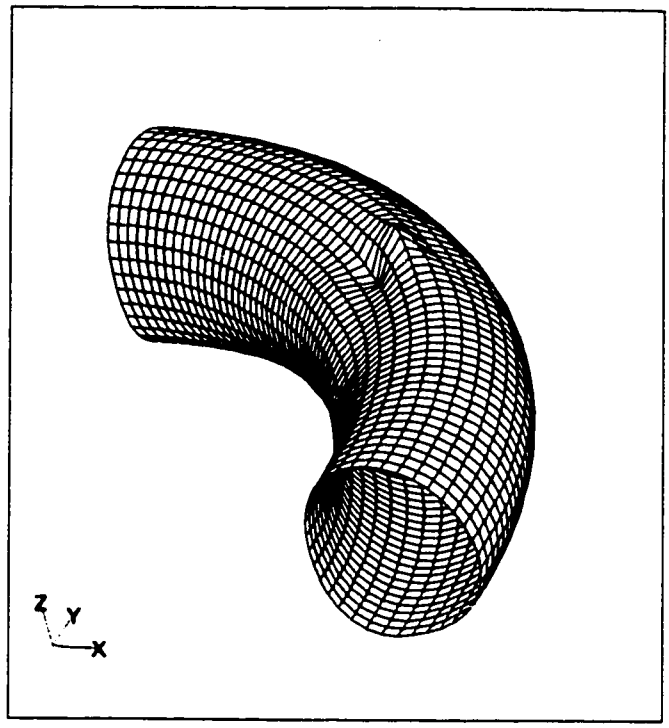

Figure 4.8b: Case 6 - mode shape 2

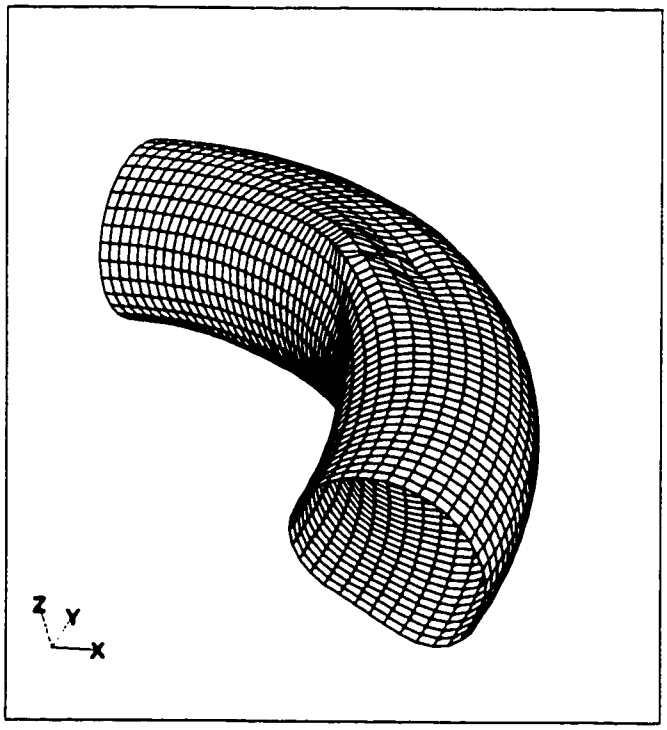

Figure 4.8c: Case 6 - mode shape 3

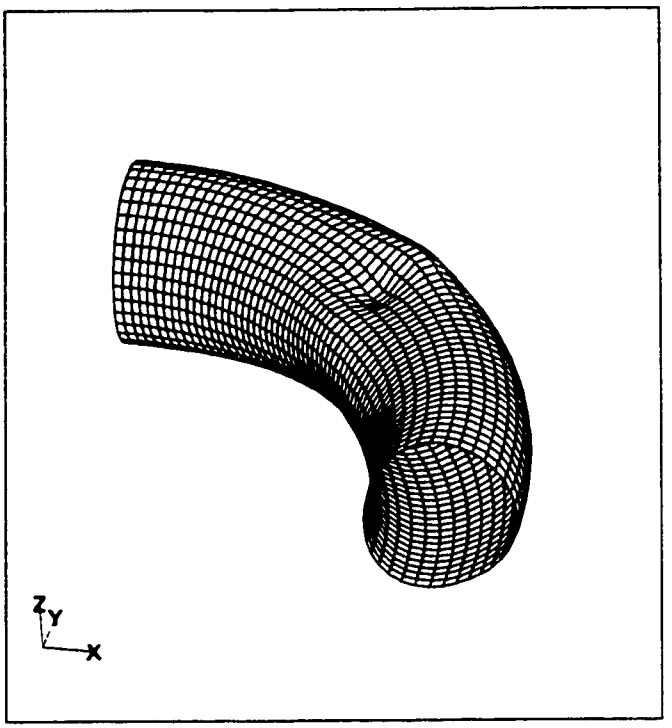

Figure 4.9a: Case 7 - mode shape 1

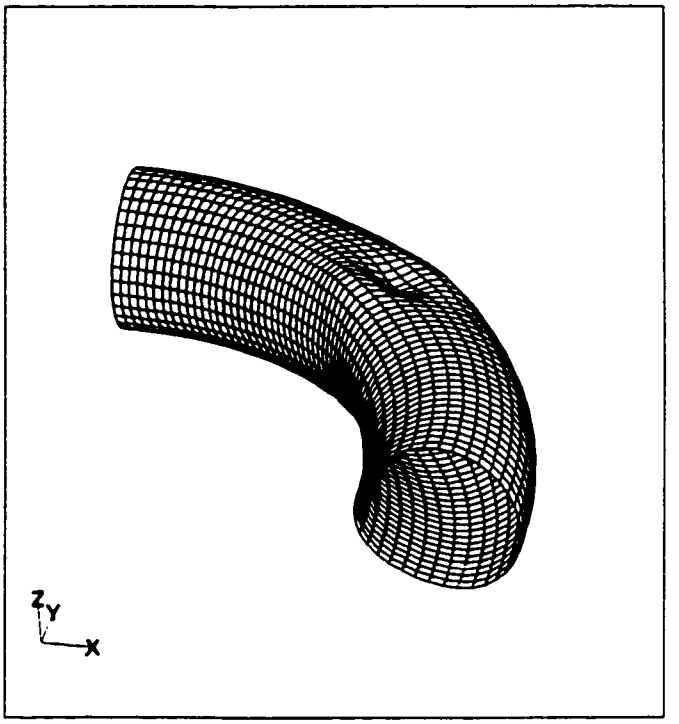

Figure 4.9b: Case 7 - mode shape 2

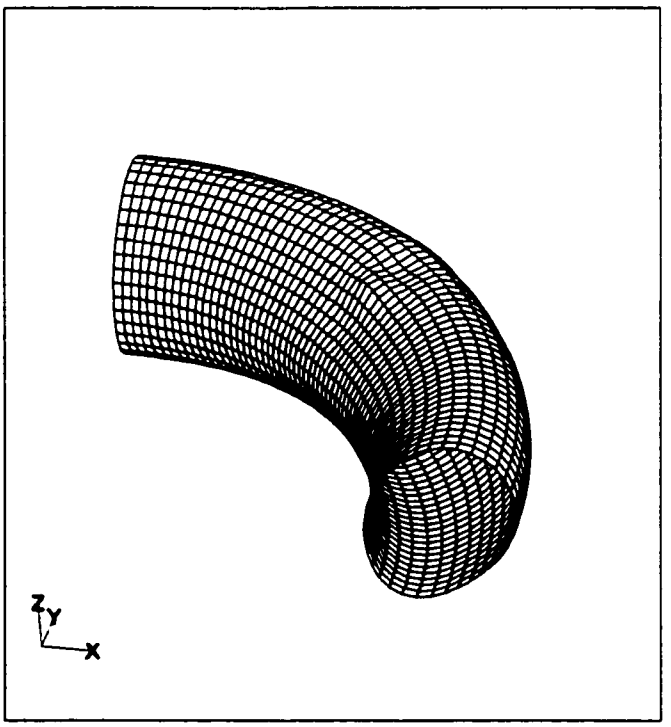

Figure 4.9c: Case 7 - mode shape 3

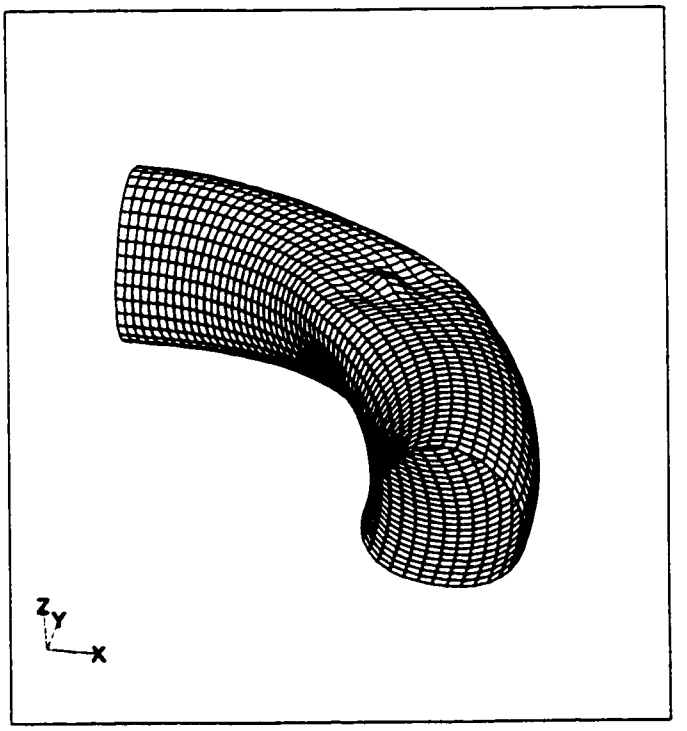

Figure 4.9d: Case 7 - mode shape 4

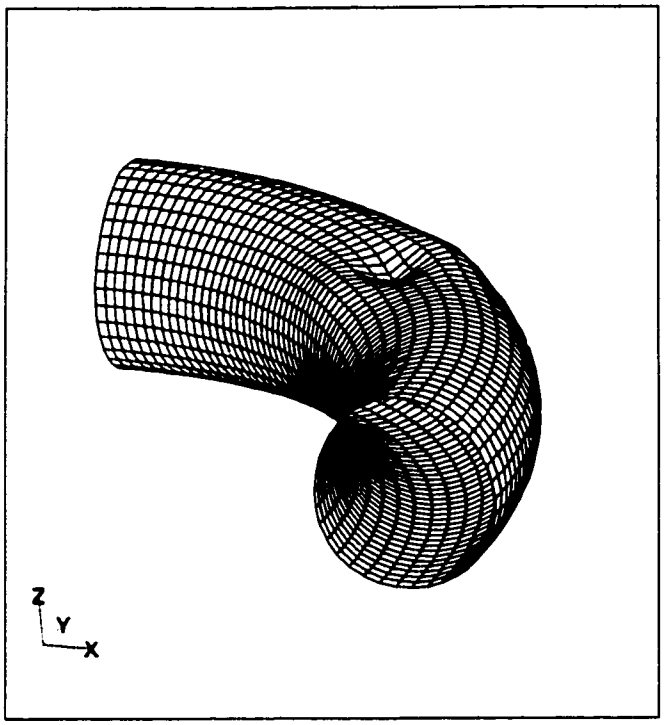

Figure 4.10a: Case 8 - mode shape 1

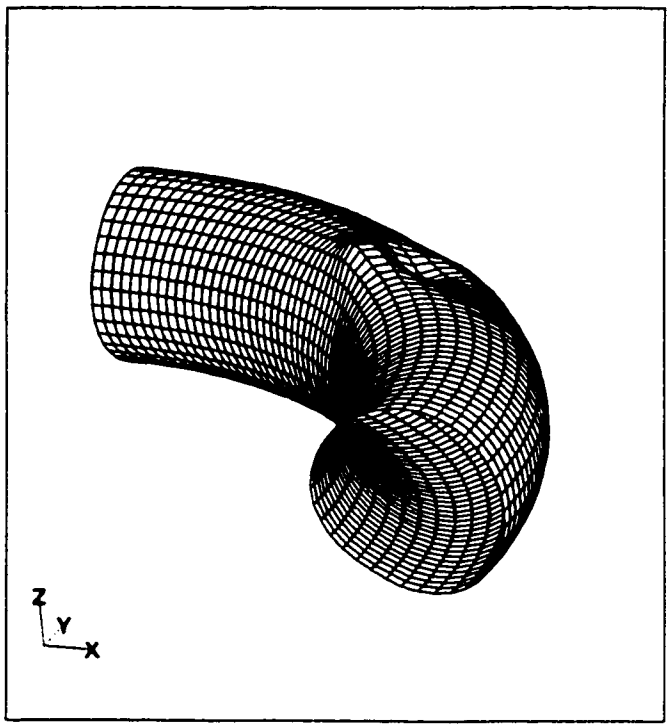

Figure 4.10b: Case 8 - mode shape 2

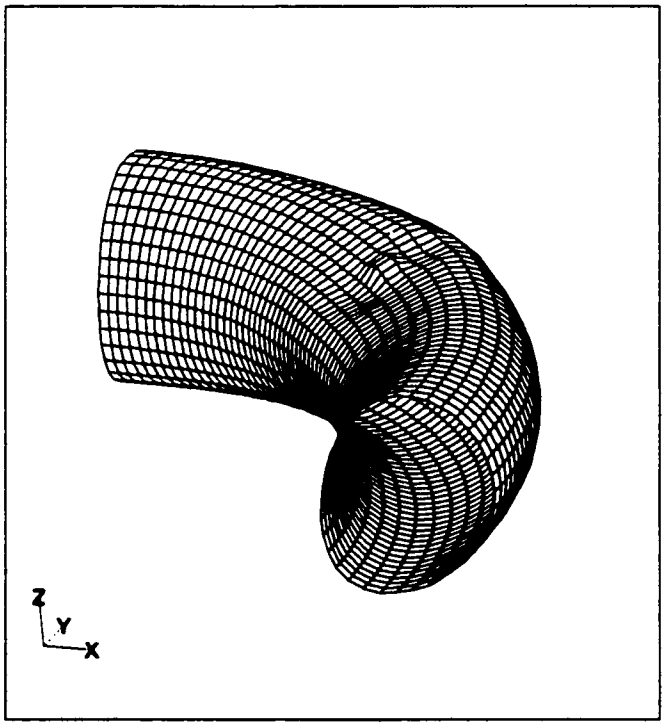

Figure 4.10c: Case 8 - mode shape 3